MECHANISM OF ENTOMOPATHOGENIC BACTERIAL EXTRACT AGAINST DRUG RESISTANT BACTERIA

WIPANEE MEESIL

A Thesis Submitted to the Graduate School of Naresuan University
in Partial Fulfillment of the Requirements
for the Doctor of Philosophy in Parasitology
2024

MECHANISM OF ENTOMOPATHOGENIC BACTERIAL EXTRACT AGAINST DRUG RESISTANT BACTERIA

WIPANEE MEESIL

A Thesis Submitted to the Graduate School of Naresuan University
in Partial Fulfillment of the Requirements
for the Doctor of Philosophy in Parasitology
2024

Thesis entitled " MECHANISM OF ENTOMOPATHOGENIC BACTERIAL EXTRACT AGAINST DRUG RESISTANT BACTERIA "

By Wipanee Meesil

has been approved by the Graduate School as partial fulfillment of the requirements for the Doctor of Philosophy in Parasitology of Naresuan University

Oral Defense Committee

..... Chair
(Professor Narisara Chantratita, Ph.D.)

..... Advisor
(Aunchalee Thanwisai, Ph.D.)

..... Co Advisor
(Assistant Professor Triwit Rattanarojpong, Ph.D.)

..... Co Advisor
(Associate Professor Apichat Vitta, Ph.D.)

..... Co Advisor
(Associate Professor Sutthirat Sitthisak, Ph.D.)

..... Internal Examiner
(Associate Professor Duangkamol Kunthalert, Ph.D.)

..... External Examiner
(Professor Helge B. Bode, Ph.D.)

..... External Examiner
(Associate Professor Triwit Rattanarojpong, Ph.D.)

Approved

.....
(Associate Professor Krongkarn Chootip, Ph.D.)
Dean of the Graduate School

TABLE OF CONTENTS

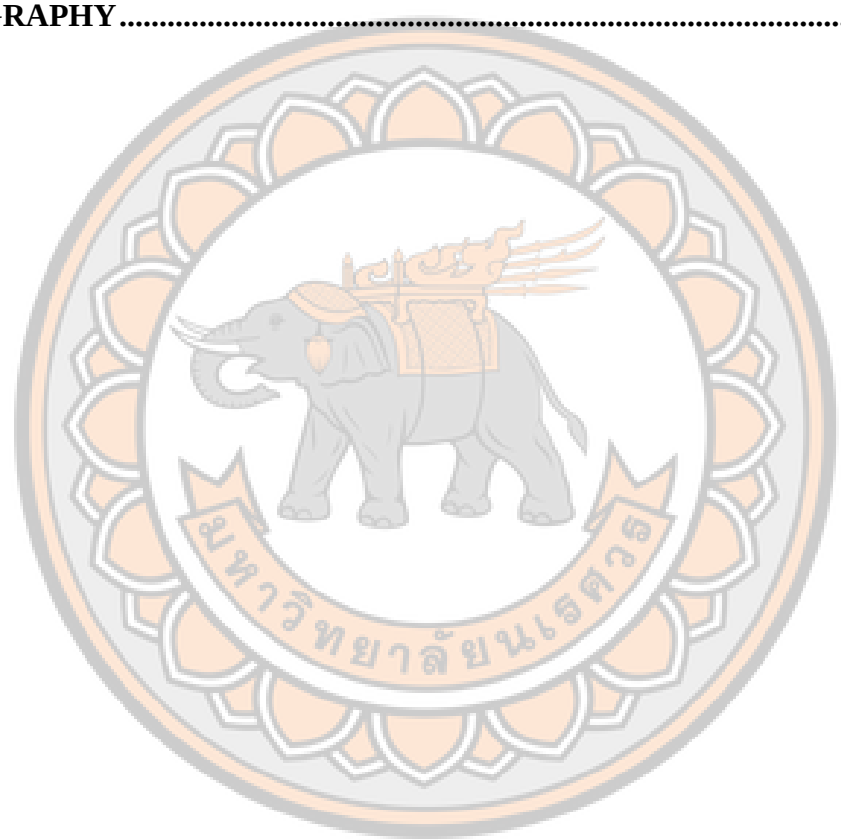

LIST OF TABLES

LIST OF FIGURES

CHAPTER I

INTRODUCTION

Background and significance of the study

Entomopathogenic bacteria are widely distributed and include genera such as *Photorhabdus*, *Xenorhabdus*, *Yersinia*, and *Providencia*. A major challenge for these bacteria in infecting diverse insect species is adapting to and evading varying host immune responses and microbial communities. In order to overcome the challenges, these bacteria have evolved general strategies, including the production of protein toxins that ultimately lead to the death of their insect hosts.

Notably, *Photorhabdus* and *Xenorhabdus* face an additional challenge as a significant portion of their life cycle is spent in symbiosis with nematodes (Patricia Stock et al., 2001; Poinar et al., 1990; Waterfield et al., 2009). These bacteria are mutualistic partners of nematodes from the genera *Heterorhabditis* and *Steinernema*, respectively. The nematode acquires its symbiotic bacteria during the development of the infective juvenile (IJ) stage and subsequently seeks insect hosts (Han & Ehlers, 2000). Upon successfully penetrating an insect, the nematodes released the bacteria into the insect's hemocoel. The bacteria then produce a variety of natural products (NPs) that facilitate infection and eventually cause the insect's death. The resulting nutrient-rich environment supports the reproduction of both the bacteria and nematodes, after which newly developed IJs reacquire their bacterial symbionts and search for new insect prey (Beemelmanns et al., 2016). The natural products synthesized by these bacteria play critical roles in symbiosis and exhibit diverse functionalities, reflecting their remarkable versatility (Beemelmanns et al., 2016; Bode et al., 2015; Bode, 2009; Challinor & Bode, 2015; Piel, 2009).

These products are also of significant interest in drug discovery, as researchers continually explore their potential for novel medicines. *Photorhabdus* and *Xenorhabdus* exhibit substantial capacity for NP production, with numerous biosynthetic gene clusters (BGCs) predicted in all species (Bode, 2009; Chaston et al., 2011). Thus, in this study, the genomes of these bacteria were analysed to discover specialized compounds that had never been detected in the laboratory, an approach that

represents one of the crucial strategies in bioprospecting for new antibiotics. As a result, antimicrobial activity screenings were conducted against pathogenic bacteria. These outcomes will enhance our understanding of the potential therapeutic applications of bioactive compounds derived from entomopathogenic bacteria.

Purposes of the study

To explore the genomes of entomopathogenic bacteria to uncover previously unobserved specialized metabolites in the laboratory and to study the antimicrobial activities of their extracted compounds.

Scope of the study

This study was divided into three main parts, each building upon the previous findings. First, genome sequencing and mining were performed to prioritize the candidate strain. Next, whole-genome sequencing of the selected strain was conducted to identify biosynthetic gene clusters associated with secondary metabolite production. Based on these findings, the antimicrobial activity of the crude extract was evaluated in detail through minimum inhibitory concentration (MIC), minimum bactericidal concentration (MBC), time-kill curve analysis, and morphological examination of treated bacteria using transmission electron microscopy. Finally, to further understand the extract's mode of action, proteomic analysis was conducted to identify differentially expressed protein profiles in antibiotic-resistant bacteria in response to the treatment.

CHAPTER II

Related works and studies

Entomopathogenic bacteria

Entomopathogenic bacteria, recognized for their production of a variety of virulence factors, which are commonly found in nature and include genera such as *Serratia*, *Peanibacillus*, *Bacillus*, *Pseudomonas*, *Brevibacillus*, *Xenorhabdus*, and *Photorhabdus* (Boemare & Tailliez, 2009; Glare et al., 2017). Among these, *Photorhabdus* and *Xenorhabdus* are unique as they are symbiotic of infective juveniles (IJs) of entomopathogenic nematodes (EPNs) from the genera *Steinernema* and *Heterorhabditis*, respectively (Patricia Stock et al., 2001; Poinar et al., 1990; Steven et al., 1997; Waterfield et al., 2009). These bacteria spend part of their lifecycle inside nematodes, using them as vectors to efficiently infect insect hosts (Heather & Randy, 2009; Herbert & Goodrich-Blair, 2007). In *Steinernema* nematodes, the bacteria are housed in the receptacle, located at the anterior part of the gut. In contrast, *Heterorhabditis* lack such a specialized structure and harbor the bacteria in their intestinal lumen (Bird & Akhurst, 1983; Boemare, 2002; Snyder et al., 2007).

1. *Xenorhabdus* bacteria

Firstly, *Xenorhabdus* spp. are named *Achromobacter nematophilus* and associated with *Steinernema carpocapsae* (Poinar & Thomas, 1966). The location of the bacteria in the IJ stage was first demonstrated using light microscopy and later confirmed through electron microscopy (Poinar, 1966; Poinar Jr & Leutenegger, 1968). The activities of the bacterium in the nematode's development and the host's death have been elucidated (Poinar & Thomas, 1966; Poinar Jr & Thomas, 1967) leading to the establishment of a new genus, named *Xenorhabdus*. This genus was proposed for entomopathogenic bacteria, gram-negative, large, rod-shaped, and facultatively anaerobic. The bacterial cell is shown in Figure 1. These bacteria primarily inhabit the intestinal lumen of nematodes or the body cavity of host insects, which they enter via the nematodes. The genus is classified within the family Morganellaceae (Ricardo et al., 2021).

The diameter of the colony on nutrient agar (NA) is approximately 1 mm after 24 to 48 hours at 24°C. Colony morphologies were circular in shape with slightly uneven edges, moist, smooth, some granular, and with a low convex shape, and exhibit a coloration that ranges from cream to yellow-brown or yellow. On triphenyl-tetrazolium chloride agar (T-7+TTC agar), colonies gradually acquire a distinctive blue pigment with maroon centers, or a blue-green shade with dark blue centers.

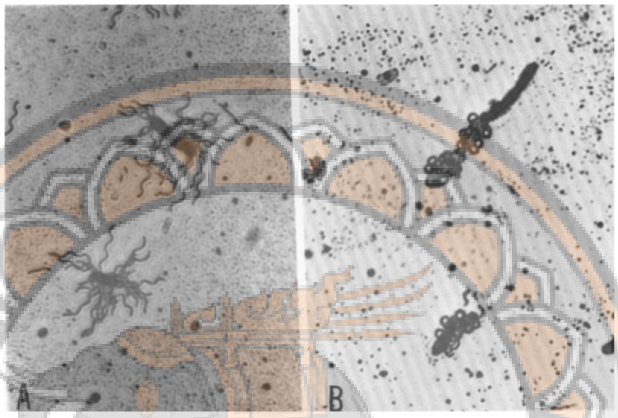

Figure 1 Bacterial cells stained by the Leifson method for flagella, demonstrating the peritrichous cells of *X. nematophilus* (A) and *P. luminescens* (B).

Source: Thomas and Poinar (1979)

In 1975, the entomopathogenic nematode *Heterorhabditis* spp. was first identified, and in 1979, the symbiotic bacterium associated with *H. bacteriophora* was characterized as *Xenorhabditis luminescens* (Poinar, 1975; Thomas & Poinar, 1979). Due to the intriguing ability of this bacterium to produce fluorescence, further studies were conducted. The entire insect cadavers infected with the bacteria glowed in the dark (Figure 2), and light was even detectable from a single infective stage (G. O. Poinar Jr et al., 1980). The bacteria were later reclassified under the genus *Photorhabdus* as *Photorhabdus luminescens* (Boemare et al., 1993).

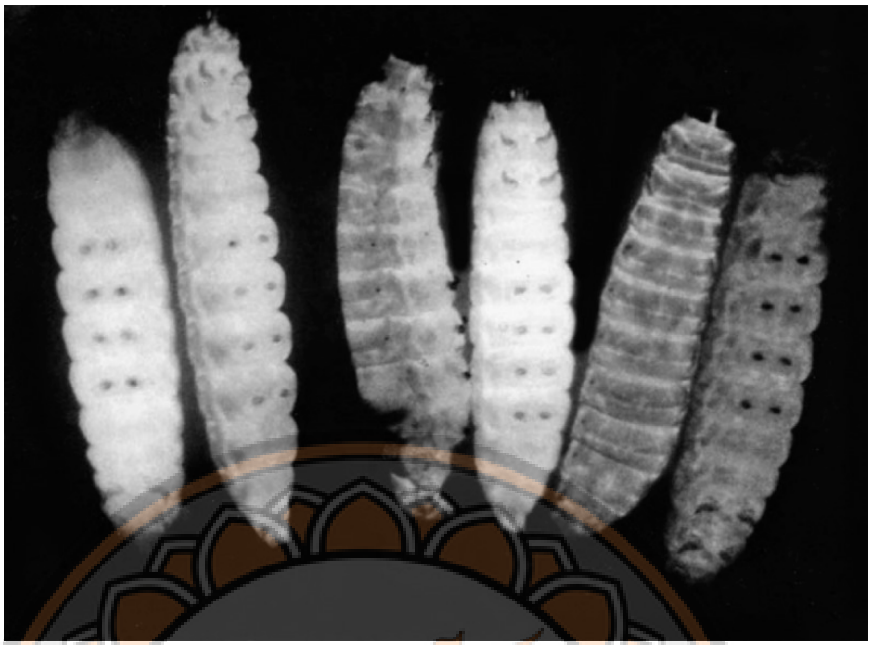

Figure 2 Cadavers of the wax moth glowing in the dark after being infected with *Heterorhabditis bacteriophora* 48 hours earlier.

Source: Poinar Jr and Grewal (2012)

2. *Photorhabdus* bacteria

Photorhabdus is belonging to the family Morganellaceae (Machado et al., 2021). This bacterium is motile, gram-negative, facultatively anaerobic, peritrichous rods measuring 5.1–6.0 µm in length and 0.8–1.4 µm in width (Figure 1B). They are chemoorganotrophic in terms of nutrition and grow well on meat extract media and peptone agar. *Photorhabdus* differ from *Xenorhabdus* in being catalase-positive, with an irreversible phase transition from the primary to the secondary form. A notable characteristic of *Photorhabdus* spp. is their capability to bioluminescence. Furthermore, *Photorhabdus* is the only known non-marine luminous bacterium. The bioluminescence of *Photorhabdus* is attributed to the sequence similarity of the *lux* genes, which are closely related to those found in marine bacteria of the genera *Vibrio* and *Photobacterium* (Szittner & Meighen, 1990). *P. luminescens* has been observed to exhibit bioluminescence on various media, including nutrient agar (NA), nutrient broth, triphenyl-tetrazolium chloride agar (T-7+TTC agar), peptone water, and in infected

insects. On nutrient agar (NA), colonies are measuring approximately 1 mm in diameter after 24 to 48 hours at 24°C. They appear smooth, with a texture ranging from slightly granular to mucoid or highly mucoid and exhibit a low convex profile. They are circular with slightly irregular margins and range in colour from brown, rust brown to brick red. On T-7+TTC agar, colonies slowly acquire a unique coloration, transitioning from greenish with red-brown centres to a dull olive green.

3. EPNs, *Xenorhabdus* and *Photorhabdus* life cycle

Xenorhabdus spp. and *Photorhabdus* spp. are two bacterial genera that form mutualistic relationships with entomopathogenic nematodes (EPNs) and are key players in insect-pathogenic processes (Martens et al., 2003; Popiel et al., 1989). *Xenorhabdus* bacteria reside in the intestines (receptacle) of *Steinernema* spp. nematodes (Bird & Akhurst, 1983), while *Photorhabdus* bacteria colonize the intestines of *Heterorhabditis* spp. nematodes (Figure 3). Both genera of bacteria utilize their nematode hosts to invade insect cadavers, where they suppress the insect's immune system and produce virulence factors that lead to host mortality (Caldas et al., 2002; Dunphy & Webster, 1988). These bacteria also produce antimicrobial compounds and exoenzymes to inhibit microbial competitors and degrade macromolecules, providing essential nutrients for nematode growth (Akhurst, 1982; Ji & Kim, 2004). As shown in Figure 4, the nematodes mature and deplete the insect's resources, they re-associate with the bacteria, transforming into infective juvenile (IJ) nematodes that emerge from the insect carcass to find new hosts. This tripartite interaction between the bacteria, nematode, and insect serves as a model system for studying both mutualistic and pathogenic relationships within a single bacterial species (Akhurst & Boemare, 1990; Richards & Goodrich-Blair, 2010).

Photorhabdus and *Xenorhabdus* share similar lifestyles but differ in the molecular mechanisms they use to overcome insect immunity. *Photorhabdus* modifies lipopolysaccharide (LPS) to resist antimicrobial peptides (AMPs), while *Xenorhabdus* prevents AMP expression altogether. The bacterial species also differ in how they colonize their nematode hosts, with *Photorhabdus* requiring colonization of maternal rectal glands in *Heterorhabditis* spp., a feature not observed in *Xenorhabdus*. These differences highlight the adaptability of bacteria to their ecological roles and provide valuable insights into bacterial pathogenesis and mutualism. Understanding the

interactions between these bacteria, their nematode hosts, and insect hosts may inform biocontrol strategies and deepen our comprehension of bacterial virulence mechanisms.

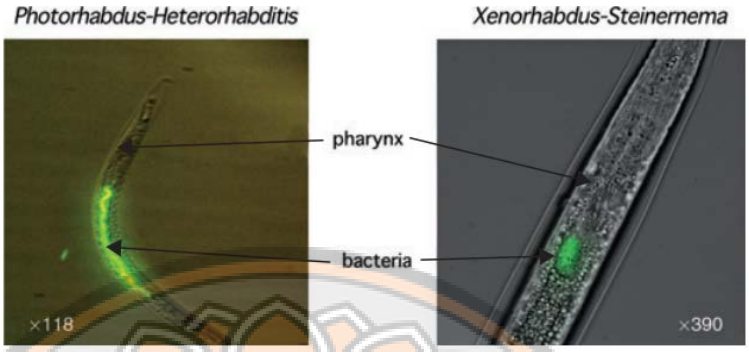

Figure 3 GFP-labelled *Xenorhabdus* and *Photorhabdus* colonize different sites in the IJ stage of their nematode hosts.

Source: Goodrich-Blair and Clarke (2007)

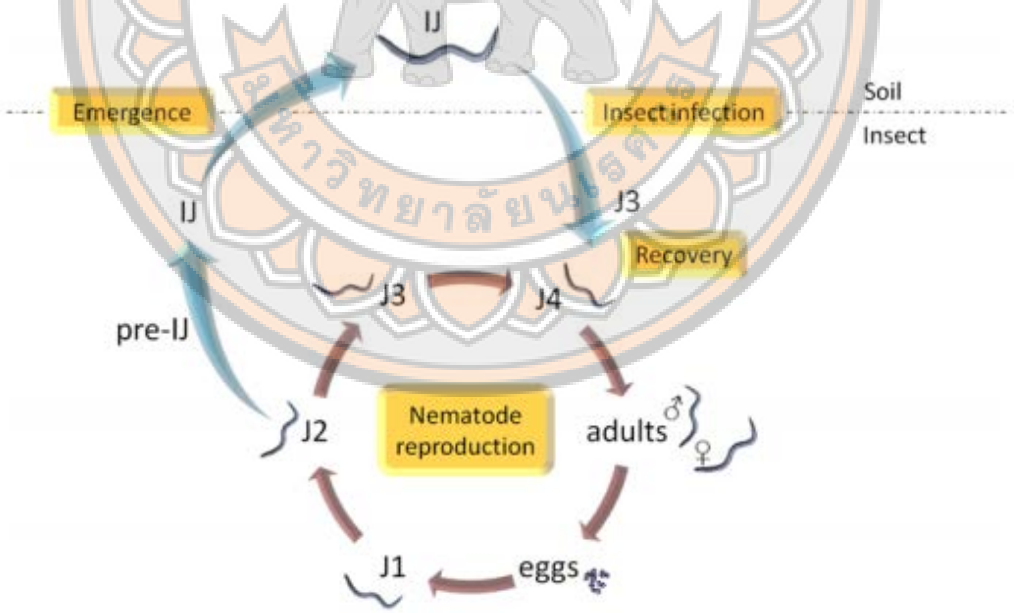

Figure 4 The Entomopathogenic nematodes (EPNs) life cycle.

The infective juvenile (IJ) nematodes infect a suitable insect host and develop into the fourth stage juvenile (J4), a developmental step that is known as recovery. During reproduction nematodes undergo four juvenile stages. The depletion of all nutrients leads to the development of IJs again, prompting the nematodes to leave the empty carcass.

Source: Reimer (2013)

4. Secondary metabolites from *Xenorhabdus* and *Photorhabdus* bacteria

In 1959, the first antibiotic activity in bacteria associated with *Steinernema* spp. was observed by Dutky, who noted that insect cadaver putrefaction was inhibited (Dutky, 1959). Later, Akhurst (Akhurst, 1980) discovered that *Xenorhabdus* existed in two or more identical phase variants with distinct colony morphologies, colors, and antimicrobial properties. The primary phase, which is carried out by the IJ nematode stages in nature, facilitates optimal nematode growth and antibiotic production. However, the primary phase can rapidly transition into a secondary phase, which supports less nematode growth and generates only a limited amount of antibiotic activity. The phase transition presented challenges for commercial nematode production, and its underlying cause remained uncertain until the discovery of a bacteriophage in *Heterorhabditis* that specifically targeted the primary phase. As a result, the shift to the secondary phase is believed to be a bacterial survival response. (Poinar et al., 1989; G. Poinar Jr et al., 1980). Since then, a variety of compounds produced by these bacteria has been extensively studied, resulting in the identification of various classes of compounds derived from non-ribosomal peptide synthetase (NRPS) and polyketide synthase (PKS). Many of these substances and their derivatives have shown efficacy against bacterial and fungal infections of medical and agricultural importance. To date, several classes of secondary metabolites, including antibacterial, antifungal, insecticidal, nematicidal, and cell-toxic agents, have been isolated from these bacterial genera (Figure 5 and Table 1).

Indole-derived metabolites from *Xenorhabdus,* such as xenocyloins, exhibit antibacterial, antifungal, and anti-insect activity. First reported in 1981 by Paul and colleagues, xenocyloins and related compounds, found in *Xenorhabdus* strains like *X.*

nematophila (Newman & Cragg, 2012) and *X. bovienii* (Li et al., 1995), shown antibacterial effects on various bacteria with thick and thin cell walls, by inhibiting RNA synthesis inducing the accumulation of guanosine-3',5'-bis-pyrophosphate, and also show antifungal activity. An additional promising group of indole derivatives from *Xenorhabdus*, known as nematophin, shows high activity against drug-resistant *Staphylococcus aureus* strains (Jianxiong, Genhui, & Webster, 1997; Li et al., 1997).

Phenethylamides synthesized by various strains of *Xenorhabdus* display cytotoxic activity against eukaryotic cells, including human cancer cell lines like gastric adenocarcinoma and hepatoblastoma. This cytotoxicity is mediated through apoptosis induced by caspase activation, as well as against insect cells, depending on the acyl chain length (Proschak et al., 2011).

A notable group of compounds is the xenorhabdins, derived from NRPS, which feature a distinct heterobicyclic pyrrolinonodithiole core, characteristic of dithiolopyrrolone antibiotics. These dithiolopyrrolones exhibit activity against both Gram-positive and Gram-negative pathogens, consisting of multiple drug resistance (MDR) *S. aureus* (Li et al., 2014; B. Li et al., 2015),, and are believed to inhibit RNA polymerase. Xenorhabdins include holomycin and thiolutin, antibiotics discovered in *Streptomyces* spp. (Celmer & Solomons, 1955; Ettlinger et al., 1959). The xenorhabdins represent both the N-acylpyrrothine (holomycin-type) and the Nmethyl, N-acylpyrrothine (thiolutin-type) subclasses of dithiolopyrrolone antibiotics with structural diversity generated by different chain lengths of the N-acyl substituent (Zhai et al., 2016). Oxidized derivatives of xenorhabdins, known as xenorxides, have also been identified. However, their high toxicity against mammalian cells limits their therapeutic potential in their current form (Bode et al., 2015).

A distinct phenotypic feature of *Xenorhabdus szentirmaii* is its purple metallic color, attributed to the phenazine pigment iodinin. However, the primary compounds produced by *X. szentirmaii* are xenofuranones, which resemble fungal furanones from *Aspergillus terreus* and exhibit weak cytotoxic activity (Brachmann et al., 2006). Additionally, hexadepsipeptides such as szentiamide and xenobactin have been found in *Xenorhabdus* strains, showing antiprotozoal activity against *Plasmodium falciparum*, the malaria-causing pathogen (Nollmann et al., 2012).

The major class of secondary metabolites in *Xenorhabdus* spp. appears to be nonribosomally produced compounds. For example, xenematides from *X. nematophila* are antibacterial against Gram-positive and Gram-negative bacteria and exhibit moderate insecticidal activity. The biosynthesis of xenematides is significantly enhanced under cultivation conditions with an abundance of L-proline (Lang et al., 2008).

A highly diverse class of cyclic depsipeptides identified in *Xenorhabdus* sp. is xentrivalpeptides A–Q, again having alternative structural variants that arise through promiscuity of the NRPS A domain (Zhou et al., 2012). The lysine-rich cyclo PAX-peptides of *X. nematophila* confer antifungal and antibacterial activity (Fuchs et al., 2011). Two linear hexapeptides (bicornutin) were identified from *X. budapestensis* with activity against the plant pathogens *Erwinia amylovora* and *Phytophthora nicotianae* (Böszörményi et al., 2009).

Another remarkably diverse group of cyclic depsipeptides discovered in *Xenorhabdus* includes xentrivalpeptides A–Q, which vary structurally due to the promiscuity of the NRPS A domain (Zhou et al., 2012). Lysine-rich cyclo-PAX peptides from *X. nematophila* have antifungal and antibacterial properties (Fuchs et al., 2011). *X. budapestensis* produces two linear hexapeptides (bicornutin), which are active against plant pathogens like *Erwinia amylovora* and *Phytophthora nicotianae* (Böszörményi et al., 2009).

Xenorhabdus strains also produce mixed peptide–polyketide metabolites with antimicrobial properties, such as xenocoumacins, which have broad antibacterial activity against Gram-positive bacteria and possess antiulcer properties (McInerney et al., 1991). A hybrid PKS/NRPS compound, fabclavine Ia, produced in *X. nematophila*, is a peptide–polyketide complex with extensive biological effects, similar to compounds described in *Serratia* strains (Fuchs et al., 2014).

X. nematophila and *P. luminescens* produce rhabdusin, an isocyanide- and aminoglycosyl-functionalized tyrosine derivative. It serves as a suppressor of phenoloxidase, a key enzyme in the insect immune system's melanization pathway (Crawford et al., 2012).

In *P. luminescens*, a carbapenem-backbone gene cluster has been identified (Derzelle et al., 2002). Carbapenems are β-lactam antibiotics known from other organisms like *Streptomyces* and *Erwinia* species. In *Photorhabdus*, carbapenem production is not controlled by quorum sensing (QS), unlike in *Erwinia* and *Serratia*, due to the absence of the QS protein CarR. *P. luminescens* also produces photobactin, a catechol siderophore that may contribute to antibiosis by sequestering iron in the insect cadaver (Ciche et al., 2003).

Another significant metabolite class unique to *Photorhabdus* is the anthraquinone pigments. Although anthraquinones are typically plant-produced and show weak antibiotic activity in *P. luminescens*, they are nonetheless noteworthy (Richardson et al., 1988).

Stilbenes, common plant metabolites, have been identified in all *Photorhabdus* spp. Isopropylstilbene and ethylstilbene exhibit antimicrobial activity and play a role in virulence and mutualism by signaling food recovery in the nematode (Joyce et al., 2008; Joyce et al., 2011). Epoxystilbene, which shows antibacterial activity against drug-resistant *S. aureus*, also exhibits cytotoxicity against three human cancer cell lines (Hu et al., 2006). Recently, additional stilbene derivatives, such as dihydroisopropylstilbene, were identified and shown to protect against oxidative stress in insect hemolymph (Crawford et al., 2011; Kontnik et al., 2010).

P. luminescens also produces non-ribosomal peptides like the cyclic GameXPeptides and linear mevalagmapeptide. The cyclic GameXPeptides A - D are synthesized under normal growth conditions, while peptides E - H are induced by the insect environment (Nollmann et al., 2015).

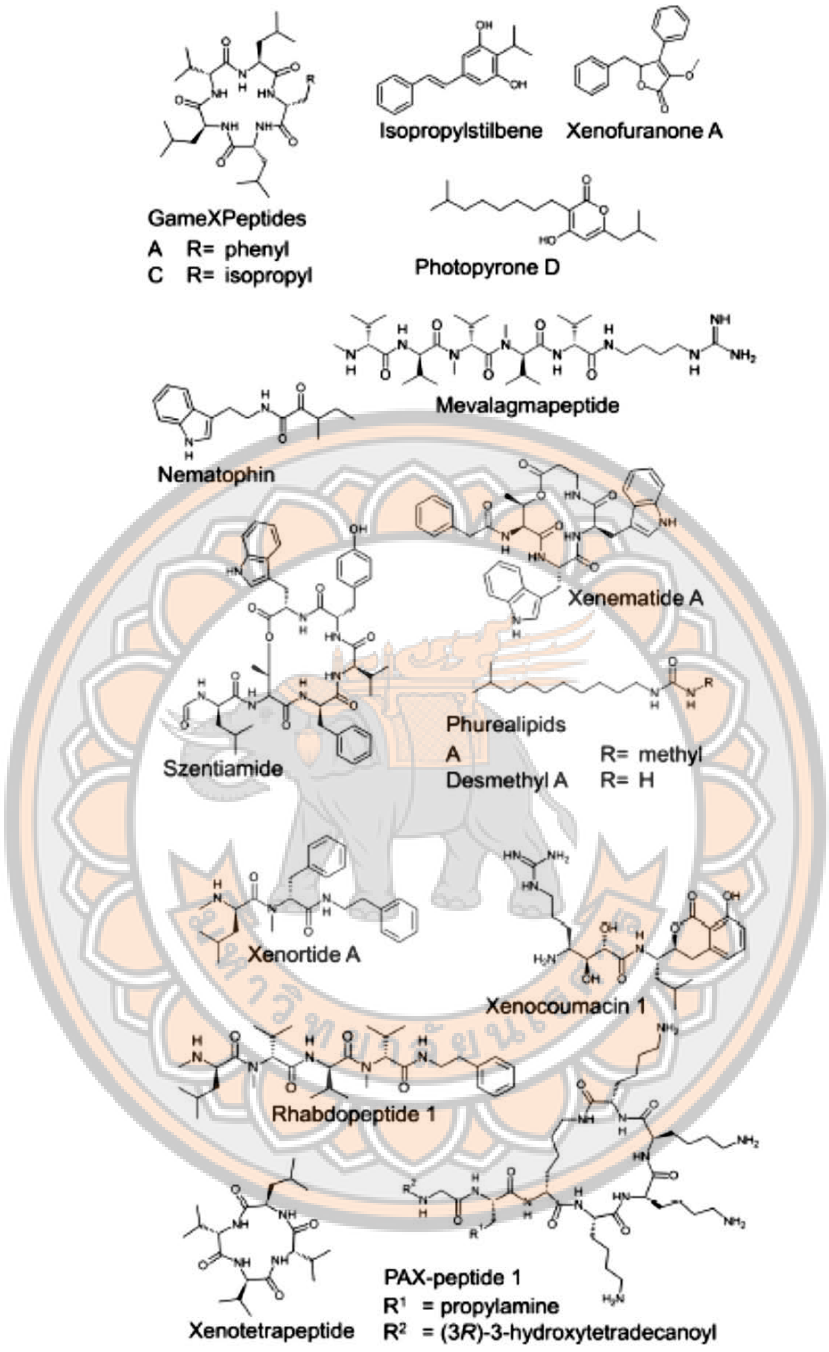

Figure 5 Examples of natural products from *Xenorhabdus* and *Photorhabdus* Bacteria

Source: Engel et al., 2017

Table 1 Secondary metabolites from *Xenorhabdus* and *Photorhabdus* bacteria and their biological activities

Secondary metabolites		Activity	Target organism	Bacteria	References
Glidobactin /Cepafungin I		Cytotoxicity against the human colon carcinoma HCT-116 cell line	HCT-116 cell line	*Photorhabdus* sp.	(Dudnik et al., 2013; Stein et al., 2012; Theodore et al., 2012)
Indigoidine		Blue pigment	None	*Photorhabdus* sp.	(Brachmann et al., 2012)
Indole and its derivatives	Indole	Nematocidal	*Caenorhabditis elegans, Meloidogyne incognita, Bursaphelenchus xylophilus,* and *B. mucronatu*	*Photorhabdus* sp.	(Hu et al., 1998)
	Xenocyloins	Insecticidal	Insects	*Xenorhabdus* sp.	(Lang et al., 2008)
	Nematophin	Antimicrobial	MDR *S. aureus*	*Xenorhabdus* sp.	(Li et al., 1997; Webster et al., 2002)
	Tryptamide and Rhabduscin	Cytotoxic activity	Eukaryotic cells	*Xenorhabdus* sp.	(Proschak et al., 2011)
	Rhabduscin	Insecticidal	Nanomolar-level inhibitor of phenoloxidase, a key component of the insect's innate immune system	*Photorhabdus* sp.	(Crawford et al., 2012)

Table 1 (Cont.)

Secondary metabolites		Activity	Target organism	Bacteria	References
Kollisin A		Unknown	Unknown	*Photorhabdus* sp.	(Bode et al., 2015)
Lumizinone A		Cytotoxic	Human plasma	*Photorhabdus* sp.	(Park & Crawford, 2015)
Phurealipids		Unknown	None	*Photorhabdus* sp.	(Nollmann et al., 2015)
Probactin		Antibiotic	None	*Photorhabdus* sp.	(Ciche et al., 2003)
Pyrone		Antimycotic, Cytotoxic	None	*Photorhabdus* sp.	(Brachmann et al., 2013)
Stilbene and its derivatives	3,5-Dihydroxy-4-isopropyl stilbene (syn. 2-isopropyl-5-[(E) - 2-phenylethenyl] benzene-1,3-diol)	Nematicidal	*C. elegans, B. xylophilus, B. mucronatus*, and *Aphelenchoides rhytium*	*Photorhabdus* sp.	(Chen, 1996; Hu et al., 1996; Paul et al., 1981; Shi et al., 2012)
		Antibacterial	*B. subtilis*		
		Antimycotic	*Aspergillus flavus, A. fumigatus, Candida tropicales, Cryptococcus neoformans, Botrytis cinerea, Pythium aphanidermatum, Exserohilum turcicum,* *R. solani,* and *Fusarium oxysporum*		

Table 1 (Cont.)

Secondary metabolites		Activity	Target organism	Bacteria	References
Stilbene and its derivatives	3-hydroxy-2- isopropyl-5-phenethyl phenyl carbamate	Insecticidal potential Antimycotic	*P. aphanidermatum*, *R. solani, E. turcicum*		
	2-isopropyl-5-(3-phenyl-2-oxiranyl) -benzene-1,3-diol (syn. 2-Isopropyl-5- (3-phenyl-2-oxiranyl)-1,3-benzenediol)	Antibacterial	*B. subtilis, E. coli, Streptococcus pyogenes*, and *Staphylococcus aureus*	*Photorhabdus* sp.	(Hu et al., 2006)
Pyrrothine	Xenorhabdins Xenorxides	Antibacterial Antifungal Insecticidal Inhibition of RNA polymerase. Note: Sub-classes of dithiolopyrrolone antibiotics	high toxicity against mammalian cells	*Xenorhabdus* sp.	(Bode et al., 2015; Qin et al., 2013) (Li et al., 1995)

Table 1 (Cont.)

Secondary metabolites		Activity	Target organism	Bacteria	References
Xenocoumacins		Antimicrobial	*Micrococcus luteus*	*Xenorhabdus* sp.	(McInerney et al., 1991; Park et al., 2009; Reimer et al., 2009)
Hydroxystil-benes	Isopropyl stilbene	Antibacterial (Inhibition of RNA synthesis)	Gram-positive and Gram-negative pathogens,	*P. luminescens*	(Paul et al., 1981; Proschak et al., 2014; Richardson et al., 1988)
		Antifungal	*A. flavus, A. fumigatus, Botrytis cinere, Candida tropicales and Cryptococcus neoformans*		(Li et al., 1995)
		Nematicidal	*Aphelenchoides rhytium, Bursaphelenchus* spp. and *Caenorhabditis elegans*		(Webster et al., 1999)

Table 1 (Cont.)

Secondary metabolites		Activity	Target organism	Bacteria	References
Cyclic hexadepsipeptide	Szentiamide Xenobactin	Antiprotozoal	*P. falciparum*	*X. szentirmai*	(Nollmann et al., 2012) (Ohlendorf et al., 2011) (Grundmann et al., 2013)
Xenematides		Antiprotozoal	*P. falciparum*	*X. nematophilus*	(Crawford et al., 2011; Lang et al., 2008)
Xentrivalpeptides A–Q		Unknown	None	*Xenorhabdus* sp.	(Zhou et al., 2012).
Xenoamicins	Xenoamicin A	Antiprotozoal	*P. falciparum* and *Trypanosoma brucei*	*X. doucetiae*	(Bode et al., 2015; Zhou et al., 2013)
Lysine-rich PAX	PAX 1–5	Antifungal pathogen	*Fusarium oxysporum*	*X. nematophilus*	(Gualtieri et al., 2009)
Rhabdopeptides 1-6	Rhabdopeptide 1 Rhabdopeptide 7–8	Unknown	None	*X. nematophila* *X. cabanillasii*	(Reimer et al., 2013)
Bicornutin A		Antibacterial and cytotoxic	Broad-spectrum	*X. budapestensis*	(Böszörményi et al., 2009)

Table 1 (Cont.)

Secondary metabolites	Activity	Target organism	Bacteria	References
Mevalagma-peptides A and B	Unknown Note: *cpm*A–H involved in the biosynthesis of carbapenem-like antibiotics	None	*P. luminescens*	(Derzelle et al., 2002)
Trans-cinnamic acid	Antimycotic	*Fusicladium effusum*	*Photorhabdus* sp.	(Bock et al., 2014)
Fabclavines	Biological activity	Broad-spectrum	*Photorhabdus* sp.	(Fuchs et al., 2014)
Darobactin	Antibacterial (The addition of darobactin to *E. coli* resulted in membrane blebbing, followed by cell swelling and eventual lysis. Within 15–30 minutes, darobactin rapidly triggered the sigma E and Rcs envelope stress responses and broadly activated genes across all five envelope stress pathways.	drug resistant Gram-negative pathogens (e.g., *E. coli*, *P. aeruginosa*, *A. baumannii* ATCC 17978, *K. pneumoniae*, and *S. aureus* HG003)	*P. khanii*	(Imai et al., 2019)

5. Regulation of secondary metabolite biosynthesis in *Xenorhabdus* and *Photorhabdus* bacteria

The ability of *Xenorhabdus* and *Photorhabdus* to adapt to environmental changes plays a crucial role in microbial interaction with hosts and the regulation between mutualism and pathogenesis, particularly in the context of secondary metabolite biosynthesis. The sequencing of several *Xenorhabdus* and *Photorhabdus* strain genomes has greatly facilitated the identification of novel compound classes. Detailed genomic studies have revealed numerous biosynthetic gene clusters involved in secondary metabolite production. For instance, 7.5% of the genome of *Xenorhabdus nematophila* ATCC 19061 and 5.9% of the genome of *Photorhabdus luminescens* TT01 are dedicated to proteins involved in secondary metabolite biosynthesis (Chaston et al., 2011; Duchaud et al., 2003).

One key player in regulating these processes is the global regulator Lrp or leucine-responsive regulatory protein which is widely present in bacteria and acts as a sensor for several amino acids, thus linking it to nutrient availability responses (Brinkman et al., 2003; Hart & Blumenthal, 2011). In *Salmonella enterica*, Lrp weakens *Salmonella* virulence by repressing genes within pathogenicity islands 1 and 2 (SPI-1 and SPI-2) (Baek et al., 2009), while in *Vibrio* species, Lrp has been demonstrated to play a key role in virulence (Lin et al., 2007). In *X. nematophila*, Lrp functions as a global regulator, influencing both symbiotic relationship with nematodes and pathogenicity in insects (Cowles et al., 2007; Hussa et al., 2015). Studies have shown that a *lrp* deletion mutant of *X. nematophila* loses antibiotic activity against *Micrococcus luteus* and *Bacillus subtilis*, unlike the wild-type strain, which retains antibiotic activity (Cowles, 2007). Similarly, in *Photorhabdus*, *lrp* mutant exhibits reduced levels of isopropylstilbene (IPS) and its precursor, cinnamic acid (Lango-Scholey et al., 2013).

Lrp is also involved in pathogenesis by modulating the expression of the transcriptional regulator LrhA (LysR homologue A), which controls l-proline uptake. Mutants lacking LrhA exhibit a significant reduction in insect-killing ability, highlighting LrhA as a critical virulence factor factors (Herbert & Goodrich-Blair, 2007; Richards et al., 2008). This is because l-proline is a prevalent amino acid composition of insect hemolymph. Therefore, increased levels of l-proline could

stimulate the production of insecticidal compounds, such as stilbene, and anthraquinone (AQ) in *Xenorhabdus* and *Photorhabdus*, respectively. This phenotype depends on proline uptake, there is evidence suggesting that proline plays a key role in regulating secondary metabolite production (Crawford et al., 2010). However, global regulators control the secondary metabolite biosynthesis of *Xenorhabdus* remains largely unexplored.

In *Photorhabdus* strains, HexA is a transcriptional inhibitor of the LysR-type family. It is essential for the interaction with the nematode in *P. temperata*, as it inhibits antibiotic production (Joyce & Clarke, 2003). Kontnik in 2010 demonstrated that Δ*hexA* mutants of *P. temperata* and *P. luminescens* produce significantly higher levels of isopropylstilbene (IPS) and its derivatives (Kontnik et al., 2010b). More recently, it has been found that *hexA* functions within a regulatory cascade regulated by the Hfq protein. Deletion of *hexA* leads to restored secondary metabolite production, whereas a Δ*hfq* mutant exhibits minimal secondary metabolite production (Tobias et al., 2016).

The BarA-UvrY two-component system (2CP) triggers gene transcription that associated with secondary metabolism in *Photorhabdus*. A *uvrY* knockout mutant in *P. luminescens* exhibited a substantial reduction in the expression of genes that essential for bioluminescence, as well as stilbene and anthraquinone (AQ) biosynthesis. However, the majority of the transcriptional modifications observed in the *uvrY* mutant did not align with protein or phenotypic changes, indicating that the regulation belonging to these genes may occur at the post-transcriptional level (Kontnik et al., 2010; Krin et al., 2008; Lango-Scholey et al., 2013). In other bacteria, the 2CP system has been established to interact with small RNA regulators. A notable target of the system is the CsrA-CsrB regulatory (Pernestig et al., 2003; Weilbacher et al., 2003). In this system, as illustrated in Figure 6, CsrA is an RNA-binding protein that inhibits protein synthesis by attaching to the ribosome-binding site of the target mRNA (Liu & Romeo, 1997). The CsrB RNA contains multiple binding sites for CsrA, and when expressed, it titrates CsrA away from target mRNAs, thereby facilitating more efficient translation of these transcripts (Babitzke & Romeo, 2007; Romeo, 1998).

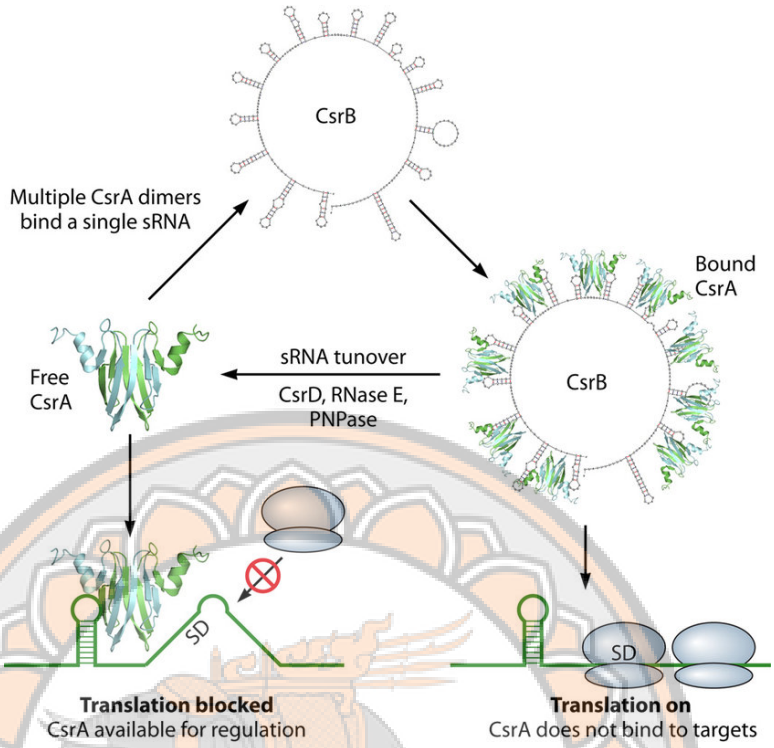

Figure 6 The regulation of bacterial virulence by Csr systems

Source: Vakulskas et al. (2015)

In *P. luminescens* TTO1, the CsrA-CsrB regulatory system has been found to regulate certain UvrY targets (Krin et al., 2008). The 2CP, also referred to as GacS-GacA in other bacteria like *Pseudomonas*, plays a crucial role in regulating secondary metabolism (Lapouge et al., 2008). Mutations in the GacS-GacA 2CP have been shown to block secondary metabolism in various pseudomonad species (Heeb & Haas, 2001). Recent studies have revealed that *gacS* mutations in *Pseudomonas aeruginosa* M18 cause variation in phenotype, leading to the development of small colony variants (SCVs) both *in vivo* and *in vitro* (Davies et al., 2007; Nelson et al., 2010). The GacS-GacA system also plays a role in the interaction among *Pseudomonas fluorescens* and the amoeba, *Dictyostelium discoideum*. Notably, many *D. discoideum* amoebae engage in bacterial husbandry, transporting and distributing bacteria during the spore stage to secure a food source after spore germination. Initially, *D. discoideum* carried two strains of *P. fluorescens*, but only one provided a food source (Brock et al., 2011). Moreover, the second strain was shown to produce secondary metabolites, including pyrrolnitrin

and chromene which promoted spore formation and benefited the amoeba. Interestingly, losing function in *gacA* altered the secondary metabolite-producing strain, turning it into a food source gene (Stallforth et al., 2013). This suggests that *gacA* mutations create functional heterogeneity within the *P. fluorescens* population. Similarly, *Photorhabdus* plays a role in mutualistic interactions with nematodes, acting both as a food source and regulating nematode development. Although no evidence exists of non-functional alleles of *uvrY* (the *gacA* homologue) arising and coexisting within insect cadavers, it is conceivable that the activity of the 2CP is regulated post-transcriptionally, leading to variation in function in the bacterial community (Camacho et al., 2015). Therefore, both the BarA-UvrY and GacS-GacA 2CPs play essential roles in regulating functional heterogeneity and secondary metabolism in various bacteria-host interactions.

Phenylalanine ammonia-lyase (PAL), the first enzyme in stilbene synthesis, converts phenylalanine into cinnamic acid (CA), highlighting the correlation between amino acid metabolism and secondary metabolism (Williams et al. 2005). It is well established throughout the Gammaproteobacteria, nutrient limitation triggers the production of (p)ppGpp, an alarmone that regulates gene expression during stress adaptation (Gaca, Colomer-Winter, et al., 2015; Hauryliuk et al., 2015). (p)ppGpp synthesis is controlled by the RelA and SpoT proteins. RelA activates (p)ppGpp synthesis in response to amino acid limitation, while SpoT integrates various signals into (p)ppGpp metabolism, with its hydrolysis activity necessary for upholding proper (p)ppGpp levels during growth (Brown et al., 2016). The accumulation of (p)ppGpp leads to significant transcriptional changes in bacteria (Bowden et al., 2013; Gaca, Kudrin, et al., 2015; Hesketh et al., 2007; Traxler et al., 2011; Vercruysse et al., 2011).

In *Photorhabdus*, a *relA spoT* double mutant, which cannot produce (p)ppGpp, was found to be unable to produce light, stilbene, or AQ pigments and could not support nematode growth. However, this mutant exhibited virulence comparable to the wild-type strain in insects, suggesting that (p)ppGpp production is not necessary for pathogenicity. Mutant of RelA spoT was quickly outcompeted by the wild-type strain after extended incubation in insects, highlighting the role of (p)ppGpp in nutrient-limited conditions (Bager et al., 2016). Similarly, a *relA spoT* mutant in *P. fluorescens*

CHAO displayed reduced antimicrobial and biocontrol effects, indicating that (p)ppGpp regulates secondary metabolism in this bacterium (Takeuchi et al., 2012).

Primary metabolism, including glycolysis and the TCA cycle, produces energy and precursors for cell growth, while secondary metabolism provides an alternative carbon and energy flux to produce bioactive compounds. This close relationship between primary and secondary metabolism is both regulatory and metabolic. In *P. luminescens* TTO1, mutations in the *mdh* or *fumC* genes, encoding key TCA cycle enzymes, blocked the production of light, stilbene antibiotics, and AQ pigments. These mutants were also unable to support nematode growth but did not affect virulence, suggesting that a metabolic switch between pathogenicity and mutualism is regulated by the TCA cycle (Lango & Clarke, 2010). A similar mutation in the *fumA* gene of *P. fluorescens* CHAO, encoding fumarase, which additionally suppressed secondary metabolism, indicating that TCA cycle imbalance impairs proper activation of the GacS-GacA 2CP (Takeuchi., 2009). Interestingly, A genetic modification in *acnB*, the gene encoding aconitase in *V. fischeri*, led to enhanced bioluminescence, which was regulated through the Gac/Rsm signaling pathway (Septer et al., 2015). Thus, the BarA-UvrY (GacS-GacA) 2CP acts as a regulatory connection between primary and secondary metabolism across various bacteria.

Numerous bacteria also use quorum sensing through AI-2, a signaling molecule produced by the LuxS enzyme, which plays a role in the activated methyl cycle. LuxS converts S-ribosylhomocysteine into AI-2, which accumulates extracellularly and induces transcriptional changes in some bacteria (Pereira et al., 2013). In *Photorhabdus*, AI-2 has been linked to carbapenem antibiotic production, as a *luxS* deletion mutant expressed greater amounts of *cpm* mRNA (Derzelle et al., 2002). The *luxS* mutant also exhibited decreased bioluminescence, increased polyamine production, heightened sensitivity to oxidative stress, reduced biofilm formation, and hyper-motility in comparison with the wild type (Krin et al., 2006). Furthermore, the BarA-UvrY 2CP in *Photorhabdus* is essential for maximal AI-2 production, and some phenotypes in the uvrY mutant, such as lowered bioluminescence, could be restored adding exogenous AI-2 (Krin et al., 2008). Thus, AI-2 plays multifunctional roles in *Photorhabdus*, linking secondary metabolism and stress resistance.

Particular secondary metabolic pathways in *Photorhabdus* remain underexplored. In bacteria, it is common for global regulators to work in conjunction with pathway-specific regulators to maintain the correct expression of secondary metabolites. For example, The AQ pigment is synthesized by proteins encoded by the 9-gene *antA-I* locus (Brachmann et al., 2007), and HdfR has been identified as a repressor of *antA-I* expression and AQ production (Easom & Clarke, 2012), Additionally, the induction of *stlA* expression during nutrient limitation facilitates stilbene production (Chalabaev et al., 2008).

In conclusion, *Photorhabdus* utilizes a sophisticated network to regulate secondary metabolism. In which global and specific regulators influence primary metabolism to coordinate the temporal regulation of secondary metabolite production (Figure 7). Secondary metabolites synthesized during the post-exponential phase of *Photorhabdus* growth are linked to its mutualistic relationship with the nematode. Nutrient limitation, mediated by the production of the alarmone (p)ppGpp, has been identified as a key environmental factor controlling secondary metabolism in *Photorhabdus*. The synthesis of (p)ppGpp acts as an intracellular signal that translates scarcity into a broad regulatory response. This response, whether directly or indirectly, involves various regulators that initiate the transition from pathogenicity to mutualism. Further elucidation of the regulatory networks involved is crucial for a more comprehension understanding of the three-way interaction between *Photorhabdus*, the nematode, and the insect prey.

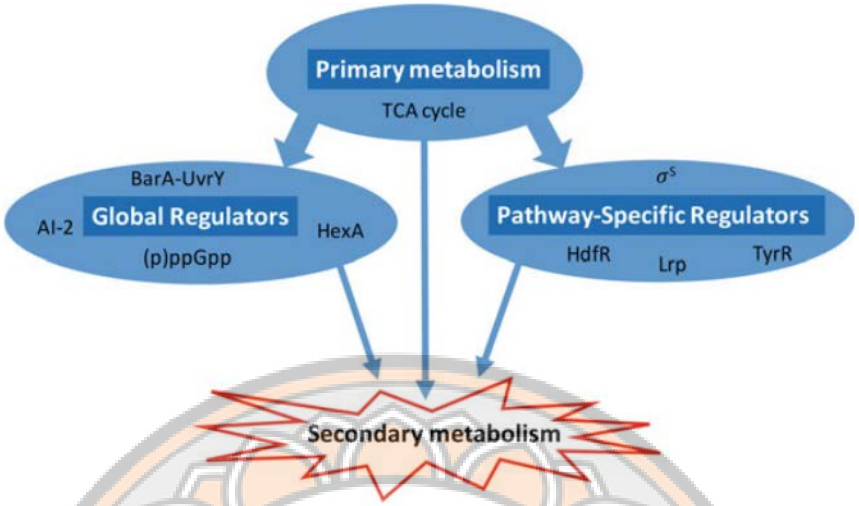

Figure 7 The regulatory network controlling secondary metabolism in *P. luminescens*

Source: Clarke (2016)

6. Genome sequencing of *Xenorhabdus* and *Photorhabdus* bacteria

Research into the genome sequencing of *Xenorhabdus* and *Photorhabdus* bacteria has significantly advanced our understanding of their biology, symbiotic relationships, and potential applications. The genomes of *Xenorhabdus* and *Photorhabdus* species are typically circular DNA molecules. For instance, *Xenorhabdus nematophila* ATCC 19061 has a genome size of approximately 4.43 million base pairs (Mb), while *Xenorhabdus bovienii* SS-2004 possesses a genome of about 4.23 Mb. Recent studies have reported genome sizes for various *Xenorhabdus* strains ranging from 4.07 to 4.94 Mb, with a GC content between 42.8% and 45.4% (Chaston et al., 2011; Palma et al., 2024). In comparison, the genome of *Photorhabdus luminescens* TT01 is approximately 5.7 Mb in size. This larger genome reflects the bacterium's extensive repertoire of genes dedicated to secondary metabolism and symbiotic functions (Tobias et al., 2016).

The complete genome sequence of *Photorhabdus luminescens* TT01, published in 2003, revealed that up to 6% of its genome is dedicated to secondary metabolism, underscoring its capacity to produce a diverse array of bioactive compounds (Sajnaga et al., 2024). Building upon this foundational knowledge, recent

studies have developed advanced genetic tools to facilitate the manipulation of these bacteria. For instance, researchers have created expression vectors and a CRISPR-Cpf1 genome editing system based on the Standard European Vector Architecture (SEVA) plasmids. These tools enable efficient genetic modifications, including the activation and refactoring of biosynthetic gene clusters to enhance the production of valuable compounds like safracin B, a precursor for the anti-cancer drug ET-743 (Rill et al., 2024).

Moreover, investigations into the phylogenetic diversity of *Xenorhabdus* and *Photorhabdus* species have been conducted worldwide. In Thailand, researchers isolated and identified various strains of these bacteria from entomopathogenic nematodes, utilizing *recA* gene sequencing and phylogenetic analyses. The study revealed multiple isolates closely related to *X. stockiae*, *X. miraniensis*, and different subspecies of *P. luminescens*(Fukruksa et al., 2017). Such studies are crucial for understanding the distribution and evolutionary relationships of these bacteria. In addition, the mutualistic relationship between these bacteria and their nematode hosts plays a vital role in their life cycles and pathogenicity. *Xenorhabdus* and *Photorhabdus* species assist nematodes in infecting and killing insect hosts, making them effective biological control agents against agricultural pests. Advancements in genomic tools have transformed the systematics of these organisms, reshaping our understanding of their phylogenetic relationships and co-evolution (Půža & Machado, 2024). Recent studies have characterized novel isolates of these bacteria. For example, two isolates from northwestern Iran were identified as *Photorhabdus thracensis* and *Xenorhabdus nematophila*. Molecular techniques, including phylogenetic analysis of 16S rDNA and *gyrB* sequences, were employed for identification. These studies also examined growth dynamics, virulence, and antibacterial susceptibility, contributing to a deeper understanding of their potential applications in pest control and medicine (Azar et al., 2025).

In summary, genome sequencing and related studies of *Xenorhabdus* and *Photorhabdus* bacteria have provided profound insights into their genetic makeup, symbiotic mechanisms, and practical applications. Ongoing research continues to explore their diversity, evolutionary biology, and potential in biotechnology and agriculture.

Antibiotic resistant bacteria

Antimicrobial resistance (AMR) occurs when microorganisms are exposed to antimicrobial agents and evolve resistance. These resistant microorganisms, often referred to as “superbugs,” render treatments ineffective, causing infections to persist in the body and increasing the risk of transmission to others. AMR poses an escalating global public health threat, requiring coordinated action across all sectors of society and government. In the absence of potent antimicrobial agents for infection prevention and therapy, as well as medical interventions like organ transplantation, chemotherapy, diabetes management, and major surgical procedures (e.g., caesarean sections or hip replacements) become considerably more risky. Patients with resistant infections face greater costs than those with treatable infections, primarily owing to prolonged durations of illness, the need for additional diagnostic tests, and the use of more expensive medications.

In 2016, around 490,000 individuals worldwide contracted multi-drug-resistant tuberculosis (TB), with drug resistance increasingly complicating the treatment of HIV and malaria (World Health Organization, 2020). To address this issue, the World Health Organization (WHO) has issued a list of high-priority antibiotic-resistant pathogens – 12 families of bacteria posing the significant threat to human health. This list is categorized into three groups based on the urgency for new antibiotics: critical, high, and medium priority (Tacconelli et al., 2017). The most critical group includes multidrug-resistant bacteria, which are a particular risk in hospitals, nursing homes, and for patients requiring medical devices like ventilators and blood catheters. These include *Acinetobacter*, *Pseudomonas*, and various Enterobacteriaceae (such as *Klebsiella*, *Escherichia coli*, *Enterobacter*, *Serratia*, *Proteus*, *Providencia*, and *Morganella* species). These bacteria are responsible for severe, often fatal infections such as septicemia and pneumonia, with resistance to multiple antibiotics, including carbapenems and third-generation cephalosporins — critical treatments for multi-drug-resistant infections. The high and intermediate priority groups include additional bacteria with growing resistance responsible for widespread diseases, including *Gonorrhoea* and *Salmonella*-induced food poisoning (Table 2).

Table 2 WHO priority pathogens list for research and development (R&D) of new antibiotics

Priority	Bacteria	Antibiotics
CRITICAL	*Acinetobacter baumannii*	carbapenem-resistant
	Pseudomonas aeruginosa	carbapenem-resistant
	Enterobacteriaceae	ESBL-producing
HIGH	*Enterococcus faecium*	vancomycin-resistant
	Staphylococcus aureus	methicillin-resistant, vancomycin-intermediate, and resistant
	Helicobacter pylori	clarithromycin-resistant
	Campylobacter spp.	fluoroquinolone-resistant
	Salmonella spp.	fluoroquinolone-resistant
	Neisseria gonorrhoeae	cephalosporin-resistant, fluoroquinolone-resistant
MEDIUM	*Streptococcus pneumoniae*	penicillin-non-susceptible
	Haemophilus influenzae	ampicillin-resistant
	Shigella spp.	fluoroquinolone-resistant

Tuberculosis, which has increasingly developed resistance to traditional treatments in recent years were excluded from the list as they are already recognized as a global priority, with urgent need for innovative new treatments. Other bacteria, such as *Streptococcus* A and B and *Chlamydia* spp., were also excluded from the list due to their limited resistance to current treatments and because they do not present a major public health risk at this time (Tacconelli et al., 2017).

1. *Acinetobacter baumannii*

Acinetobacter spp. are Gram-negative coccobacilli, aerobic, glucose-non-fermentative, non-motile, non-fastidious, catalase-positive, and oxidase-negative. Within *Acinetobacter* spp., *A. baumannii* stands out as the most critical pathogen linked to hospital-acquired infections worldwide. Additionally, there has been a gradual increase in community-acquired *A. baumannii* infections (Lin & Lan, 2014). Genomic

and phenotypic studies have identified several virulence factors, such as outer membrane porins, phospholipases, proteases, lipopolysaccharides (LPS), capsular polysaccharides, protein secretion systems, and iron-chelating systems (Antunes et al., 2011; Lin & Lan, 2014; McConnell et al., 2013).

Several studies have indicated that *A. baumannii* rapidly develops resistance to antimicrobials, with strains resistant to multiple drugs being isolated (McConnell et al., 2013). The WHO has notified that *A. baumannii* is one of the most serious infections in ESKAPE group (*E, faecium, S. aureus, K. pneumoniae, A. baumannii, P. aeruginosa,* and *Enterobacter* spp.), known for its ability to evade the effects of antibacterial drugs. *A. baumannii* employs various resistance mechanisms, including enzymatic drug degradation, target site alterations, multidrug efflux pumps, and reduced membrane permeability (Gordon & Wareham, 2010; Kim et al., 2012; Lin & Lan, 2014). The remarkable adaptive ability of *A. baumannii*, along with the acquisition and transmission of antibiotic resistance factors, undermines the effectiveness of the latest therapeutic approaches, including last-resort and combination antibiotic therapies. A summary data from Lee and his co-workers, shows the virulence factors, mechanisms of antibiotic resistance, and the treatment preferences for *A. baumannii* infections (Figure 8).

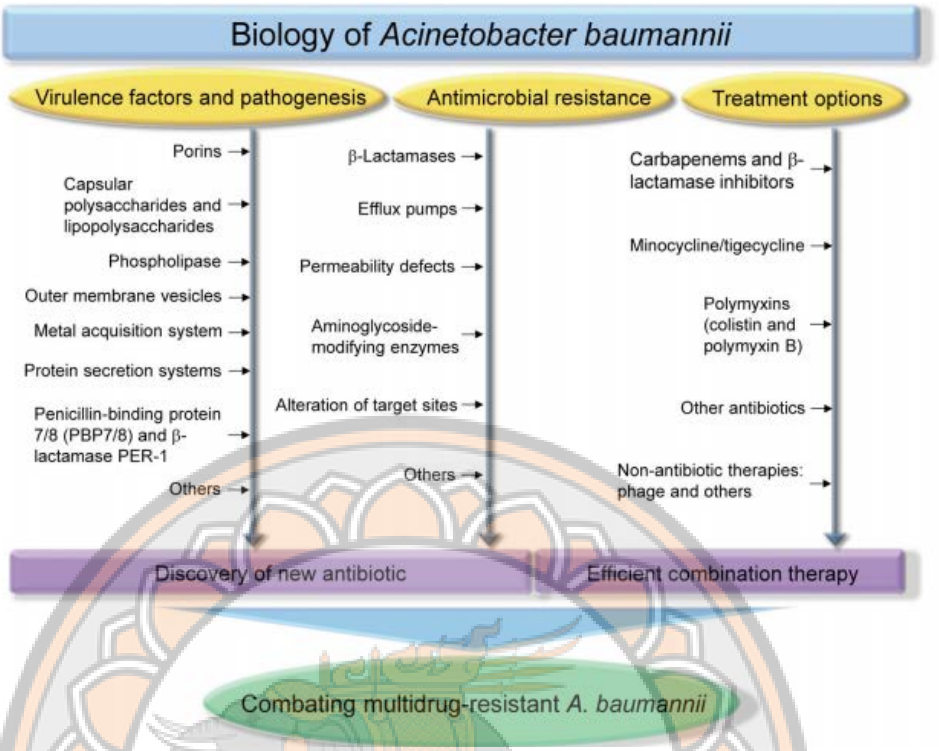

Figure 8 Biology of *Acinetobacter baumannii*

Source: Lee et al. (2017)

1.1 Virulence factors and pathogenesis of *Acinetobacter baumannii*

There are several virulence factors of *A. baumannii* have been described for its pathogenicity. The major virulence factors discovered through genomic and phenotypic analysis are outer membrane porins, phospholipases, capsular polysaccharides, lipopolysaccharides (LPS), proteases, iron-chelating systems, and protein secretion systems. Summary of *A. baumannii* virulence factors are concluded in Table 3.

Table 3 The key virulence factors of *Acinetobacter baumannii*

Virulence factors	Proposed role in pathogenesis	References
Outer membrane proteins	Adherence and invasion, serum resistance, biofilm formation, surface motility, and induction of apoptosis in host cells or causes cytotoxicity	(Choi et al., 2005; Fernández-Cuenca et al., 2011; Gaddy et al., 2009; Huang et al., 2016; Kim et al., 2009; Lee et al., 2010; Rumbo et al., 2014; Smani et al., 2013; Smani et al., 2012; Wang et al., 2014)
Capsule	Peptide resistance, mediates cationic antimicrobial, serum resistance and *in vivo* survival	(Antunes et al., 2011; Geisinger & Isberg, 2015; Iwashkiw et al., 2012; Lees-Miller et al., 2013; Russo et al., 2010)
Biofilm-associated protein (Bap)	Biofilm development and cell-to-cell adhesion	(Loehfelm et al., 2008)
Lipopolysaccharide (LPS)	Evasion of the host immune response, resistance to cationic antimicrobial peptides, activation of the host inflammatory response, reduction of TLR4 signalling, and enhanced survival under desiccation conditions.	(Lin et al., 2012; Luke et al., 2010; McConnell et al., 2013; McQueary et al., 2012)
Phospholipase - PLD -PLC	Serum resistance, *in vivo* survival, and dissemination of bacteria Exhibiting hemolytic activity against human red blood cells and facilitating the uptake of iron	(Camarena et al., 2010; Fiester et al., 2016; Jacobs et al., 2010; Stahl et al., 2015)

Table 3 (Cont.)

Virulence factors	Proposed role in pathogenesis	References
Outer membrane vesicle (OMV)	Delivering virulence genes to the host cell cytoplasm and facilitating the horizontal transfer of antibiotic resistance genes between bacterial cells.	(Jin et al., 2011; Jun et al., 2013; Kwon et al., 2009; Z. T. Li et al., 2015; Moon et al., 2012; Rumbo et al., 2011)
Acinetobactin (Siderophore mediated iron acquisition mechanism)	Provides iron for the survival of both the bacterium and the host, while also inducing cell death.	(Ali et al., 2017; Fiester et al., 2016; Gaddy et al., 2012; Penwell et al., 2012; Zimbler et al., 2012) (Hood et al., 2012; Nairn et al., 2016) -Zn (Juttukonda et al., 2016) -Mg
Penicillin-binding protein 7/8 (pbpG) and β-lactamase PER-1	Biosynthesis of peptidoglycan, cellular stability, and growth in serum	(Russo et al., 2009; Sechi et al., 2004)
Poly-β-1-6-N-Acetylglucosamine (PNAG)	Formation of biofilm, cell-cell adherence, and protection against innate host defenses	(Choi et al., 2008)
AbaI autoinducer synthase	Biofilm development	(Niu et al., 2008)
CsuA/BABCDE chaperone usher pili assembly system	Pilus assembly, biofilm formation on abiotic surfaces	(Tomaras et al., 2003; Tomaras et al., 2008)
Type II protein secretion system	*In vivo* survival	(Elhosseiny et al., 2016; Harding et al., 2016; Johnson et al., 2016)
Type VI protein secretion system	Killing of competing bacteria, host colonization	(Carruthers et al., 2013; Jones et al., 2015; Repizo et al., 2015; Ruiz et al., 2015; Wright et al., 2014)
Type V protein secretion system	Biofilm formation and adherence	(Bentancor et al., 2012)

1.1.1 Outer membrane proteins and outer membrane vesicles

Outer membrane proteins (Omps), located in the outer membrane, are essential core components that regulate both cell membrane permeability and virulence in *A. baumannii*. These β-barrel porins, which can exist as monomers or trimers, link the external environment to the periplasm, facilitating the transport of nutrients, small molecules, antibiotics, and disinfectants (Ambrosi et al., 2017; Ayoub Moubareck & Hammoudi Halat, 2020; Harding et al., 2018; Srinivasan et al., 2015; Uppalapati et al., 2020). To date, identified Omps in *A. baumannii* are OmpA, OmpW, Omp33-36 kDa, AbuO, CarO, OprD-like, TolB, NmRmpM, DcaP, LptD, Oma87/BamA, CadF, and OprF (Ayoub Moubareck & Hammoudi Halat, 2020; Harding et al., 2018; Uppalapati et al., 2020). The main outer membrane protein OmpA is one of the most abundant porins in *A. baumannii*. This 38kDa protein is involved in cell invasion and apoptosis, also small solute penetration occurs as it binds to the host cell surface, becomes localized in both the mitochondria and nuclei, and triggers cell death (Choi et al., 2005). OmpA is a thoroughly studied virulence factor with a range of intriguing biological characteristics (McConnell et al., 2013; Smith et al., 2007). In a previous report investigating the ability of *A. baumannii* to penetrate epithelial membranes in a murine pneumonia model, prominent lung histopathological changes, including a large quantity of white blood cells and alveolar damage, were detected in mice infected with the wild-type strain, but not in those infected with OmpA-mutants (Choi et al., 2008). In addition to its role as a porin for transport, OmpA can induce host cell apoptosis, promote biofilm formation, enable dissemination into the bloodstream, and interact with epithelial cells, mainly through host fibronectin (Smani et al., 2012). A additional outer membrane protein of *A. baumannii* is Omp33, also known as Omp33-36 kDa or Omp34, which functions as a water channel and associated with carbapenem resistance (Smani et al., 2013). In Rumbo study, this protein induced apoptosis by inhibiting autophagy, which allowed for intracellular persistence and led to the development of cytotoxicity (Rumbo et al., 2014). Moreover, knockout strains of *A. baumannii* lacking Omp33 exhibited reduced growth rates and a marked decline in their ability to adhere, invade, and induce cytotoxicity, indicating that Omp33 is essential for the survival and virulence of *A. baumannii* (Smani et al., 2013). Other porins, such as carbapenem associated outer membrane protein (CarO) and OccAB1

(OprD or porinD), are considered a virulence factor contributing to diminished virulence in a mouse model (Fernández-Cuenca et al., 2011). Moreover, OccAB1 together with OmpW were found linked to iron uptake in *A. baumannii* (Catel-Ferreira et al., 2016). OmpW is an outer membrane β-barrel protein which has many similar characteristics with OmpA, highly cytotoxic against the host cells, immunogenic, greatly concentrated in outer membrane vesicles (OMVs) (Catel-Ferreira et al., 2016; Huang et al., 2015; Tiku et al., 2021). OMVs are 20-200 nm micro-spherical vesicles secreted through the secretory system, apart from conventional systems (Ahmadi Badi et al., 2017). These vesicles can be composed of Omps, LOS, phospholipids, DNA and RNA molecules, as well as periplasmic proteins. OMVs are generally secreted and play a role in the delivery of virulence factors targeting other bacteria or host cells leading host cell injury and innate immune reactions (Geisinger et al., 2019; Li et al., 2018; Morris et al., 2019; Pires & Parker, 2019; Tiku et al., 2021).

1.1.2 Capsule and lipopolysaccharides (LPS)

Besides OmpA, *A. baumannii* envelope is also associated with the pathogenicity. The cell wall polysaccharide (LPS) is a key virulence factor involved in various stages of the disease process. It plays a crucial role in resisting normal human serum and offers a survival advantage *in vivo*. Additionally, in animal models, it may induce a proinflammatory response (Knapp et al., 2006). The antigenic O-polysaccharide of LPS, along with pili, may promote adherence to host cells as the initial stage of colonization (Haseley et al., 1997). In addition, a key structural factor contributing to *A. baumannii* virulence is the capsule that surrounds the bacterial surface. The tightly packed, repetitive sugar units in the capsule create a protective barrier against environmental challenges, such as dryness and disinfection, as well as immune defences like phagocytosis. It also offers protection against certain antimicrobials (Geisinger & Isberg, 2015; Singh et al., 2019). In spite of the diversity of capsular sugars in *A. baumannii*, with over 100 different types, the capsule remains a crucial factor for the pathogen's survival during infections and its capacity to grow in serum (Kenyon & Hall, 2013). These results suggest that blocking LPS synthesis is a promising strategy for discovering novel antibiotics, whereas numerous studies have shown that LPS modifications contribute to the antimicrobial resistance of *A. baumannii* to several clinically important antibiotics, such as colistin (Arroyo et al.,

2011; Beceiro et al., 2011; Boll et al., 2015; Chin et al., 2015; Moffatt et al., 2010; Pelletier et al., 2013).

1.1.3 Biofilm

Biofilm formation is crucial for *A. baumannii*'s ability to evade the immune system (de Breij et al., 2010), and pili are vital for its adherence to surfaces, biofilm development on abiotic materials, and overall virulence (Tomaras et al., 2003; Tomaras et al., 2008). Biofilm formation shown increased tolerance to antibiotics (Van Dessel et al., 2004; Vidal et al., 1997). Complex microbial biofilms consist of proteins, ions, nucleic acids, and polysaccharide polymers (Morikawa et al., 2006; Schooling & Beveridge, 2006; Steinberger & Holden, 2005; Whitchurch et al., 2002). Other important factors involved in biofilm formation are proteins in Repeats-in-Toxin (RTX)-like domain, poly-β (1-6)-N-acetyl-glucosamine (PNAG), capsule, and others. For PNAG, this polysaccharide polymer has been well described as a major component of biofilms of *S. epidermidis* (Mack et al., 1996) and *S. aureus* (Maira-Litrán et al., 2002). Its roles are in surface and cell-to-cell adherence (Cramton et al., 1999; Mack et al., 1996). PNAG is also protects bacteria from innate host defences (Vuong et al., 2004). Moreover, a specific cell surface protein called biofilm-associated protein (Bap) was found related to an initial adherence of abiotic surfaces and biofilm formation in both gram-negative and gram-positive bacteria (Loehfelm et al., 2008). The protein was firstly characterized in *S. aureus* and have been identified in many gram-positive and gram-negative pathogenic bacteria (Lasa & Penadés, 2006). Production of Bap in *A. baumannii* is essential for stabilization of mature biofilms on glass, affecting both thickness and biovolume (Loehfelm et al., 2008). Lastly, the Csu pili, or Csu fimbriae, which are encoded by the six-gene operon csuA/BABCDE, are assembled via the chaperone-usher (CU) pathway (Tomaras et al., 2003). Along with biofilm-associated proteins (Bap), Csu pili play a crucial role in the formation and maintenance of biofilms on abiotic surfaces (Loehfelm et al., 2008; Tomaras et al., 2003).

1.1.4 Phospholipase

Phospholipases, lipolytic enzymes recognized as additional virulence factors of *A. baumannii*, play important roles in the bacterium's pathogenicity. Phospholipase D aids *A. baumannii* in persisting in human serum, while phospholipase C is toxic to epithelial cells (Camarena et al., 2010). Moreover, the glycan-specific

adamalysin-like protease (CpaA) has been identified as a virulence factor that inhibits blood coagulation by deactivating factor XII. CpaA may reduce important antimicrobial defence mechanisms such as intravascular thrombus formation, allowing *A. baumannii* to disseminate (Waack et al., 2018).

1.1.5 Acinetobactin or siderophore mediated iron acquisition system

A main cause contributing to *A. baumannii*'s persistence as a hospital-acquired microorganism is its ability to capture host nutrients, such as manganese, iron, and zinc, allowing it to adapt to the metal-limited environment imposed by the host (Tipton & Rather, 2017). The primary mechanism, known as siderophores, involves five clusters of high-affinity iron-chelating molecules. Siderophores are classified into hydroxamate, catecholate, and mixed types based on the moiety that donates oxygen ligands to coordinate Fe^{3+} (Saha et al., 2013). *A. baumannii* also produces acinetobactin, the best-characterized siderophore of *A. baumannii*, a mixed-type siderophore with an oxazoline ring derived from threonine (McConnell et al., 2013). Additionally, the organism contains transporters and receptors, including FecA and FecI, that facilitate direct iron uptake and enable the utilization of heme (Morris et al., 2019). Damage to iron transporters has been shown to reduce virulence by impairing biofilm production and diminishing resistance to oxidative stress (Ajiboye et al., 2018).

Acinetobactin is a key virulence factor in *A. baumannii*. Disruption of acinetobactin biosynthesis and transport notably decreases the ability of *A. baumannii* ATCC 19606 to survive within epithelial cells. A mutation in the *entA* gene, which is essential for the synthesis of the acinetobactin precursor 2,3-dihydroxybenzoic acid, substantially reduces the persistence of *A. baumannii* ATCC 19606 in human alveolar epithelial cells and its ability to infect and kill *Galleria mellonella* larvae. One study found that acinetobactin production was significantly more common in multidrug-resistant *A. baumannii* isolates than in avirulent strains (Ali et al., 2017; Gaddy et al., 2012; Penwell et al., 2012).

The *A. baumannii* NfuA Fe-S scaffold protein involved in the formation of Fe-S clusters and playing a role in cellular responses to iron chelation and oxidative stress. The *nfuA* mutant demonstrates increased sensitivity to reactive oxygen species (ROS), such as cumene hydroperoxide and, hydrogen peroxide and shows

significantly impaired growth in human epithelial cells. In a *G. mellonella* infection model, more than 50% of larvae injected with the parental strain die within 6 days, while fewer than 30% of larvae infected with the *nfuA* mutant die (Zimbler et al., 2012). Additionally, a report indicated that iron starvation leads to an increase in the production of phospholipases C (PLCs), which enhances the hemolytic activity of *A. baumannii* (Fiester et al., 2016).

A. baumannii also relies on an efficient zinc scavenging system, comprising the ZnuABC transporter and the ZigA GTPase. The ZnuABC transporter facilitates intracellular zinc uptake, while ZigA plays a role in zinc metabolism (Moore et al., 2014; Nairn et al., 2016). Additionally, *A. baumannii* evades calprotectin, an immune system protein that binds zinc, manganese, and other divalent metal ions, thereby limiting bacterial growth. In a murine pneumonia model, *zigA* mutants with limited zinc availability demonstrated reduced systemic dissemination from the lungs after infection (Nairn et al., 2016). Although the mechanisms by which *A. baumannii* overcomes manganese limitation are not fully understood, it is thought that a transporter from the resistance-associated macrophage protein (NRAMP) family aids in manganese accumulation, allowing growth in the presence of calprotectin (Juttukonda et al., 2016).

1.1.6 Protein secretion systems

Multiple protein secretion systems have been discovered in *A. baumannii*, with the most recently characterized being the Type II secretion system (T2SS) (Johnson et al., 2016). The T2SS is a multi-protein assembly with structural similarities to Type IV pili systems, which are commonly found in Gram-negative bacteria. This system facilitates the translocation of a diverse set of proteins from the periplasmic space to the external environment or outer membrane surface. The T2SS comprises 12–15 proteins organized into four subassemblies: a pseudopilus, a cytoplasmic secretion ATPase, an inner-membrane platform, and a dodecameric outer-membrane complex (Harding et al., 2016; Korotkov et al., 2012). The secretion process is carried out in two steps. First, target proteins are translocated into the periplasm by either the general secretory (Sec) system or the twin-arginine translocation (Tat) system. These proteins are then secreted out of the cell via the T2SS. Deletion of genes encoding T2SS components, such as *gspD* or *gspE*, results in the loss of LipA secretion,

suggesting that LipA is a T2SS substrate. LipA is a lipase that breaks down long-chain fatty acids, and strains with mutations in *lipA*, *gspD*, or *gspE* cannot grow on long-chain fatty acids as their sole carbon source, exhibiting impaired *in vivo* growth in a neutropenic murine bacteraemia model (Johnson et al., 2016). Lipases (LipA, LipH, and LipAN) as well as the metallopeptidase CpaA have been recognized as substrates of the T2SS. Interestingly, two of these secreted proteins, LipA and CpaA, depend on specific chaperones for their secretion. These chaperones are encoded adjacent to their corresponding effectors, and their inactivation completely prevents the secretion of LipA and CpaA (Elhosseiny et al., 2016; Harding et al., 2016).

Acinetobacter baumannii also possesses a type VI secretion system (T6SS), first identified in *Vibrio cholerae* and *Pseudomonas aeruginosa*. The T6SS is used by many bacteria to inject effector proteins, providing a colonization advantage during eukaryotic host infections (Mougous et al., 2006) or to eliminate competing bacterial species (Basler et al., 2013). The T6SS in *Vibrio cholerae* results in DNA release and horizontal gene transfer, which may facilitate the spread of antibiotic resistance (Borgeaud et al., 2015). This secretion system is composed of several conserved structural proteins and accessory factors, and it features a contractile bacteriophage sheath-like structure that forms a needle or spike for penetrating target cells. Hcp is a structural protein that polymerizes into a tubular structure, which is then secreted from the cell. VgrGs are involved in attaching effector domains to the spike, while a proline-alanine-alanine-arginine (PAAR) repeat protein forms the sharp tip of the needle-like structure (Shneider et al., 2013; Zoued et al., 2014).

While the role of the T6SS in *A. baumannii* ATCC 17978 remains undetermined (Weber et al., 2013). , studies on the *A. baumannii* strain M2 have shown that this strain produces a functional T6SS, which is involved in the killing of competing bacteria (Carruthers et al., 2013). Additionally, research has demonstrated that the T6SS is active in six pathogenic strains of *A. baumannii* (Ruiz et al., 2015). It appears that the T6SS plays a strain-specific role in *A. baumannii* virulence (Repizo et al., 2015).

The type V autotransporter system, Ata, has also been characterized in *A. baumannii*. Ata is a trimeric membrane protein that facilitates biofilm formation, adhesion to extracellular matrix components like collagen I, III, and

IV, and contributes to virulence in a murine model of systemic *Acinetobacter* infection. In a pneumonia infection model using both immunocompetent and immunocompromised mice, Ata was identified as a potential vaccine candidate against *A. baumannii* infections (Bentancor et al., 2012). Additionally, a type IV secretion system, located on a plasmid, has been bioinformatically identified in *A. baumannii* system present in the plasmid was bioinformatically identified in *A. baumannii* (Liu et al., 2014), although no experimental data has been presented to elucidate its function.

1.1.7 Penicillin-Binding Protein 7/8 (PBP7/8) and β-Lactamase PER-1

Penicillin-binding proteins (PBPs) are typically involved in resistance to β-lactam antibiotics, but PBP7/8, encoded by the *pbpG* gene, also functions as a virulence factor in *A. baumannii*. The *pbpG* mutant strain displays normal growth in Luria-Bertani medium but shows reduced growth in human serum and significantly decreased survival rates in rat soft-tissue infection and pneumonia models. Electron microscopy analysis of bacterial morphology indicated that the loss of PBP7/8 may disrupt the peptidoglycan structure, which could increase susceptibility to host defense mechanisms (Russo et al., 2009). Interestingly, the β-lactamase PER-1 has also been proposed as a virulence factor in *A. baumannii*. PER-1, an extended-spectrum β-lactamase (ESBL), has been linked to cell adhesion (Sechi et al., 2004). Many β-lactamases are believed to contribute to virulence in other pathogenic bacteria, such as *E. coli* (Dubois et al., 2009), *P. aeruginosa* (Fernández-Cuenca et al., 2011), and *K. pneumonia* (Sahly et al., 2008), though no unified mechanisms have been established (Rumbo et al., 2014).

1.1.8 AbaI autoinducer synthase

Quorum sensing in bacteria (QS) is a cell-to-cell signaling mechanism that utilizes molecules known as 'auto-inducers'. These molecules enable bacteria to detect their population density and regulate gene expression in response (Rutherford & Bassler, 2012). QS systems play a vital role in the regulation of motility, virulence factor expression, biofilm formation, conjugation, and interactions with eukaryotic host cells (Bhargava et al., 2010; Zarrilli, 2016). Only one QS system has been reported in *A. baumannii* currently, consisting of *abaI* and *abaR* genes (Niu et al., 2008). AbaI is the autoinducer synthase which catalyse the synthesis of acyl-homoserine lactone (AHL) signals. The most common AHLs (N-acyl homoserine

lactones) produced by *A. baumannii* are 3-hydroxy-C12-homoserine lactones. The *abaR* gene encodes the receptor protein that binds to these AHLs and functions as a transcriptional regulator. The previous study found that the mutation of *abaI* gene could greatly reduce biofilm formation (Tang et al., 2020). Other actions that interfere with quorum sensing also significantly reduced *A. baumannii* motility and biofilm formation. (Castillo-Juarez et al., 2017; Stacy et al., 2012).

1.1.9 Others

A. baumannii CipA is a novel plasminogen-binding protein that inhibits complement activation and facilitates serum resistance. When CipA binds plasminogen, it is converted to active plasmin, which degrades fibrinogen and complement component C3b, contributing to the organism's serum resistance. Consequently, the *cipA* mutant strain is more vulnerable to killing by human serum and demonstrates a reduced ability to penetrate endothelial monolayers (Koenigs et al., 2016). In a similar manner, the *A. baumannii* translation elongation factor Tuf also binds plasminogen, which is subsequently converted into active plasmin, leading to the degradation of fibrinogen and C3b (Koenigs et al., 2015). RecA, a protein involved in homologous recombination and the SOS response, has been recognized as a virulence factor in *A. baumannii* as well. The mutant of *recA* exhibits significantly reduced survival within macrophages and decreased lethality in a mouse model of systemic infection (Aranda et al., 2011). The surface antigen protein SurA1 plays an important role in the fitness and virulence of *A. baumannii*. The *surA1* mutant shows decreased serum resistance compared to the wild-type strain CCGGD201101. In the *G. mellonella* insect model, the *surA1* mutant has a lower survival rate and reduced dissemination (Liu et al., 2016).

A comprehensive growth analysis of 250,000 isolates of *A. baumannii* transposon mutants conducted within *Galleria mellonella* larvae identified 300 genes that are essential for the survival and growth of *A. baumannii* in this host. These genes were categorized into six groups: micronutrient uptake, cysteine metabolism and sulfur assimilation, aromatic hydrocarbon breakdown, cell envelope and membrane components, stress response pathways, antibiotic resistance mechanisms, and transcriptional control. Within this group, four transcriptional regulators essential for growth in *G. mellonella* larvae were designated as *gig* genes,

abbreviated from growth in *Galleria*. The deletion of gig A - D led to significant defects in growth and lethality in the larvae (Gebhardt et al., 2015). The study also identified stress proteins, such as UspA, as important factors for growth in *G. mellonella*. Furthermore, UspA was found to be critical for the pathogenesis of pneumonia and sepsis caused by *A. baumannii* (Elhosseiny et al., 2015). Among the 300 genes, several were involved in aromatic hydrocarbon metabolism (Gebhardt et al., 2015). One study emphasized the role of GacS, a transcription factor that regulates genes like *paaE*, which is involved in the phenylacetic acid catabolic pathway, *in A. baumannii* virulence. Experiments with a paaE deletion mutant confirmed the contribution of aromatic hydrocarbon metabolism to *A. baumannii* virulence (Cerqueira et al., 2014), although the precise molecular mechanism remains unclear. Interestingly, a recent study found that the accumulation of phenylacetate in *A. baumannii* induces a rapid neutrophil influx to the infection site, enhancing bacterial clearance (Bhuiyan et al., 2016). The authors suggested that phenylacetate acts as a neutrophil chemoattractant, promoting bacterial-guided neutrophil chemotaxis, which may uncover a novel molecular mechanism linking the phenylacetic acid catabolic pathway to *A. baumannii* virulence.

Biofilm formation contributes a critical role in immune evasion by *A. baumannii* (de Breij et al., 2010), and pili are essential for its adherence to abiotic surfaces, biofilm formation, and virulence (Tomaras et al., 2003; Tomaras et al., 2008). Notably, imipenem treatment of imipenem-resistant *A. baumannii* isolates induces the expression of key genes involved in type IV pili synthesis, suggesting that the overproduction of pili confers a biological advantage to *A. baumannii*. Other virulence-related proteins, including OmpR/EnvZ (Tipton & Rather, 2017), FhaBC (Pérez et al., 2017), and the resistance-nodulation-division-type membrane transporter AbeD (Srinivasan, 2015), have been identified, although their molecular mechanisms remain to be determined.

2. Antimicrobial resistance mechanism of *Acinetobacter baumannii*

A. baumannii has become one of the most highly resistant pathogens to the majority of antibiotics currently used in clinical practice (Lin & Lan, 2014). The bacterium employs various resistance mechanisms, including efflux pumps, β-lactamase production, enzymes that modify aminoglycosides, defects in membrane

permeability, and changes to target sites. As a result, the accumulation of these resistance mechanisms has progressively reduced the number of effective antibiotic classes available for treating *A. baumannii* infections. Figure 9 illustrates the mechanisms of antibiotic resistance in *A. baumannii* (Ayoub & Hammoudi, 2020), with further details provided below.

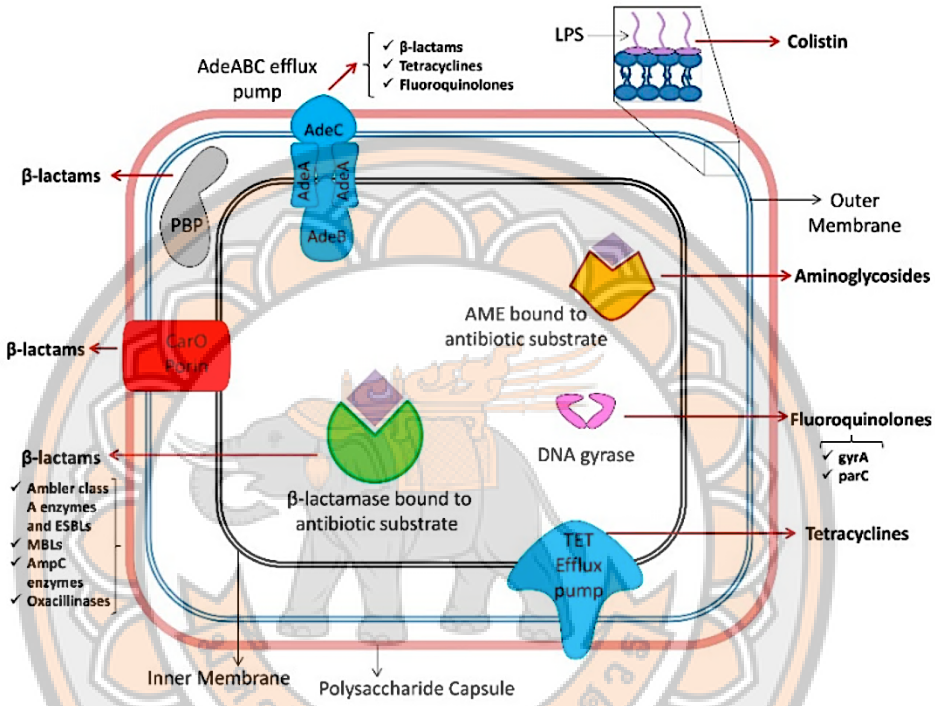

Figure 9 A diagram illustrating the various resistance mechanisms of *A. baumannii* to antimicrobial agents is shown.

It highlights antibiotic-modifying enzymes, efflux pumps, porins, drug targets, and the specific antibiotics affected by each resistance mechanism. Abbreviations include AMEs (Aminoglycoside Modifying Enzymes), AmpC (Ambler Class C Cephalosporinases), ESBLs (Extended-Spectrum β-Lactamases), MBLs (Metallo-β-Lactamases), LPS (Lipopolysaccharide), and PBP (Penicillin-Binding Protein).

Source: Ayoub Moubareck and Hammoudi Halat (2020)

2.1 Enzymatic Mechanisms

β-Lactamases

The primary resistance mechanism of *A. baumannii* to β-lactams is enzymatic hydrolysis by β-lactamases. These enzymes are categorized into four molecular classes ; A, B, C, and D according to sequence homology (Jeon et al., 2015). All four Ambler classes of β-lactamases are found in *A. baumannii*. Classes A, C, and D include enzymes with a serine-based active site, while class B consists of Zn-dependent metallo-enzymes (Ambler, 1980). In the functional classification by Bush, Jacoby, and Medeiros, β-lactamases are divided into three groups based on their substrate profile and inhibitor susceptibility. Group 1 includes class C cephalosporinases, group 2 contains β-lactamases with serine at the active site, and group 3 comprises metallo-β-lactamases (MBLs), corresponding to class B in the molecular structural classification (Bush et al., 1995).

Class A β-lactamases are the most common cause of β-lactam resistance in *A. baumannii*. These enzymes can be inhibited by clavulanate and hydrolyze penicillins and cephalosporins more effectively than carbapenems, with exceptions like *Klebsiella pneumoniae* carbapenemase (KPC)-type enzymes (Jeon et al., 2015). Several class A β-lactamases have been identified in *A. baumannii*, including TEM, GES, CTX-M, SHV, SCO, PER, CARB, VEB, and KPC, with most being broad-spectrum β-lactamases (e.g., SHV-5, PER-1, PER-2, PER-7, TEM-92, CTX-M-15, VEB-1, GES-14, CARB-10, CTX-M-2) and some narrow-spectrum (e.g., TEM-1, SCO-1, CARB-4). Carbapenemases like GES-14 and KPC-2 have also been detected in *A. baumannii* (Bogaerts et al., 2010; Moubareck et al., 2009).

Class B β-lactamases, known as metallo-β-lactamases (MBLs), require zinc or other heavy metals for catalysis (Jeon et al., 2015). These enzymes hydrolyze almost all β-lactam antibiotics, including carbapenems, except for monobactams such as aztreonam aztreonam (Jeon et al., 2015; Queenan & Bush, 2007). Various MBLs have been identified in *A. baumannii*.

Class C β-lactamases, also known as *Acinetobacter* derived cephalosporinases (ADCs), are encoded by the *ampC* gene and are intrinsic to all *A. baumannii* strains (Gordon & Wareham, 2010; Jeon et al., 2015). These enzymes confer resistance to cephamycins, penicillins, cephalosporins, and β-lactamase inhibitor

combinations, but are not inhibited by common β-lactamase inhibitors like clavulanic acid (Jeon et al., 2015).

Class D β-lactamases, or oxacillinases (OXA), are serine-dependent and typically hydrolyze oxacillin more effectively than benzylpenicillin (Jeon et al., 2015). Over 400 OXA enzymes have been characterized, and many variants exhibit carbapenemase activity. Carbapenem-hydrolyzing OXAs, such as OXA-23, OXA-24, OXA-51, and OXA-58, are prevalent in *A. baumannii*. The first carbapenem-hydrolyzing OXA enzyme, OXA-23, was identified in Scotland in 1985 (McLeod & Lyon, 1985) and has since spread globall. Insertion of the *ISAba1* element in the *bla*OXA-23 promoter has been linked to the overexpression of *bla*OXA-23, *bla*OXA-51, and *bla*OXA-58 in *A. baumannii* (Turton et al., 2006).

Aminoglycoside-Modifying Enzymes

Aminoglycoside-modifying enzymes (AMEs) are a major resistance mechanism in *A. baumannii* against aminoglycosides. These enzymes can be classified as acetyltransferases, adenyl transferases, and phosphotransferases, and are typically found on transposable elements, facilitating horizontal gene transfer between bacteria (Lin & Lan, 2014). Many multi-drugs resistant (MDR) *A. baumannii* isolates produce a combination of these enzymes (Gallego & Towner, 2001; Nemec et al., 2004).

2.2 Non-Enzymatic Mechanisms

In addition to β-lactamases, *A. baumannii* resistance to β-lactams is also attributed to non-enzymatic mechanisms, such as alterations in outer membrane proteins and multidrug efflux pumps (Jeon et al., 2015).

Activation of the Efflux Pumps

Efflux systems are critical in *A. baumannii* resistance to various antibiotics, especially when overexpressed (Chen et al., 2017). Efflux pump genes are often located on mobile genetic elements (MGEs) such as transposons, integrons, and plasmids (Butaye et al., 2003). Four types of efflux pumps have been identified in *A. baumannii*: RND superfamily, MATE (multidrug and toxic compound extrusion family), MFS (major facilitator superfamily), and SMR (small multidrug resistance transporters) (Lin & Lan, 2014). The RND system is the most prevalent and includes the AdeABC pump, which plays a key role in resistance to β-lactams, fluoroquinolones, erythromycin, chloramphenicol, trimethoprim, tetracyclines, aminoglycosides and

macrolides (Jeon et al., 2015). The AdeABC pump consists of three components: AdeA (inner membrane pump), AdeB (major fusion protein), and AdeC (outer membrane factor) (Coyne et al., 2011), all encoded by the adeRS operon. In wild-type *A. baumannii*, the AdeABC pump is usually cryptic but becomes active upon exposure to high concentrations of antibiotics, leading to a multidrug-resistant (MDR) phenotype (Yoon et al., 2015). Point mutations in the *adeR* and *adeS* genes or insertion of *ISAba1* upstream of the *adeABC* operon can trigger overexpression of this efflux pump (Marchand et al., 2004). However, other pathways for efflux pump overexpression remain to be explored (Chopra & Roberts, 2001).

Decreased Membrane Permeability

Changes in outer membrane porins significantly affect *A. baumannii* resistance and virulence by controlling the transport of molecules. The loss of porins such as CarO is associated with resistance to imipenem and meropenem (Benmahmod et al., 2019). Decreased membrane permeability, involving porins like Omp22–23 (Bou et al., 2000), Omp43 (Dupont et al., 2005), Omp37, 44, 47 (Quale et al., 2003), Omp33–36 (del Mar Tomás et al., 2005; Hood et al., 2010), and CarO (Catel-Ferreira et al., 2011; Jin et al., 2011; Mussi et al., 2005; Siroy et al., 2005). OmpA, another key porin, is associated with resistance to aztreonam, chloramphenicol, and nalidixic acid (Smani et al., 2014) and its role in virulence has been highlighted in recent studies (Espinal et al., 2019). OmpA and CarO also interact physically with OXA-23 carbapenems, contributing to antibiotic resistance (Wu et al., 2016), providing new insights into bacterial resistance mechanisms.

Changing the Target Site

This resistance mechanism is driven by random mutations. For instance, overexpression of modified penicillin-binding proteins (PBPs) with reduced affinity for imipenem results in *A. baumannii* developing resistance to this antibiotic (Gehrlein et al., 1991). Resistance to quinolones is linked to changes in GyrA (DNA gyrase subunit) and ParC (topoisomerase IV subunit) in various *A. baumannii* isolates (Vila et al., 1995). Ribosomal protection by the TetM protein, which shares 100% homology with *S. aureus* TetM, is related with tetracycline resistance (Ribera et al., 2003b). Dihydrofolate reductases (DHFR and FolA), responsible for trimethoprim resistance, have also been found in MDR *A. baumannii* isolates (Lin & Lan, 2014; Mak

et al., 2009; Taitt et al., 2014). Additionally, the 16S rRNA methylase ArmA, which confers aminoglycoside resistance, is present in many *A. baumannii* strains, often coexisting with OXA-type carbapenemases like OXA-23. Changes in or loss of lipopolysaccharides (LPS) can reduce the sensitivity of *A. baumannii* to colistin.

Prospective treatment options

Carbapenems are effective for treating *A. baumannii* (Cisneros & Rodríguez-Baño, 2002; Turner et al., 2003), however, carbapenem-resistant *A. baumannii* isolates have become more prevalent gradually (Kuo et al., 2012; Mendes et al., 2010; Su et al., 2012). As a result, there are fewer effective antibiotic options available for treating multidrug-resistant (MDR) *A. baumannii* infections (Gordon & Wareham, 2010; Lee & Zhang, 2015). To address MDR or pandrug-resistant (PDR) strains, combination therapies such as imipenem/sulbactam, colistin/teicoplanin, colistin/imipenem, colistin/tigecycline, colistin/rifampicin, colistin/meropenem, and colistin/sulbactam have been extensively studied.

CHAPTER III

RESEARCH PROCEDURES OF THE STUDY

Bacterial strains

Thirteen entomopathogenic bacterial strains, listed in Table 4, were selected from those collected at the Department of Microbiology and Parasitology, Faculty of Medical Sciences, Naresuan University. The selection was based on screening for antimicrobial and anti-mosquito activities. Identification of all isolates was performed using the *recA* gene sequence. In briefly, genomic DNA was extracted from bacterial pellets with the Genomic DNA Mini Kit (Blood/Cultured Cell) (Geneaid Biotech Ltd., Taiwan). PCR amplification was performed using EconoTaq® PLUS 2X Master Mixes (Lucigen, USA) on a thermal cycler (Applied Biosystems, Pittsburgh, PA, USA). An 890 bp fragment of the *recA* gene from bacteria was amplified using specific primers. The components of the PCR reagents and thermal cycling conditions for *recA* amplification are detailed in Table 5 and Table 6. Then, the PCR products were analysed on a 1.2% agarose gel via electrophoresis at 100 volts for 30 minutes. Gels were stained with ethidium bromide (EtBr), de-stained with distilled water, and visualized under UV light. The resulting *recA* sequences were edited using SeqManII (DNASTAR Inc., Wisconsin, USA) and compared with known sequences using the BLASTN program (NCBI), with a 97% identity threshold for species-level matches.

Table 4 A summary of bacterial strains was used in the study

No.	Bacteria Code	Maximum identity to	Year of isolate	Place of isolate
1	NN168.5	*P. akhurstii*	2016	Nam Nao National Park
2	SBR15.4	*P. australis*	2013	Saraburi
3	NN169.4	*P. hainanensis*	2016	Nam Nao National Park
4	MH8.4	*P. laumondii*	2013	Mae Hong Son
5	MW27.4	*P. temperata*	2014	Mae Wong National Park

Table 4 (Cont.)

No.	Bacteria Code	Maximum identity to	Year of isolate	Place of isolate
6	MH9.2	*X. ehlersii*	2013	Mae Hong Son
7	KK26.2	*X. indica*	2014	Khon Kaen
8	MW12.3	*X. japonica*	2015	Mae Wong National Park
9	MH16.1	*X. miraniensis*	2013	Mae Hong Son
10	RT25.5	*X. stockiae*	2018	Phitsanulok
11	SBR31.4	*X. stockiae*	2013	Saraburi
12	SBRx11.1	*X. stockiae*	2013	Saraburi
13	NN167.3	*X. vietnamensis*	2016	Nam Nao National Park

Table 5 Components of PCR reagent for amplification of symbiotic bacteria

Reagent (concentration)	Volume (µL)
EconoTaq PLUSMaster Mix (2X)	15
Forward primer (1 µM) recA_F (5’-GCTATTGATGAAAATAAACA-3’)	1.5
Reward primer (1 µM) recA_R (5’RATTTTRTCWCCRTTRTAGCT-3’)	1.5
DNA (10 ng/ µl)	1.5
Distilled water	10.5
Amount	30

Table 6 Thermal cycling for amplification of partial *recA* fragment

Parameter	Temperature	Time	
Initial denature	94ºC	5 min	
Denature	94ºC	1 min	
Annealing	45ºC	45 sec	30 cycles
Extension	72ºC	2 min	
Final extension	72ºC	7 min	

Genome sequencing and analysis

1. Whole genome sequencing

A single colony of the bacterial strain was inoculated into 5 mL of Luria-Bertani (Caisson LABS, USA). The culture was incubated at 28°C with agitation at 200 rpm for 24 hours. Genomic DNA extraction was performed using the DNeasy kit from Qiagen (Hilden, Germany). To begin, 1 ml of bacterial culture was transferred to a 1.5 ml microcentrifuge tube. The sample was then centrifuged at 7,500 rpm for 5 minutes to pellet the cells. Discard the supernatant and 180 µl Buffer ATL was added to the cell pellet. Then, 20 µl of proteinase K was added, the tube was mixed thoroughly by vortexing and incubate at 56°C for approximately 1 hour, occasionally vortexing or using a shaking water bath or rocking platform to ensure complete lysis of the cells. After incubation, briefly centrifuge the tube to collect any droplets from the lid, 4 µl of RNase A (100 mg/ml) was added to degrade RNA, mix by pulse-vortexing for 15 seconds, and incubated for 2 minutes at room temperature (15–25°C). The tube was centrifuged briefly to remove any drops from the lid, then 200 µl of Buffer AL was added and pulse-vortex for another 15 seconds to mix thoroughly. The tube was incubated at 70°C for 10 minutes, during which time any white precipitate formed should dissolve, as it does not interfere with the procedure. After incubation, the tube was briefly centrifuged again. 200 µl of 100% ethanol was added to the sample and mixed thoroughly by pulse-vortexing for 15 seconds. The tube was briefly centrifuged to remove droplets from the lid, ensuring the sample, Buffer AL, and ethanol form a homogeneous solution. Apply the mixture, including any precipitate, to the QIAamp Mini spin column (placed in a 2 ml collection tube) without wetting the rim. Close the

cap, centrifuge at 8,000 rpm for 1 minute, and transferred the spin column to a fresh 2 ml collection tube, and the collection tube was discarded with the filtrate. Next, open the spin column carefully, and 500 µl of Buffer AW1 was added, avoiding wetting the rim, then centrifuged at 8,000 rpm for 1 minute. The spin column was transferred to another clean 2 ml collection tube, the previous tube was discarded, and 500 µl of Buffer AW2 was added in to the tube. The tube was centrifuged at full speed (14,000 rpm) for 3 minutes to ensure thorough washing. To reduce any carryover of Buffer AW2, place the spin column in a new collection tube, and the tube was centrifuged at full speed for 1 minute. Transfer the spin column to a new clean 1.5 ml microcentrifuge tube and the collection tube with the filtrate was discarded. Elute the DNA by adding 200 µl of Buffer AE or distilled water. Incubated at room temperature for 1 minute, then the tube was centrifuged at 8000 rpm for 1 minute to collect the purified DNA in the microcentrifuge tube. Extracted DNA will roughly be quantified using nanoDrop spectrophotometer (Thermo Scientific). Whole genome sequencing using Illumina MiSeq platform and Oxford Nanopore Technology (ONT) was then performed by Macrogen, Inc. Teheran-ro, Gangnam-gu, Seoul, Republic of Korea and the Center for Biotechnology (CeBiTec), Bielefeld University, Bielefeld, Germany, respectively.

2. Genome assembly and annotation

For short reads, quality trimming was performed using FastQC (Simon, 2010) and Sickle v1.33 (Joshi & Fass, 2011), discarding any trimmed reads shorter than 125 bp. Genome assembly was then performed using SPAdes v. 3.10.1 (Andrey et al., 2020) with the following settings: --cov-cutoff auto, --careful in paired-end mode with mate pairs, and k-mer lengths of 21, 33, 55, 77, 81, and 91. Genome annotation was performed using Prokka v1.12 (Torsten, 2014) to identify coding sequences, rRNAs, tRNAs, and other genomic features. The following parameters were used: --usegenus, --genus GENUS, --addgenes, --evalue 0.0001, --rfam, --kingdom Bacteria, --gcode 11, --gram, and --mincontiglen 200. For long read, genome assembly and annotation were performed according to the Prokaryotic Genome Annotation Pipeline (PGAP) (Tatiana et al., 2016). The PGAP is a comprehensive tool used for annotating prokaryotic genomes. It begins with the input of a complete or near-complete genome assembly, accompanied by metadata such as organism name, BioSample, and BioProject information. PGAP performs quality control checks on the assembly, assessing genome

integrity, completeness, and potential contamination. Gene prediction is conducted using GeneMarkS-2+ (Alexandre et al., 2018) to identify protein-coding genes, along with tools to detect tRNA and rRNA genes. Predicted coding regions are analyzed to identify open reading frames (ORFs) and assign functions based on homology using a best-placed reference protein set version 2022-12-13.build6494. Functional domains within proteins are identified through domain databases such as Pfam and TIGRFAMs. The pipeline also detects pseudogenes and annotates non-coding RNAs (ncRNAs), including small RNAs important for regulation. Additionally, PGAP predicts operons and maps annotated genes to metabolic pathways. Protein features such as signal peptides and transmembrane domains are identified, and post-translational modifications may be annotated. The output includes a fully annotated genome in GenBank format, ready for submission to public databases. Manual curation was optional step for correcting errors or ambiguities.

3. Bioinformatics analysis

3.1 General Characteristics of the genome

Reports summarized genome size, gene predictions, G+C content, and overall genome quality, providing by Prokka v1.12 (Torsten, 2014). The genome map was created using Proksee (Grant & Stothard, 2008), a system for genome visualization. To use Proksee, a complete genome sequence in GenBank format was provided.

3.2 antiSMASH annotations and preliminary classification.

The annotated genome sequences, in GenBank format, were analyzed for biosynthetic gene clusters (BGCs) using antiSMASH 6.1.1 (antibiotics and secondary metabolite analysis shell) (Kai et al., 2021). For this analysis, detection strictness was set to "relaxed," enabling options like Known ClusterBlast, ActiveSiteFinder, ClusterBlast, Cluster PFam analysis, and SubClusterBlast to ensure a comprehensive search of BGCs. Following the initial automated classification of BGC types by antiSMASH, each cluster underwent manual inspection and reclassification to ensure accurate categorization. A summary of the annotated BGCs was generated based on this careful validation. Moreover, to refine the analysis, BiG-SCAPE (Biosynthetic Gene Similarity Clustering and Prospecting Engine) and Core Analysis of Syntenic Orthologues to Prioritize Natural Product Gene Clusters (CORASON) tool set (Jorge et al., 2020) was employed using a cutoff value of 0.65.

BiG-SCAPE is a tool designed to assess the sequence similarity of biosynthetic gene clusters (BGCs) and organize them into gene cluster families (GCFs) through similarity-based clustering. By comparing domain architecture, conserved sequence motifs, and other structural features of BGCs, BiG-SCAPE determines the relatedness of clusters at a specified similarity cutoff. This enables it to group BGCs into GCFs likely to produce related or similar molecules. BiG-SCAPE calculates a pairwise similarity score between clusters based on genetic and domain composition, presenting these relationships in a network format. This network visualization reveals the diversity of BGCs across multiple genomes and can identify clusters that may represent unique or novel bioactive metabolites. BiG-SCAPE's network analysis helps researchers explore large datasets by providing a biosynthetic diversity map, highlighting clusters with distinct genetic compositions that may hint at new chemical structures or activities. The resulting GCFs were carefully reviewed and corrected as needed within an interactive network. Additionally, BiG-SCAPE integrates with Cytoscape 3.10 (Paul et al., 2003) for visualization, facilitating the interpretation of complex networks of related clusters.

3.3 Pangenome analysis.

For comparative analysis of all genomes, a pangenome analysis was conducted primarily following the anvi'o 7.1 (Eren et al., 2015) pangenome workflow. To streamline genome analysis, the header lines of FASTA files were simplified using the anvi-script-reformat-fasta command. The FASTA files were then converted into anvi'o contigs databases via anvi-gen-contigs-database and annotated with HMM model hits using anvi-run-hmms. For functional annotation, anvi-run-ncbi-cogs was employed to assign gene functions based on NCBI's Clusters of Orthologous Groups (COGs). To map gene locations, tables with gene caller IDs and nucleotide start/stop positions were exported using anvi-export-table. Gene caller IDs were linked with biosynthetic gene clusters (BGCs) based on their nucleotide boundaries, identifying genes within BGCs as natural product biosynthetic genes. These genes were subsequently classified and assigned potential compound names corresponding to their BGC origins. This information was re-integrated into the contigs databases using anvi-import-functions.

To manage sequence data and annotations, a genome storage file was created using anvi-gen-genomes-storage, incorporating DNA and amino acid sequences alongside functional annotations for each gene. Pangenome analysis was then performed with anvi-pan-genome, utilizing the genome storage database, the --use-ncbi-blast flag, and the parameter --mcl-inflation 8. The results were visualized using anvi-display-pan, which presented pangenome organization as a dendrogram in the interface, highlighting gene presence/absence patterns.

Gene clusters were categorized into the following bins:

Core Gene Bin: Gene homology groups present in all genomes.

Singleton Bin: Gene homology groups occurring only once across genomes.

Accessory Bin: Gene clusters that were neither core nor singleton.

Detection of secondary metabolites by LC/MSMS

X. stockiae strain RT25.5 was cultured in LB media at 28°C for 3 days. The culture supernatant was subjected to a mass spectrometry experiment using a timsTOF fleX MALDI-2 instrument utilized an Acquity UPLC BEH C18 column (2.1 x 50 mm) with solvent A (H2O + 0.1% formic acid) and solvent B (acetonitrile + 0.1% formic acid), employing a gradient method from 5 to 95% B over 16 minutes. Operating in positive ionization mode with VIP-HESI source, the instrument employed specific voltage settings, gas flows, and temperatures. Isolation and fragmentation of ions were achieved by varying collision energy across a range of m/z values and charge states. Data processing involved centroid mass detection for both MS1 and MS2 spectra, chromatogram construction, local minimum resolution, isotope filtering, blank subtraction, alignment of features, and gap filling. Finally, feature-based molecular networking was performed with specified mass tolerances and minimum matching criteria. Molecular network was annotated using SIRIUS software (Dührkop, 2019), cross-referencing with in-house compound lists and online databases such as GNPS (Wang, 2016) for identification of compound families.

easyPACId (Easy Promoter Activation and Compound Identification) in *X. stockiae* Strain RT25.5

1. Construction of *hfq* deletion mutants

Deletion of the *hfq* gene, which encodes the RNA chaperone Hfq, results in a mutant deficient in natural product (NP) production (Nicholas et al., 2017). A scheme of deletion via homologous recombination in *X. stockiae* strain RT25.5 depicted in Figure 10. Approximately 1,000-bp upstream and downstream fragments of the *hfq* gene from *X. stockiae* strain RT25.5 were amplified using specific primer pairs. Details of the PCR components and cycler conditions are provided in Table 7, 8, and 9**,** respectively. These fragments were fused through complementary overhangs introduced by the primers and subsequently cloned into the pEB17 vector (kanamycin-resistant), which had been linearized using *PstI* and *BglII*. The restriction digestion mixture (total 150 µl) consisted of 10 µl plasmid DNA, 15 µl buffer, 3 µl *BglII*, 3 µl *PstI*, and 119 µl distilled water. The insert fragments and vector were combined at varying molar ratios (1:1, 1:3, and 3:1), depending on DNA concentrations. The assembly was performed using NEBuilder HiFi DNA Assembly Master Mix via a hot fusion protocol at 50°C for 1 hour in a thermal cycler. The resulting ligated constructs were stored at -20°C. The resulting plasmid was transformed into *E. coli* strain ST18, a *hemA*-deleted strain that requires 5-aminolevulinic acid hydrochloride (5-ALA) for growth, was used for growth using electroporation. To perform the transformation, 50 µl of electrocompetent cells were pipetted into the bottom of a pre-chilled 1 mm electroporation cuvette, followed by the addition of 1 µl of the ligated construct. Electroporation was conducted with the following settings: 1.8 kV, 200 Ω, and 25 µF. Immediately after pulsing, 950 µl of pre-warmed LB medium supplemented with 5-ALA (50 µg/mL) was added to the cuvette. The cells were then transferred into a 1.5 mL reaction tube and incubated at 37°C with shaking at 800 rpm for 1 hour. Following incubation, the transformed cells were plated on LB agar containing 5-ALA and the selective antibiotic. The plates were incubated overnight at 37 °C, where colonies typically appeared the next day. To verify successful transformation, colonies were screened using colony PCR with verification primers pEB17-fw (GCTATGCCATAGCATTTTTATCCATAAG) and pEB17-rv (ACATGTGGAATT GTGAGCGG). Amplification of the ligated fragment resulted in a 234 bp product for

an “empty” vector. Finally, a master plate was prepared by streaking each respective clone onto LB agar containing the corresponding selective antibiotic and 5-ALA. This plate was stored for future applications. The *E. coli_pEB17-hfq* strain was subsequently conjugated with *X. stockiae* strain RT25.5. Both strains were grown to an OD600 of 0.6–0.7, washed, and mixed in defined ratios. The mixture was then spotted onto LB agar plates and incubated at 37°C for 3 hours, followed by overnight incubation at 30°C. After incubation, conjugants were harvested, plated on LB agar supplemented with kanamycin and incubated at 28°C for 2–3 days. Single colonies were selected for further analysis, including the generation of double-crossover mutants through counterselection on LB plates containing 6% sucrose. Successful *hfq* deletion mutants were confirmed using PCR and HPLC-MS analysis. PCR verification utilized primers listed in Table 7. Components of PCR reagent for DNA and colony amplification of upstream and downstream fragments are shown in Table 8.

Table 7 A list of primers for constructing *hfq* deletion mutants, containing overlapping sequences (in bold) compatible with the cloning vector pEB17

Primers	Primer Sequences	Purpose
P1hfq_F	**GATCCTCTAGAGTCGACCTGCAG**CGTCG CGATGCGCTGGAA	*hfq* upstream amplification
P2hfq_R	CAGCGATATCATTTTCCTGTTGTGCTGCCA GGAATGGATCTTGCAAAGATTG	
P3hfq_F	GCAGCACAACAGGAAAATGATATCG	*hfq* downstream amplification
P4hfq_R	GTGGAATTCCCGGGAGAGCTCAGATCT **GTGACGAATGAAACCAACGGTGTC**	
P3hfq_F	GGCAATCTTTGCAAGATCCATTCCTGGCAG CACAACAGGAAAATGATATCG	Fusion of *hfq* fragments
P2hfq_R	CAGCGATATCATTTTCCTGTTGTGCTGCCA GGAATGGATCTTGCAAAGATTG	
P5hfq_F	GATTCTGCACTGGTTTATCGTG	Verification of *hfq* deletion
P6hfq_R	CTTCCAGAACACTGTCCACTGC	

Table 8 Components of PCR reagent for amplification of upstream and downstream fragments

Reagent (concentration)	Volume (µL)
Q5 buffer	10
dNTPs (25 mM)	1
Primer forward (10 µmol/µL)	1
Primer reverse (10 µmol/µL)	1
Q5 hot start polymerase	1
DNA (10 ng/ µl)	1 or 0.5
Distilled water	36
Amount	50

Components of reagent for colony PCR

Reagent (concentration)	Volume (µL)
Bio mix red	7.5
Primer forward (100 µmol/µL)	0.15
Primer reverse (100 µmol/µL)	0.15
Q5 hot start polymerase	1
Cell material or DNA	1 or 0.5
Distilled water	7.2
Amount	15

Table 9 Thermal cycling for amplification of partial *hfq* fragment and colony PCR

Parameter	Temperature	Time	
Initial denature	94ºC	5 min	
Denature	94ºC	1 min	
Annealing	55/60 ºC	45 sec	30 - 35
Extension	72ºC	2 min	cycles
		(or 1000 bp/60 sec)	
Final extension	72ºC	7 min	

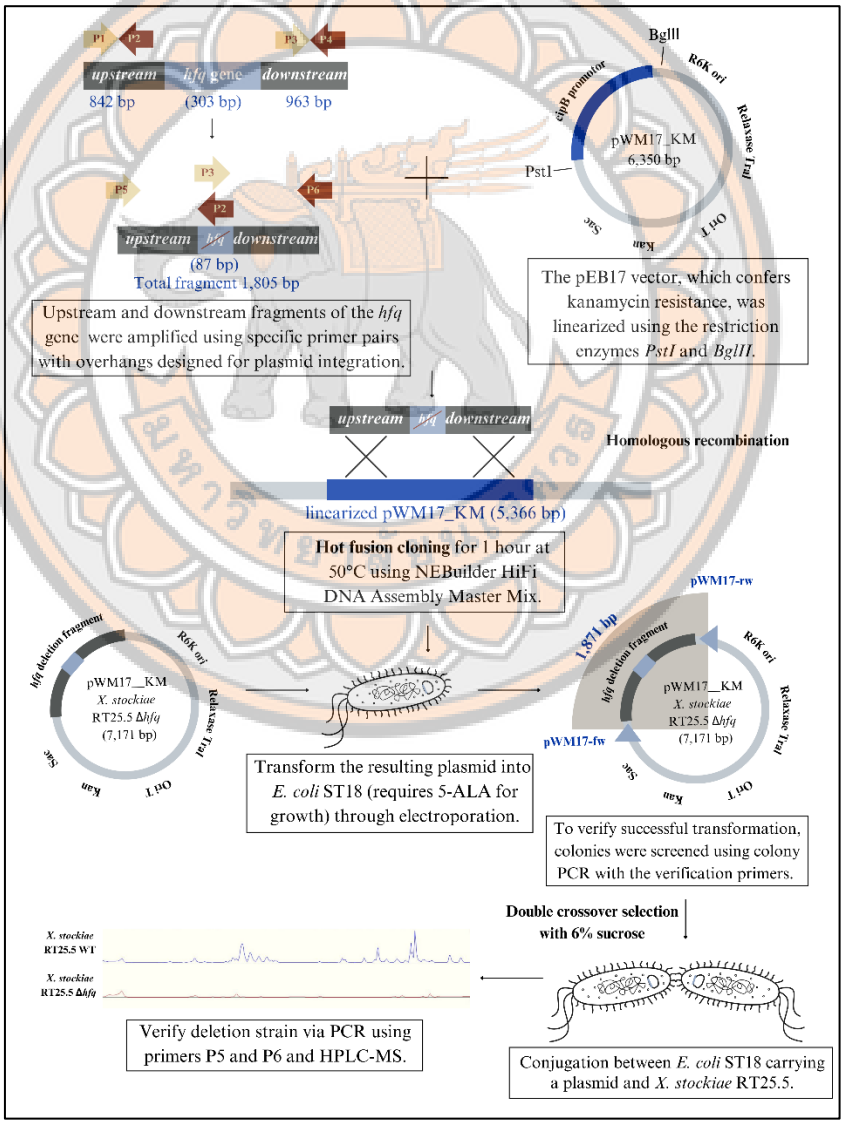

Figure 10 A scheme of deletion via homologous recombination in *X. stockiae* strain RT25.5.

2. Induced production, isolation, identification, and testing of natural products from the strain RT25.5

After generating a Δ*hfq* mutant from the strain of interest, the genome was first analyzed for potentially interesting natural product biosynthetic gene clusters (BGCs) using antiSMASH 6.0 (Blin et al., 2021). The Cluster Expression Plasmid (pCEP), a kanamycin-resistant, low-copy vector, was then used to create a promoter insertion mutant. A 500–800 bp region upstream of the target gene was amplified using the primer pair shown in Table 10. The amplified fragment was inserted into the prepared pCEP backbone via hot fusion using primers pCEP_fw and pCEP_rv. The constructed plasmid was transformed into *E. coli* ST18, and the clones were confirmed by PCR using primers VpCEP-fw and VpCEP-rv. The recipient strain, *X. stockiae* Δ*hfq*, was mated with *E. coli* ST18 (the donor strain carrying the plasmid). Both strains were grown in LB medium to an optical density of 1 at 600 nm (OD600), then washed once with fresh LB medium. The donor and recipient strains were mixed on LB agar plates at 1:3 and 3:1 ratio and incubated at 37°C for 3 hours, followed by 21 hours at 28°C. After incubation, the bacterial layer was collected using an inoculating loop, resuspended in 2 ml of fresh LB medium, and a 200-µl aliquot was plated on LB agar with kanamycin. The plates were incubated at 28°C for 2 days. Individual insertion clones were cultured and analyzed by HPLC-MS. The genotypes of all mutants were confirmed using the VpCEP-fw primer and a corresponding verification primer binding downstream of the homologous region in the genome. A list and characteristics of plasmid used in this study was shown in Table 11.

Table 10 A list of primers for promoter activation of the interest BGCs, containing overlapping sequences (in bold) compatible with the cloning vector pCEP

List	Primers	Primer Sequences
Backbone amplification of pCEP_kan	pCEP_fw	ATGTGCATGCTCGAGCTC
	pCEP_rv	ATGCTAGCCTCCTGTTAGC
PAX (with glu)	p1819-fw	**TTTGGGCTAACAGGAGGCTAGCAT**ATGACTCTAATT GTTTATCTTTATCGCC
	p1819-rv	**CCGTTTAAACATTTAAATCTGCAG**GATATATCTTAT CTACCTGCTCACG
	Vp1819	CTGCCATCGATCAGTTGCTG
PAX (with glu)	p1818-fw	**TTTGGGCTAACAGGAGGCTAGCAT**ATGAATCATCCT GAAACATTGAAACCAT
	p1818-rv	**CCGTTTAAAC**ATTTAAATCTGCAGGCCAGGTAACAT AATCCTGATAACT
	Vp1818	CGGGTAATTGTAATTCGGTTAACTC
Unknown 2984	p2984-fw	**TTTGGGCTAACAGGAGGCTAGCAT**ATGATACAAGA GAATCCTTTTTCAT
	p2984-rv	CCGTTTAAACATTTAAATCTGCAGGATAAGTTTGGTA TTTTCGGTAATG
	Vp 2984	GGAATGGATCTTGCAAAGATTG
Unknown 2981	p2981-fw	**TTTGGGCTAACAGGAGGCTAGCAT**ATGCGTAAACA CAATCAAAATG
	p2981-rv	CCGTTTAAACATTTAAATCTGCAGCGGACTGATCAGG TCAGTTTC
	Vp 2981	AGAATATTGTTCTGACTGAGCAA
Unknown 1972	p1972-fw	**TTTGGGCTAACAGGAGGCTAGCAT**ATGATGAGAAG CGATAATATGC
	p1972-rv	CCGTTTAAACATTTAAATCTGCAGATCAATAGTCAAG GATGGTCCTTG
	Vp 1972	ACCAGTACGGCTTTCTACTAT
	VpCEP-rv	ACATGTGGAATTGTGAGCGG

Table 10 (Cont.)

List	Primers	Primer Sequences
Unknown 1974	p1974-fw	**TTTGGGCTAACAGGAGGCTAGCAT**ATGAGAAAAGC GGCAGATCAT
	p1974-rv	CCGTTTAAACATTTAAATCTGCAGCTGTCGTAAGATA TTTCGGAATTTC
	Vp1974	AGTGTTTTATGATCAGTGCCTGT
Verification primer	VpCEP-fw	GCTATGCCATAGCATTTTTATCCATAAG

Table 11 A list and characteristics of plasmid used in this study

Plasmid	Genotype/Description	Reference
pCEP_kan	R6Kγ ori, oriT, araC, araBAD promoter, Kmr	(Bode et al., 2015)
pEB17	pDS132 derivative with an additional BglII recognition site, R6Kγ *ori*, *oriT*, *cipB* promoter, Km^r	(Bode et al., 2017)
pCEP *hfq*	pCEP *Xstockiae_RT25.5*, *araBAD* promoter, Km^r	This study
pEB17 *plu1818*	pEB17 *Xstockiae_RT25.5*, *cipB* promoter, Km^r	This study
pEB17 *plu1819*	pEB17 *Xstockiae_RT25.5*, *cipB* promoter, Km^r	This study
pEB17 *plu2894*	pEB17 *Xstockiae_RT25.5*, *cipB* promoter, Km^r	This study
pEB17 *plu2891*	pEB17 *Xstockiae_RT25.5*, *cipB* promoter, Km^r	This study
pEB17 *plu1972*	pEB17 *Xstockiae_RT25.5*, *cipB* promoter, Km^r	This study
pEB17 *plu1974*	pEB17 *Xstockiae_RT25.5*, *cipB* promoter, Km^r	This study
pEB17 *plu1819*	pEB17 *Xstockiae_RT25.5*, *cipB* promoter, Km^r	This study

Studying the antimicrobial activity of the bacterial extract

1. Preparation of crude compound extraction

Single colony of entomopathogenic bacteria on NBTA was inoculated into 500 ml tryptone soya broth (TSB) and incubated at room temperature with shaking at 150 rpm for 48 h. The culture was successively extracted with 1 L of ethyl acetate. The mixture was allowed to stand at room temperature at least 24 h before concentrated with

a rotary evaporator (Büchi, Konstanz, Germany) at 40°C under reduced pressure. Dried extracts were kept in airtight containers, labelled, and stored in a -20 °C until required for use.

2. Antimicrobial activities

The antibacterial activities of the bacterial extract with ethyl acetate were assessed using a disk diffusion assay were performed in triplicate against a panel of clinically relevant gram-negative and gram-positive pathogens (Table 12) including *Acinetobacter baumannii* (four clinical strains), *Escherichia coli* (two clinical strains), *E. coli* ATCC35218, *Klebsiella pneumoniae* (two clinical strains), *K. pneumoniae* ATCC700603, *Enterococcus faecalis* ATCC51299, *Staphylococcus aureus* (two clinical strains), and *S. aureus* ATCC20475. The experimental procedure involved preparing agar plates by applying pathogenic cells at a concentration of 5×10^5 CFU/mL on Muller Hinton agar (MHA) plates obtained from Oxoid Ltd., England. Standardized antibiotics corresponding to the test organisms were subsequently added to the agar plates. Sterile discs with the crude extract of the collected strains were then placed onto the agar surface. The plates were incubated at a temperature of 37°C for a duration of 24 hours. Afterwards the presence of clear zones surrounding the discs which indicated inhibition of bacterial growth were measured.

Table 12 List of antibiotic-resistant bacteria and corresponding standard antibiotics used as positive controls

Bacteria	Type	Antibiotic Disc
***Acinetobacter baumannii* AB320**	XDR[1]	Tigecycline
***Acinetobacter baumannii* AB321**	MDR[2]	Tigecycline
***Acinetobacter baumannii* AB322**	MDR[2]	Tigecycline
***Acinetobacter baumannii* AB324**	XDR[1]	Tigecycline
***Escherichia coli* ATCC 35218**	β-lactam	Ceftazidime
***Escherichia coli* PB1**	ESBL[3] + MDR[2]	Amoxicillin
***Escherichia coli* PB231**	ESBL[3] + CRE[4]	Amoxicillin
***Escherichia coli* PB30**	MDR[2]	Ceftazidime
***Klebsiella pneumonia* ATCC 700603**	ESBL[3]	Ceftazidime / clavulanic acid
***Klebsiella pneumonia* PB5**	ESBL[3] + MDR[3]	Ceftazidime / clavulanic acid

Table 12 (Cont.)

Bacteria	Type	Antibiotic Disc
***Klebsiella pneumonia* PB21**	ESBL[3] + CDR[5]	Ceftazidime / clavulanic acid
***Staphylococcus aureus* ATCC 20475**	MRSA[6]	Vancomycin
***Staphylococcus aureus* PB36**	MRSA[6]	Ampicillin
***Staphylococcus aureus* PB57**	MRSA[6]	Ampicillin
***Enterococcus faecalis* ATCC 51299**	MDR[2]	Ampicillin

[1]XDR (Extensive Drug Resistance), [2]MDR (multidrug resistance), [3]ESBL (Extended-spectrum beta-lactamases), [4]CRE (Carbapenam Resistant Enerobacteriacea), [5]CDR, [6]MRSA (Methicillin-resistant *Staphylococcus aureus*). 1. *Acinetobacter baumannii* (Resistant to multiple antibiotics): Amikacin, Colistin 2. *Escherichia coli* (Resistant to specific antibiotics): Ampicillin, Ciprofloxacin 3. *Klebsiella pneumoniae* (Resistant to multiple antibiotics): Meropenem, Gentamicin 4. *Enterococcus faecalis* (Resistant to specific antibiotics): Vancomycin, Linezolid 5. *Pseudomonas aeruginosa* (Resistant to multiple antibiotics): Tobramycin, Piperacillin/Tazobactam 6. *Staphylococcus aureus* (Methicillin-resistant): Methicillin, Vancomycin.

3. Determination of Minimum Inhibitory Concentration (MIC) and Minimum Bactericidal Concentrations (MBC)

The zone of inhibition against the most critical drug-resistant bacteria was determined and selected for further in-depth tests. The minimum inhibitory concentration (MIC) and minimum bactericidal concentration (MBC) were determined in triplicate using the microdilution method. The test medium used for the determination of MICs is Mueller Hinton Broth (cation-adjusted) (MHB ca+). Additionally, a time-kill assay was performed to evaluate the effect of the crude extract on bacterial growth. The crude extraction was diluted with DMSO to make a final concentration of 500 mg/ml. This stock was then serially dilute to obtain concentrations starting from 125 to 2 mg/ml. Then, 25 ul of 24 h cultured of drug resistance bacteria will be added to each well and incubated at 37˚C for 24 h. The MICs were determined by visual examination. The MIC was defined as the lowest concentration of crude extraction that prevented visible growth of the test organisms. In addition, the minimum

bactericidal concentrations (MBC) were evaluated. 10 µl from each well of 96-well microtiter plates from MIC was sub-cultured onto the MHA plates. The plates were incubated at 37°C for 24 h. The lowest concentration of each extract without growth of bacteria were considered.

4. Time kill assay

Concentrations equal to MIC of the extracts were prepared in MHB ca+. An inoculum size of 10^5 CFU/mL of antibiotic resistance bacteria was added. The mixtures were incubated at 37°C. Aliquots of 1. 0 mL of the mixture was taken at time intervals of 0, 0.5, 1, 2, 3, 4, 5, 6, 7, 8, 9, 10, 11, 12, and 24 h and dropped aseptically on MHA. All plates were incubated at 37 °C for 24 hours. A control test was conducted using organisms without the extracts or reference antibiotic. The colony-forming units (CFU) of the organisms were counted. The experiment was performed in triplicate (three independent trials), and a graph plotting log CFU/mL against time was generated. The data was analyzed statistically using a one-way analysis of variance (ANOVA) followed by multiple comparisons with Bonferroni correction (STATA version 13). A P-value of less than 0.05 was considered statistically significant.

5. Transmission electron microscopy

Transmission electron microscopy (TEM) was employed to observe the ultrastructural morphology of bacteria after exposure to the extracts. TEM sample preparation was conducted following an 18-hour preincubation at 37°C. *Acinetobacter baumannii* AB320 was adjusted to a final concentration of approximately 5×10^5 CFU/ml using spectrophotometric measurements. The bacteria were cultured in two conditions: in the absence of the extract (control) and in the presence of ½ MIC of the extract for 4 hours. Afterward, the cultures were harvested by centrifugation at 6000 rpm for 15 minutes at 4°C, and the pellets were fixed in 2.5% glutaraldehyde (Electron Microscope Sciences; EMS) in 0.1 M phosphate buffer (pH 7.2) for 12 hours. The samples were carefully washed twice with 0.1 M phosphate buffer. Post-fixation was carried out with 1% osmium tetroxide (EMS) in 0.1 M phosphate buffer (pH 7.2) for 2 hours at room temperature. Following further washing, the samples were dehydrated using graded ethanol (20%, 40%, 60%, 80%, and 100%) for 15 minutes at each concentration. Infiltration and embedding were then be done using Spurr's resin (EMS). The samples were sectioned with an ultramicrotome using a diamond knife and

mounted onto copper grids. Finally, the ultrathin sections were counterstained with 2% (w/v) uranyl acetate for 3 minutes and 0.25% (w/v) lead citrate for 2 minutes. After staining, the specimens were examined using a transmission electron microscope (JEOL, Tokyo, Japan) at 80 kV.

Proteomic analysis

Acinetobacter baylyi was used as a model organism instead of *A. baumannii* strain AB320 due to biosafety limitations, as *A. baylyi* is a non-pathogenic strain. Quadruplicate cultures of *A. baylyi* were grown in LB medium containing the crude extract of *X. stockiae* strain RT25.5 at a concentration of 1× MIC. Bacterial cells were cultured until an optical density (OD_{600}) of 1 was reached, which took approximately 4 hours. Subsequently, 2 mL aliquots of the culture were transferred to reaction tubes and washed twice with PBS buffer. The cell pellets were resuspended in 300 µL of lysis buffer containing 100 mM ammonium bicarbonate, 0.5% sodium lauroyl sarcosinate (SLS), and 5 mM Tris(2-carboxyethyl)phosphine (TCEP). Cells were lysed by incubating for 5 minutes at 95°C followed by 10 seconds of ultra-sonication (Vial Tweeter, Hielscher). After a 30-minute incubation at 90°C, the lysate was alkylated with 10 mM iodoacetamide for 30 minutes at 25°C. To clarify the lysate, the samples were centrifuged for 10 minutes at 15,000 rpm, and the supernatant was transferred to a new tube. Proteins in the lysate were digested overnight with 1 mg of trypsin (Promega) at 30°C. To remove the SLS, trifluoroacetic acid (TFA) was added to a final concentration of 1.5%, and the samples were left to stand at room temperature for 10 minutes. The samples were then centrifuged for 10 minutes at 10,000 rpm, and the supernatant was used for C18 peptide purification.

Peptide purification was carried out using C18 microspin columns according to the manufacturer's instructions (Harvard Apparatus). The eluted peptide solutions were dried and resuspended in 0.1% TFA. Peptide concentrations were determined using a colorimetric peptide assay (Quantitative Colorimetric Peptide Assay, Thermo Fischer Scientific). Peptide analysis was performed using liquid chromatography-mass spectrometry on a Q-Exactive Plus mass spectrometer, coupled with an Ultimate 3000 RSLC nano system, equipped with a Prowflow upgrade and nanospray flex ion source (Thermo Scientific). Peptide separation was achieved on a reverse-phase HPLC column

(75 mm x 42 cm), packed in-house with C18 resin (2.4 µm, Dr. Maisch GmbH, Germany). The separation gradient used was as follows: 98% solvent A (0.15% formic acid) and 2% solvent B (99.85% acetonitrile, 0.15% formic acid) to 25% solvent B over 105 minutes, and to 35% solvent B over the next 35 minutes at a flow rate of 300 nL/min.

Data acquisition was set to acquire one high-resolution MS scan at a resolution of 70,000 full width at half maximum (at m/z 200), followed by MS/MS scans of the 10 most intense ions. To optimize MS/MS efficiency, the charge state screening mode was enabled to exclude unassigned and singly charged ions. The dynamic exclusion duration was set to 30 seconds. The ion accumulation time was set to 50 ms for MS scans and 50 ms at 17,500 resolutions for MS/MS scans. The automatic gain control was set to 3x10^6 for MS survey scans and 1x10^5 for MS/MS scans. Label-free quantification (LFQ) was performed using Progenesis QIP (Waters), and MS/MS searches of aligned peptide features were conducted using MASCOT (v2.5, Matrix Science). The following search parameters were applied: a full tryptic search with two missed cleavage sites, 10 ppm MS1 tolerance, and 0.02 Da fragment ion tolerance. Carbamidomethylation (C) was set as a fixed modification, and oxidation (M) and deamidation (N,Q) were set as variable modifications. The Progenesis output data was further analyzed with SafeQuant, and volcano plots were generated using RStudio. To create a volcano plot in R for differential gene expression visualization, start by loading the required libraries(`tidyverse`, `RColorBrewer`, and `ggrepel` for annotations). Set the working directory and import the dataset containing gene symbols, p-values, p-adjusted values, and log2 fold changes. Begin with a basic volcano plot using `ggplot2`, plotting log2 fold change on the x-axis and -log10 p-values on the y-axis. Then, add threshold lines to distinguish upregulated (log2FC > 0.6), downregulated (log2FC < -0.6), and statistically significant genes ($p < 0.05$). Customize the plot further to enhance its readability and visual appeal.

CHAPTER IV

RESULTS

Genome sequencing and analysis

After conducting *de novo* assembly and annotation for all 13 bacterial draft genomes, a comparative analysis of their genetic and biosynthetic diversity was undertaken to prioritize these entomopathogenic bacteria for novel chemotype discovery, thereby reducing redundant investigations. The analysis commenced with general characterization, as summarized in Table 13, which detailed genome size, gene predictions, G+C content, and overall genome quality, ensuring a robust annotation process. Subsequently, a pan and core genome analysis were conducted. to examine the complete gene set, including core genes (common to all strains), accessory genes (shared by specific groups), and singleton genes (unique to individual strains). This analysis identified a total of 51,883 genes distributed across 13 genomes, organized into 10,821 gene clusters. These clusters comprise 1,763 core genes, 5,033 accessory genes, and 4,024 singleton genes (Figure 11), providing critical insights into the genetic diversity, evolutionary connections, and functional potential of the strains.

Following this, antiSMASH software was utilized for an initial evaluation of the bacterial BGCs. Across the 13 genomes, a total of 314 BGCs were identified. The highest biosynthetic diversity was observed in *X. indica* KK26.2 and *X. vietnamensis* NN167.3, followed by *P. temperata* MW27.4, *P. akhurstii* NN168.5, *P. hainaensis* NN169.4, *P. laumondii* MH8.4, *X. miraniensis* MH16.1, and *X. ehlersii* MH9.2. In contrast, the lowest BGC diversity was found in *P. australis* SBR15.4, *X. stockiae* RT25.5, SBRx11.1, and SBR31.4, as well as *X. japonica* MW12.3. In addition, the comparative analysis of BGCs revealed that nonribosomal peptide synthetases (NRPS) were the predominant class in both *Xenorhabdus* and *Photorhabdus* genomes. Which accounted for 51% of the total BGCs. The "others" and hybrid groups exhibited the second and third highest levels of enrichment and distribution, respectively. PKS, RiPPs, and terpene clusters were fairly low. Certain clusters were widely shared, particularly those resembling known BGCs responsible for betalactone (Shi et al., 2022) production, followed by GameXpeptides (Gxps) clusters (Friederike et al., 2015) and

photoxenobactin-associated clusters (Shi et al., 2022). Despite the broad diversity of BGCs across genomes, specific clusters were limited to particular strains. For example, acinetobactin, ATred, butyrolactone, cuidadopeptide, PAX peptide, and RXPs were prevalent only in *X. stockiae* genomes. Additionally, unique discoveries included althiomycin clusters in *X. indica* KK26.2, andrimid clusters in *P. temperata* MW27.4, and malonomycin clusters in *P. akhurstii* NN168.5. These findings highlight these strains as promising candidates.

Table 13 A summary of the strains used in the preliminary analysis and their general characteristics across all genomes. The sequences have been submitted under project PRJNA990961.

Features / Bacteria Code	***P. akhurstii* NN168.5**	***P. australis* SBR15.4**	***P. hainanensis* NN169.4**	***P. laumondii* MH8.4**	***P. temperata* MW27.4**	***X. ehlersii* MH9.2**	***X. indica* KK26.2**	***X. japonica* MW12.3**	***X. miraniensis* MH16.1**	***X. stockiae* RT25.5**	***X. stockiae* SBR31.4**	***X. stockiae* SBRx11.1**	***X. vietnamensis* NN167.3**
Entomopathogenic nematode host	NA	*H. indica*	NA	*H.* sp. SGmg3	*H. zealandica*	*S. scarabaei*	*Steinernema* sp.	*S. kushidai*	*S. websteiri*	NA	*S. surkhetense*	NA	NA
Accession number	SAMN 36278239	SAMN 36278238	SAMN 36278241	SAMN 36278240	SAMN 36278242	SAMN 36278243	SAMN 36278244	SAMN 36278245	SAMN 36278246	SAMN 36278249	SAMN 36278248	SAMN 36278247	SAMN 36278250
Estimated genome size	5,629,344	4,699,665	5,260,969	4,937,123	5,247,567	3,916,271	4,506,415	3,495,382	4,378,409	4,509,455	4,496,578	4,509,288	4,654,759
Number of predicted genes	4,805	4,152	4,337	4,351	4,582	3,383	3,907	3,008	3,739	3,921	3,832	3,919	3,947
Num Contigs	79	87	50	110	161	47	95	52	80	132	52	132	83
Num Contigs > 100 kb	18	12	20	13	9	14	14	13	16	6	17	6	15
Num Contigs > 50 kb	32	32	28	33	29	21	38	24	24	34	29	34	33

Table 13 (Cont.)

Features / Bacteria Code	*P. akhurstii* NN168.5	*P. australis* SBR15.4	*P. hainanensis* NN169.4	*P. laumondii* MH8.4	*P. temperata* MW27.4	*X. ehlersii* MH9.2	*X. indica* KK26.2	*X. japonica* MW12.3	*X. miraniensis* MH16.1	*X. stockiae* RT25.5	*X. stockiae* SBR31.4	*X. stockiae* SBRx11.1	*X. vietnamensis* NN167.3
Num Contigs > 10 kb	55	63	44	83	100	39	66	40	48	96	44	96	69
Num Contigs > 5 kb	66	73	49	94	129	44	84	45	61	111	48	111	75
Num Contigs > 2.5 kb	79	87	50	110	161	47	95	52	80	132	52	132	83
Longest Contig	429,773	250,279	458,435	289,965	320,441	604,063	233,439	378,067	319,343	185,193	283,943	185,483	300,582
Shortest Contig	2,679	2,612	3,974	2,707	2,537	3,204	2,595	2,766	2,608	2,687	3,386	2,687	2,501
Num Genes (prodigal)	4,805	4,152	4,337	4,351	4,582	3,383	3,907	3,008	3,739	3,921	3,832	3,919	3,947
L50[1]	11	14	10	18	22	7	17	9	10	26	10	25	15
L75	23	29	19	37	50	15	32	19	20	49	20	49	29
L90	38	47	29	61	83	24	49	29	34	76	31	76	46

Table 13 (Cont.)

Features / Bacteria Code	*P. akhurstii* NN168.5	*P. australis* SBR15.4	*P. hainanensis* NN169.4	*P. laumondii* MH8.4	*P. temperata* MW27.4	*X. ehlersii* MH9.2	*X. indica* KK26.2	*X. japonica* MW12.3	*X. miraniensis* MH16.1	*X. stockiae* RT25.5	*X. stockiae* SBR31.4	*X. stockiae* SBRx11.1	*X. vietnamensis* NN167.3
N50[2]	161,766	91,246	168,036	83,047	66,115	176,708	93,815	128,329	162,938	62,766	154,677	64,259	101,518
N75	79,874	57,975	107,734	46,313	32,744	92,215	62,268	65,480	73,980	34,367	81,111	34,367	56,847
N90	42,852	30,276	46,728	21,575	14,617	37,737	25,029	40,821	30,364	17,541	47,989	17,541	31,150
Number of predicted BGCs by antiSMASH	26	19	24	23	26	20	28	18	21	19	18	19	28

[1] L50 is the minimum number of contigs required to reach 50% of the genome, with a lower L50 reflecting a more contiguous assembly.

[2] N50 represents the length of the shortest contig (or scaffold) that, when combined with longer contigs, covers at least 50% of the total genome assembly. A higher N50 indicates greater assembly continuity. These metrics help evaluate genome completeness and fragmentation, where an ideal assembly has a high N50 and a low L50, indicating fewer but longer contigs.

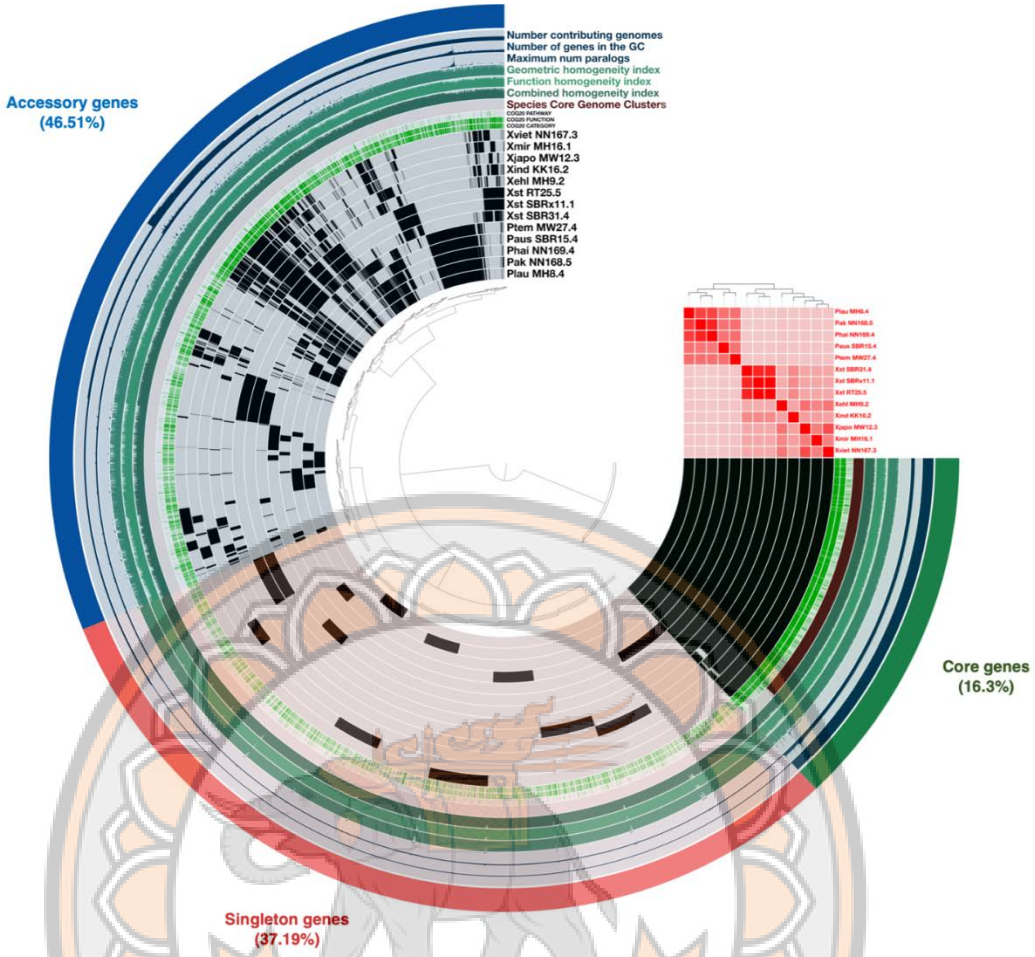

Figure 11 The detailed visualization of the pan- and core-genome analysis incorporates an average nucleotide identity (ANI) layer

A circular dendrogram was generated based on the presence or absence of gene clusters. Each genome is represented as a circle, containing all genes (depicted in black) from the 13 bacterial genomes. Moving inward from the outermost layer, the diagram distinguishes core genes (green), accessory genes (blue), and singleton genes (red). The figure also includes additional data such as the number of genes in the gene cluster (GC), the maximum number of paralogs, the geometric homogeneity index, the functional homogeneity index, the combined homogeneity index, Species Core Genome (SCG) clusters, Cluster of Orthologous Groups (COG20) categories, COG20 functions, and COG20 pathways.

After manually verifying the antiSMASH results with our in-house database, the filtered data were analyzed using BiG-SCAPE/CORASON (Navarro-Muñoz et al., 2020). BiG-SCAPE organizes BGCs identified by antiSMASH into gene cluster families (GCFs) based on sequence similarity. Meanwhile, CORASON establishes phylogenetic relationships among the detected BGCs and the generated GCFs. These tools facilitate the exploration of BGCs diversity across large genome datasets by constructing BGC sequence similarity networks, grouping BGCs into GCFs, and linking gene cluster diversity to enzyme phylogenies. Together, they provide powerful approaches for identifying novel compounds. Here we reported 181 potential biosynthetic clusters remains from 314 clusters due to limited information from the predicted modules. (Table 14). 181 putative BGCs including 92 NRPS, 8 PKS, 22 hybrids, 6 Terpenes, 15 RiPPs, 1 lanthipeptide, and 37 others as depicted in Figure 12 and Table 14. Among the remaining clusters, 145 showed similarity to known BGCs, while 36 clusters belonged to unrelated groups with no homologous gene clusters identified implying the potential novelty of the metabolites related to these clusters. Considering this analysis, the strains *X. stockiae* RT25.5, *X. stockiae* SBRx11.1, *X. japonica* MW12.3, *X. indica* KK26.2, *X. miraniensis* MH16.1, *P. akhurstii* NN168.5, *P. temperata* MW27.4, and *P. hainanensis* NN169.4 are particularly promising candidates for further exploration in the discovery of novel compounds. When applying comparative analysis, *X. stockiae* RT25.5, *X. stockiae* SBRx11.1, *X. indica* KK26.2, *P. temperata* MW27.4, and *P. hainanensis* NN168.5 stand out as strong candidates for experimental natural product discovery due to their richness in unique and unknown clusters.

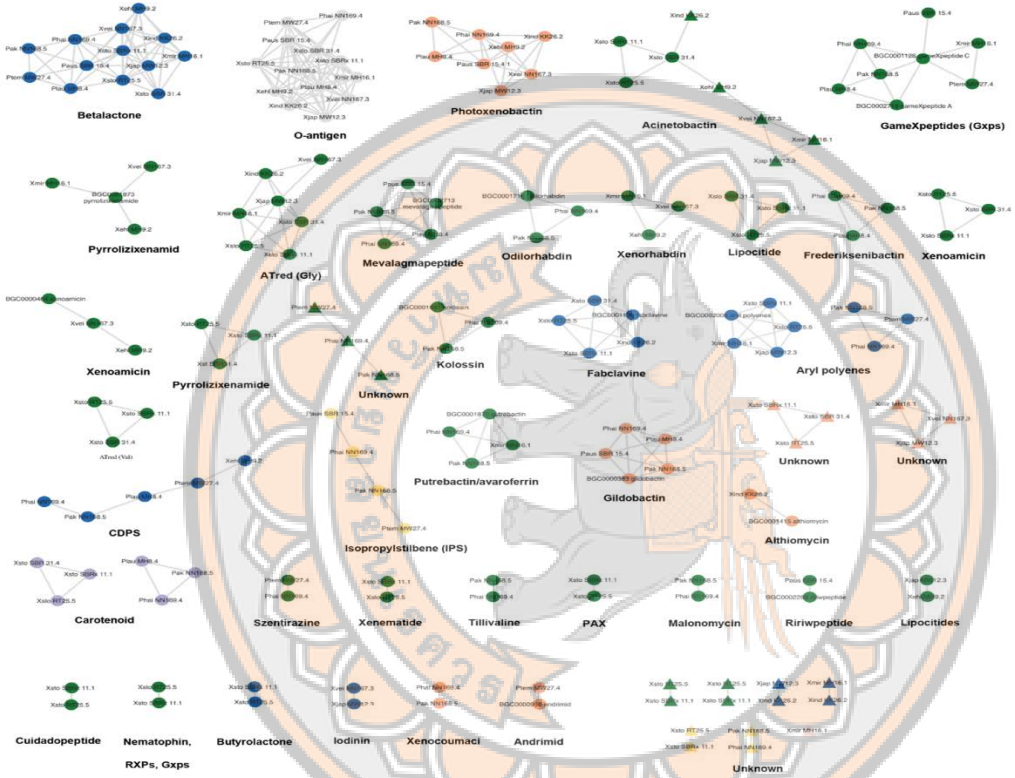

Figure 12 A sequence-based similarity network of BGCs across 13 genomes

The network displays identified BGCs, with circular shapes representing known BGCs and triangular shapes representing unknown BGCs. These clusters are categorized by type: NRPS (green), PKS (yellow), hybrid (orange), RiPPs (gray), terpene (purple), and others (blue).

Table 14 Explorations and classifications of annotated BGCs across 13 genomes

No.	XP isolates	Region	Clusters type	Predicted compounds
1	*P. hainaensis*	Phai NN169.4 region 1.1	NRP+Polyketide	Xenocoumacin
2	*P. hainaensis*	Phai NN169.4 region 1.2	NRPS	Szentirazine like
3	*P. hainaensis*	Phai NN169.4 region 10.1	NRPS	Frederiksenibactin
4	*P. hainaensis*	Phai NN169.4 region 11.2	NRP+Polyketide	Photoxenobactin
5	*P. hainaensis*	Phai NN169.4 region 13.1	NRPS	tillivaline
6	*P. hainaensis*	Phai NN169.4 region 16.1	NRPS.independent. siderophore	Putrebactin
7	*P. hainaensis*	Phai NN169.4 region 17.1	NRPS	Odilorhabdin
8	*P. hainaensis*	Phai NN169.4 region 18.1	RiPPs	O-antigen
9	*P. hainaensis*	Phai NN169.4 region 2.1	NRPS	Gxps
10	*P. hainaensis*	Phai NN169.4 region 25.1	NRPS	Mevalagmapeptide
11	*P. hainaensis*	Phai NN169.4 region 3.1	NRPS	Unknown
12	*P. hainaensis*	Phai NN169.4 region 3.2	Others	Betalactone
13	*P. hainaensis*	Phai NN169.4 region 34.1	RiPPs	O-antigen
14	*P. hainaensis*	Phai NN169.4 region 4.1	NRPS	Kolossin
15	*P. hainaensis*	Phai NN169.4 region 49.1	PKS	Unknown
16	*P. hainaensis*	Phai NN169.4 region 5.1	NRP+Polyketide	Glidobactin
17	*P. hainaensis*	Phai NN169.4 region 6.1	Others	Arylpolyene
18	*P. hainaensis*	Phai NN169.4 region 6.2	PKS	Isopropylstilbene (IPS)
19	*P. hainaensis*	Phai NN169.4 region 7.1	Others	CDPS
20	*P. australis*	Phai NN169.4 region 1.3	Terpene	Carotenoid
21	*P. hainaensis*	Phai NN169.4 region 9.1	NRPS	Malonomycin
22	*P. laumondii*	PLau MH8.4 region 1.1	NRP+Polyketide	Glidobactin
23	*P. laumondii*	PLau MH8.4 region 10.1	Others	CDPS
24	*P. laumondii*	PLau MH8.4 region 11.1	NRPS	Gxps
25	*P. laumondii*	PLau MH8.4 region 19.2	RiPPs	O-antigen
26	*P. laumondii*	PLau MH8.4 region 3.1	NRP+Polyketide	Photoxenobactin
27	*P. laumondii*	PLau MH8.4 region 38.1	RiPPs	O-antigen
28	*P. laumondii*	PLau MH8.4 region 4.1	NRPS	Frederiksenibactin
29	*P. laumondii*	PLau MH8.4 region 5.1	NRPS	Mevalagmapeptide
30	*P. australis*	Plau MH8.4 region 79.1	Terpene	Carotenoid
31	*P. laumondii*	PLau MH8.4 region 9.1	Others	Betalactone
32	*P. akhurstii*	Pak NN168.5 region 28.1	Terpene	Carotenoid

Table 14 (Cont.)

No.	XP isolates	Region	Clusters type	Predicted compounds
33	*P. akhurstii*	Pak NN168.5 region 1.1	NRP+Polyketide	Xenocoumacin
34	*P. akhurstii*	Pak NN168.5 region 12.1	Others	CDPS
35	*P. akhurstii*	Pak NN168.5 region 13.1	NRPS	Gxps
36	*P. akhurstii*	Pak NN168.5 region 15.1	NRPS	Odilorhabdin
37	*P. akhurstii*	Pak NN168.5 region 16.1	Others	Betalactone
38	*P. akhurstii*	Pak NN168.5 region 2.1	NRP+Polyketide	Photoxenobactin
39	*P. akhurstii*	Pak NN168.5 region 24.1	NRPS	Malonomycin
40	*P. akhurstii*	Pak NN168.5 region 3.1	NRP+Polyketide	Glidobactin
41	*P. akhurstii*	Pak NN168.5 region 3.2	RiPPs	O-antigen
42	*P. akhurstii*	Pak NN168.5 region 41.1	NRPS	Unknown
43	*P. akhurstii*	Pak NN168.5 region 5.1	NRPS.independent. siderophore	Putrebactin
44	*P. akhurstii*	Pak NN168.5 region 5.2	NRPS	Tillivaline
45	*P. akhurstii*	Pak NN168.5 region 6.1	NRPS	Kolossin
46	*P. akhurstii*	Pak NN168.5 region 6.2	NRPS	Frederiksenibactin
47	*P. akhurstii*	Pak NN168.5 region 64.1	PKS	Unknown
48	*P. akhurstii*	Pak NN168.5 region 7.1	Others	Arylpolyene
49	*P. akhurstii*	Pak NN168.5 region 7.2	PKS	Isopropylstilbene (IPS)
50	*P. akhurstii*	Pak NN168.5 region 9.1	NRPS	Mevalagmapeptide
51	*P. australis*	Paus SBR 15.4 region 51.1	NRPS	Mevalagmapeptide
52	*P. australis*	Paus SBR15.4 region 11.1	PKS	Isopropylstilbene (IPS)
53	*P. australis*	Paus SBR15.4 region 13.1	NRP+Polyketide	Glidobactin
54	*P. australis*	Paus SBR15.4 region 25.1	NRPS	Ririwpeptide
55	*P. australis*	Paus SBR15.4 region 34.1	NRP+Polyketide	Photoxenobactin
56	*P. australis*	Paus SBR15.4 region 46.1	NRPS	Gxps
57	*P. australis*	Paus SBR15.4 region 7.1	Others	Betalactone
58	*P. australis*	Paus SBR15.4 region 8.1	RiPPs	O-antigen
59	*P. temperata*	Ptem MW27.4 region 2.2	Others	Betalactone
60	*P. temperata*	Ptem MW27.4 region 20.1	NRP+Polyketide	Andrimid
61	*P. temperata*	Ptem MW27.4 region 25.1	NRPS	Unknown

Table 14 (Cont.)

No.	XP isolates	Region	Clusters type	Predicted compounds
62	*P. temperata*	Ptem MW27.4 region 4.1	PKS	Isopropylstilbene (IPS)
63	*P. temperata*	Ptem MW27.4 region 40.1	Others	CDPS
64	*P. temperata*	Ptem MW27.4 region 41.1	NRPS	Szentirazine like
65	*P. temperata*	Ptem MW27.4 region 47.1	NRPS	Gxps
66	*P. temperata*	Ptem MW27.4 region 58.1	Others	Arylpolyene
67	*P. temperata*	Ptem MW27.4 region 64.1	RiPPs	O-antigen
68	*X. ehlersii*	Xehl MH9.2 region 1.1	Others	Betalactone
69	*X. ehlersii*	Xehl MH9.2 region 1.2	NRPS	Unknown
70	*X. ehlersii*	Xehl MH9.2 region 17.1	NRPS	Pyrrolizixenamide
71	*X. ehlersii*	Xehl MH9.2 region 2.1	RiPPs	O-antigen
72	*X. ehlersii*	Xehl MH9.2 region 3.2	NRPS	Xenoamicin
73	*X. ehlersii*	Xehl MH9.2 region 5.1	NRP+Polyketide	Photoxenobactin
74	*X. ehlersii*	Xehl MH9.2 region 6.1	NRPS	Xenorhabdin
75	*X. ehlersii*	Xehl MH9.2 region 8.1	Others	CDPS
76	*X. ehlersii*	Xehl MH9.2 region 9.1	NRPS	Lipocitides
77	*X. indica*	Xin KK26.2 region 1.1	Others	Fabclavine la
78	*X. indica*	Xin KK26.2 region 14.1	Others	Unknown
79	*X. indica*	Xin KK26.2 region 2.1	NRPS	Unknown
80	*X. indica*	Xin KK26.2 region 22.1	Others	Unknown
81	*X. indica*	Xin KK26.2 region 28.1	NRPS	ATred
82	*X. indica*	Xin KK26.2 region 34.1	RiPPs	O-antigen
83	*X. indica*	Xin KK26.2 region 44.1	NRP+Polyketide	Althiomycin
84	*X. indica*	Xin KK26.2 region 5.1	Others	Betalactone
85	*X. indica*	Xin KK26.2 region 7.1	NRP+Polyketide	Photoxenobactin
86	*X. japonica*	Xjap MW12.3 region 1.2	NRP+Polyketide	Photoxenobactin
87	*X. japonica*	Xjap MW12.3 region 16.1	NRPS	ATred
88	*X. japonica*	Xjap MW12.3 region 17.1	RiPPs	O-antigen
89	*X. japonica*	Xjap MW12.3 region 2.1	NRPS	Unknown
90	*X. japonica*	Xjap MW12.3 region 24.1	Others	Iodinin (phenazine)
91	*X. japonica*	Xjap MW12.3 region 3.1	Others	Arylpolyene
92	*X. japonica*	Xjap MW12.3 region 30.1	NRP+Polyketide	Unknown
93	*X. japonica*	Xjap MW12.3 region 38.1	NRPS	Unknown (fragment)
94	*X. japonica*	Xjap MW12.3 region 43.1	Others	Unknown

Table 14 (Cont.)

No.	XP isolates	Region	Clusters type	Predicted compounds
95	*X. japonica*	Xjap MW12.3 region 5.1	NRPS	Lipocitides
96	*X. japonica*	Xjap MW12.3 region 6.1	Others	Betalactone
97	*X. miraniensis*	Xmir MH16.1 region 1.1	RiPPs	O-antigen
98	*X. miraniensis*	Xmir MH16.1 region 1.3	NRPS.independent. siderophore	Putrebactin
99	*X. miraniensis*	Xmir MH16.1 region 16.2	NRPS	Pyrrolizixenamide
100	*X. miraniensis*	Xmir MH16.1 region 2.1	NRPS	Unknown
101	*X. miraniensis*	Xmir MH16.1 region 23.1	Others	Unknown
102	*X. miraniensis*	Xmir MH16.1 region 26.1	NRPS	Gxps
103	*X. miraniensis*	Xmir MH16.1 region 3.1	NRPS	Xenorhabdin
104	*X. miraniensis*	Xmir MH16.1 region 32.1	lanthipeptide.class.II	Unknown
105	*X. miraniensis*	Xmir MH16.1 region 32.1	NRP+Polyketide	Unknown
106	*X. miraniensis*	Xmir MH16.1 region 4.1	Others	Arylpolyene
107	*X. miraniensis*	Xmir MH16.1 region 4.2	NRPS	ATred
108	*X. miraniensis*	Xmir MH16.1 region 6.1	Others	Betalactone
109	*X. stockiae*	Xsto SBR31.4 region 5.1	NRPS	Pyrrolizixenamide
110	*X. stockiae*	Xsto SBR31.4 region 5.1	NRPS	ATred
111	*X. stockiae*	Xsto SBR31.4 region 25.1	NRPS	Acinetobactin/ metallophore
112	*X. stockiae*	Xsto SBR31.4 region 26.1	NRPS	lipocitides
113	*X. stockiae*	Xsto SBR31.4 region 35.1	Terpene	Carotenoid
114	*X. stockiae*	Xsto SBR31.4 region 4.1	NRPS	Xenoamicin
115	*X. stockiae*	Xsto SBR 31.4 region 3.2	Others	Betalactone
116	*X. stockiae*	Xsto SBR31.4 region 11.1	NRP+Polyketide	Unknown
117	*X. stockiae*	Xsto SBR31.4 region 31.1	NRPS	ATred
118	*X. stockiae*	Xsto SBR31.4 region 6.1	Others	Fabclavine la
119	*X. stockiae*	Xsto SBR31.4 region 13.1	RiPPs	O-antigen
120	*X. stockiae*	Xsto RT25.5 region 18.1	Terpene	Carotenoid
121	*X. stockiae*	Xsto RT25.5 region 15.1	RiPPs	O-antigen
122	*X. stockiae*	Xsto RT25.5 region 16.1	NRP+Polyketide	Unknown
123	*X. stockiae*	Xsto RT25.5 region 17.1	Others	Arylpolyene
124	*X. stockiae*	Xsto RT25.5 region 18.1	NRPS	Cuidadopeptide
125	*X. stockiae*	Xsto RT25.5 region 20.1	Others	Betalactone
126	*X. stockiae*	Xsto RT25.5 region 24.1	NRPS	Pyrrolizixenamide

Table 14 (Cont.)

No.	XP isolates	Region	Clusters type	Predicted compounds
127	*X. stockiae*	Xsto RT25.5 region 24.1	NRPS	ATred
128	*X. stockiae*	Xsto RT25.5 region 3.1	Others	Fabclavine la
129	*X. stockiae*	Xsto RT25.5 region 34.1	NRPS	ATred
130	*X. stockiae*	Xsto RT25.5 region 37.1	NRPS	Acinetobactin (NRP-metallophore)
131	*X. stockiae*	Xsto RT25.5 region 4.1	NRPS	Xenoamicin
132	*X. stockiae*	Xsto RT25.5 region 49.1	NRPS	Lipocitides
133	*X. stockiae*	Xsto RT25.5 region 56.1	Others	Butyrolactone
134	*X. stockiae*	Xsto RT25.5 region 58.1	NRPS	Unknown (fragment)
135	*X. stockiae*	Xsto RT25.5 region 59.1	NRPS	Unknown (fragment)
136	*X. stockiae*	Xsto RT25.5 region 61.1	NRPS	Xenematide
137	*X. stockiae*	Xsto RT25.5 region 8.1	PKS	Unknown
138	*X. stockiae*	Xsto RT25.5 region 8.1	NRPS	Unknown
139	*X. stockiae*	Xsto RT25.5 region 8.1	NRPS	Nematophin,
140	*X. stockiae*	Xsto RT25.5 region 8.1	NRPS	Rhabdopeptide (RXPs)
141	*X. stockiae*	Xsto RT25.5 region 8.1	NRPS	GameXpeptide
142	*X. stockiae*	Xsto RT25.5 region 81.1	NRPS	Unknown (fragment)
143	*X. stockiae*	Xsto RT25.5 region 85.1	NRPS	PAX (with glutamine)
144	*X. stockiae*	Xsto RT25.5 region 90.1	NRPS	Unknown (fragment)
145	*X. stockiae*	Xsto RT25.5 region 3.1	NRPS	Unknown
146	*X. stockiae*	Xsto SBRx11.1 region 18.1	Terpene	Carotenoid
147	*X. stockiae*	Xsto SBRx11.1 region 10.1	Others	Betalactone
148	*X. stockiae*	Xsto SBRx11.1 region 15.1	RiPPs	O-antigen
149	*X. stockiae*	Xsto SBRx11.1 region 16.1	NRP+Polyketide	Unknown
150	*X. stockiae*	Xsto SBRx11.1 region 17.1	Others	Arylpolyene
151	*X. stockiae*	Xsto SBRx11.1 region 18.1	NRPS	Cuidadopeptide
152	*X. stockiae*	Xsto SBRx11.1 region 24.1	NRPS	Pyrrolizixenamide
153	*X. stockiae*	Xsto SBRx11.1 region 24.1	NRPS	ATred
154	*X. stockiae*	Xsto SBRx11.1 region 3.1	Others	Fabclavine la
155	*X. stockiae*	Xsto SBRx11.1 region 34.1	NRPS	ATred
156	*X. stockiae*	Xsto SBRx11.1 region 37.1	NRPS	Acinetobactin (NRP-metallophore)
157	*X. stockiae*	Xsto SBRx11.1 region 4.1	NRPS	Xenoamicin

Table 14 (Cont.)

No.	XP isolates	Region	Clusters type	Predicted compounds
158	*X. stockiae*	Xsto SBRx11.1 region 49.1	NRPS	lipocitides
159	*X. stockiae*	Xsto SBRx11.1 region 56.1	Others	butyrolactone
160	*X. stockiae*	Xsto SBRx11.1 region 58.1	NRPS	Unknown (fragment)
161	*X. stockiae*	Xsto SBRx11.1 region 59.1	NRPS	Unknown (fragment)
162	*X. stockiae*	Xsto SBRx11.1 region 61.1	NRPS	Xenematide
163	*X. stockiae*	Xsto SBRx11.1 region 8.1	PKS	Unknown
164	*X. stockiae*	Xsto SBRx11.1 region 8.1	NRPS	Unknown
165	*X. stockiae*	Xsto SBRx11.1 region 8.1	NRPS	Nematophin
166	*X. stockiae*	Xsto SBRx11.1 region 8.1	NRPS	Rhabdopeptide (RXPs)
167	*X. stockiae*	Xsto SBRx11.1 region 8.1	NRPS	GameXpeptide
168	*X. stockiae*	Xsto SBRx11.1 region 81.1	NRPS	Unknown (fragment)
169	*X. stockiae*	Xsto SBRx11.1 region 85.1	NRPS	PAX (with glutamine)
171	*X. stockiae*	Xsto SBRx11.1 region 90.1	NRPS	Unknown (fragment)
172	*X. vietnamensis*	Xvei NN167.3 region 1.1	RiPPs	O-antigen
173	*X. vietnamensis*	Xvei NN167.3 region 10.1	Others	Betalactone
174	*X. vietnamensis*	Xvei NN167.3 region 12.1	Others	Iodinin (phenazine)
175	*X. vietnamensis*	Xvei NN167.3 region 15.1	NRPS	Unknown
176	*X. vietnamensis*	Xvei NN167.3 region 2.1	NRPS	Xenorhabdin
177	*X. vietnamensis*	Xvei NN167.3 region 22.1	NRP+Polyketide	Photoxenobactin
178	*X. vietnamensis*	Xvei NN167.3 region 24.1	NRPS	Xenoamicin
179	*X. vietnamensis*	Xvei NN167.3 region 35.1	NRPS	Pyrrolizixenamide
180	*X. vietnamensis*	Xvei NN167.3 region 42.1	NRP+Polyketide	Unknown
181	*X. vietnamensis*	Xvei NN167.3 region 5.1	NRPS	ATred
182	*X. vietnamensis*	Xvei NN167.3 region 55.1	NRPS	Unknown (fragment)

Out of the 36 unidentified clusters, 10 were excluded due to their BGCs being too short for analysis. The remaining clusters were further characterized and classified into ten putative BGCs. Among these, three were identified as NRPS clusters, two as type I T1PKS clusters, two displayed hybrid NRPS/PKS characteristics, and three were categorized under the “others” category.

NRPS Clusters: The nrpks-1 gene clusters were located in region 25.1 of *P. temperata* MW27.4, region 3.1 of *P. hainaensis* NN169.4, and region 24.1 of *P.*

akhurstii NN168.5 (Figure 13A). Spanning approximately 37 kb, these clusters contained over 30 biosynthetic genes but included only a single module, showing low sequence similarity to characterized NRPS clusters. As a result, their metabolites could not be predicted. The nrpks-2 gene clusters were found in region 3.1 of *X. stockiae* strain RT25.5, and *X. stockiae* SBRx11.1, (Figure 13B). Although these clusters were not fully sequenced and did not match existing database entries, they contained two modules, suggesting that their products are likely dipeptides, specifically hydrophobic-aliphatic peptides with valine (Val)–valine (Val) as the primary building blocks.

Type I T1PKS Clusters: In regions 8.1 of *X. stockiae* strain RT25.5, and *X. stockiae* SBRx11.1, one novel t1pks-1 cluster and one unidentified nrpks-3 cluster (Figure 13C) were identified. These clusters, named "*plu00736*" and "*plu00747*," respectively, did not match entries in the MIBiG, KnownClusterBlast, or in-house databases, highlighting their uniqueness and suggesting the presence of two novel compounds in this genomic region. The t1pks-1 gene clusters were hypothesized to contain domains such as PKS_KS (Modular-KS), PKS_AT (Modular-AT), PKS_DH (Modular-DH), and PKS_KR (Modular-KR), utilizing methylmalonyl-CoA as a substrate. Furthermore, within the t1pks-2 gene clusters located in region 64.1 of *P. akhurstii* (NN168.5) and region 49.1 of *P. hainaensis* (NN169.4), an 81.37% similarity was observed with t1pks-1 from *X. stockiae* region 8.1, except for the phosphopantetheine-binding protein (PP-binding) domain. These clusters may represent analogues of the same compound (Figure 13D).

Hybrid NRPS/PKS Clusters: The hybrid-1 gene clusters, containing both NRPS-like and T1PKS genes, were identified in region 16.1 of *X. stockiae* strain RT25.5 and SBRx11.1, and region 11.1 of *X. stockiae* SBR31.4. These clusters, spanning 57.4 kb, contained up to 40 related genes and featured an assembly line of seven modules. (Figure 13E). Based on assembly line predictions and substrate domains, these clusters were predicted to synthesize a compound resembling a bacterial small molecule commonly used as a protease inhibitor, as identified in the NORINE database (Figure 13F). This molecule is significant in autophagy and immunoproteasome research (Li et al., 2020). The *hybrid-2* gene clusters, a hybrid of NRPS-like and transAT-PKS-like genes, were found in region 32.1 of *X. miraniensis* MH16.1, region 42.1 of *X. veitnamensis* NN167.3, and region 30.1 of *X.*

japonica MW12.3. These clusters encoded proteins comprising five modules and one domain, predicted to incorporate cysteine (Cys) as substrates. The resulting products were hypothesized to be hexapeptides containing one cysteine molecule (Figure 13G, 14H). Other clusters; Among the remaining clusters, three distinct types were identified: Nucleotide-Related Clusters: Found in region 23.1 of *X. miraniensis* strain MH16.1 and region 22.1 of *X. indica* KK26.2. Phosphonate-Related Clusters: Detected in region 43.1 of *X. japonica* MW12.3 and region 14.1 of *X. indica* strain KK26.2. Lastly, Lanthipeptide-Class-II Clusters: Located in region 32.1 of *X. miraniensis* MH16.1.

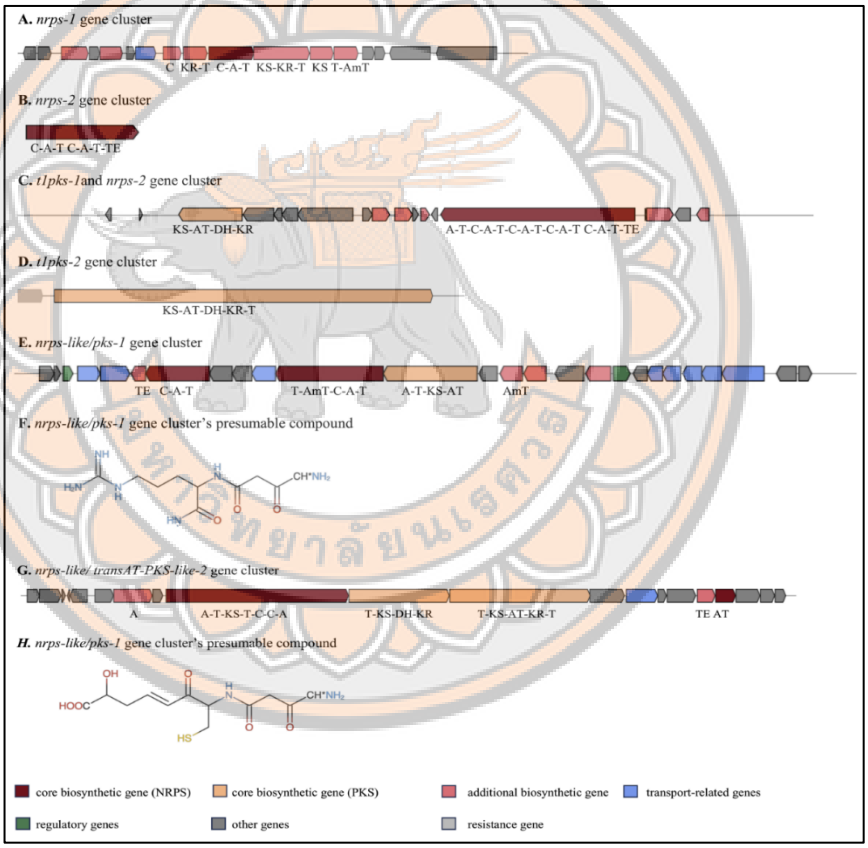

Figure 13 The summary of the domain composition and organization of the uncharacterized clusters

The clusters including *nrps-1* gene cluster (A), *nrps-2* gene cluster (B), *t1pks-1*and *nrps-2* gene cluster (C), *t1pks-2* gene cluster (D), *nrps-like/pks-1* gene cluster (E) and its presumable compound (F), and *nrps-like/ transAT-PKS-like-2* gene cluster (G) and its presumable compound (*H*)

Based on the results above, the strain *X. stockiae* RT25.5 was first selected for further studies, including complete genome sequencing, comparative genomics among *Xenorhabdus* species, secondary metabolite detection, antimicrobial activity assessments, preliminary mode of action analysis of its crude extract, promoter activation, and compound identification. The circular complete genome of strain RT25.5 was estimated to be 4.5 Mbp. The *de novo* genome assembly resulted in 10 contigs, with the largest contig spanning 1,082,361 bp. The observed average G + C content was 43.34%. A map of the complete chromosome of *X. stockiae* strain RT25.5 was created using the Proksee (Grant & Stothard, 2008) and is shown in figure 14. Most of the genes were associated with the metabolism of amino acids and their derivatives, cofactors, vitamins, prosthetic groups, pigments, and carbohydrates. Additional details regarding the annotated genome of strain RT25.5 are presented in Table 15.

Table 15 A summary of the general genomic features of the complete genome of *X. stockiae* strain RT25.5

Characteristics	Genome Annotation Data
Estimated genome size	4,586,701 bp
Total genes	4,050
Total Coding Sequences (CDSs)	3,941
Coding genes	3,858
CDSs with protein	3,858
RNA genes	109
rRNAs	8, 7, 7 (5S, 16S, 23S)
complete rRNAs	8, 7, 7 (5S, 16S, 23S)
tRNAs	79
ncRNAs	8
Total pseudo genes	83
CDSs without protein	83
Pseudo genes (ambiguous residues)	0 of 83
Pseudo genes (frameshifted)	26 of 83
Pseudo genes (incomplete)	61 of 83
Pseudo genes (internal stop)	13 of 83
Pseudo genes (multiple problems)	14 of 83

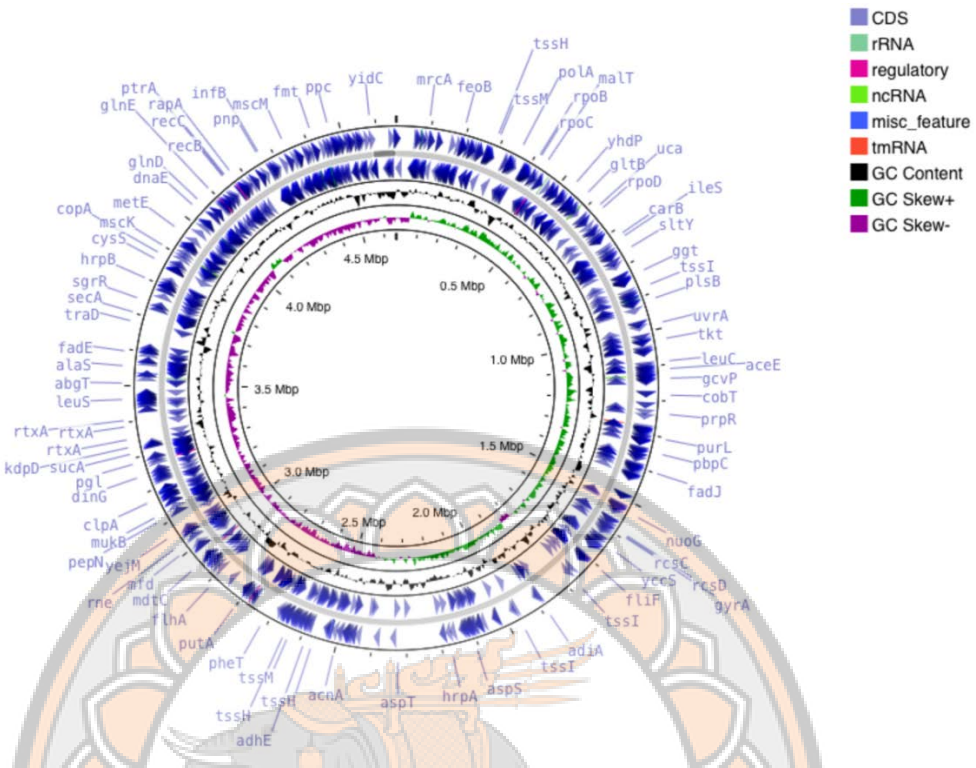

Figure 14 The map of the complete chromosome of *X. stockiae* strain RT25.5

Comparative genomics among the *Xenorhabdus* spp.

Further comparison of the genome of *X. stockiae* strain RT25.5 with publicly available *Xenorhabdus* genomes in the National Center for Biotechnology Information (NCBI) database was performed. At present, 122 *Xenorhabdus* spp. genome sequences have been deposited in the database, including 9 complete and 113 draft genome sequences. These genome sequences were downloaded from the NCBI database, and their accession numbers were listed in Table 16. The genome sizes of the complete *Xenorhabdus* spp. strains ranged from 3.7 Mb to 4.8 Mb, and the GC contents ranged from 43.50 to 45.50 %. A phylogenetic tree revealed a close association between RT25.5 and *X. stockiae* DSM 17904 (Figure 16), with an average nucleotide identity (ANI) of 0.956. The results confirmed that both strains belong to the same species. In contrast, the ANI values of RT25.5 with other *Xenorhabdus* spp. were consistently below the suggested species boundary cut-off of 95–96% (Arahal, 2014).

Table 16 The genome sequences downloaded from the NCBI database

Assembly number	Organism name	Strain	Isolation country
ASM212754v1	*X. beddingii*	DSM4764	Australia: Queensland
ASM1774301v1	*X. budapestensis*	C72	China: Jilin
ASM338666v1	*X. cabanillasii*	DSM17905	USA: Texas
ASM812467v1	*X. doucetiae*	DSM17909	France
ASM96819v1	*X. doucetiae*	FRM16	France: Martinique
ASM190810v1	*X. eapokensis*	DL20	Vietnam
ASM361046v1	*X. ehlersii*	DSM16337	China
ASM190809v1	*X. thuongxuanensis*	30TX1	Vietnam
ASM263272v1	*X. hominickii*	DSM17903	Kenya
ASM1446723v1	*X. indica*	DSM17382	India
ASM90015535v1	*X. innexi*	HGB1681	NA
ASM263275v1	*X. ishibashii*	DSM22670	China
IMG-taxon 2684622846	*X. japonica*	DSM16522	Japan
IMG-taxon 2684622845	*X. koppenhoeferi*	ppDSM18168	USA: New Jersey
ASM263287v1	*X. kozodoii*	DSM17907	Russia
ASM263261v1	*X. miraniensis*	DSM17902	Australia; Queensland
ASM25295v1	*X. nematophila*	ATCC19061	NA
ASM263282v1	*X. stockiae*	DSM17904	Thailand
ASM212753v1	*X. vietnamensis*	DSM22392	Vietnam

Figure 15 A phylogenetic tree generated using whole genome sequences

Secondary metabolites biosynthetic gene clusters of complete *X. stockiae* strain RT25.5 genome

To identify the potential BGCs, the complete genome of *X. stockiae* RT25.5 were analyzed using antiSMASH (Kai et al., 2021), followed by manual refinements using MIBiG database (Barbara et al., 2023), previous public researches, and an in-hose database. A total of 21 biosynthetic gene clusters were identified including 13 NRPS, 4 Hybrid, 1 Terpene and 3 other clusters as shown in table 17. Notably, using antiSMASH, five clusters—clusters 2, 3, 4, 15, and 21—were identified as being associated with butyrolactone, aryl polyenes (Gina et al., 2019), fabclavine (Fuchs et al., 2014), carotenoid, and betalactone, respectively. Meanwhile, gene clusters 1, 6, 7, 8, 9, 10, 11, 12, 13, 16, 17, 18, and 19 were manually verified and found to share module structure similarities with known BGCs including ATRed (1) (Tietze et al., 2020), xenobactin (Grundmann et al., 2013), PAX (Dreyer et al., 2019), nematophin (Jianxiong, Genhui, & John, 1997), rhabdopeptide/xenortide-like peptides (RXPs)

(Reimer, 2013), GameXpeptide (Nollmann et al., 2015), cuidadopeptide (inhouse data), ATRed (2) (Tietze et al., 2020), pyrrolizixenamide (Olivia et al., 2015), and xenoamicin (Qiuqin et al., 2013), respectively. Intriguingly, the remaining three clusters (gene clusters 5, 14, and 20) did not match any known gene clusters, suggesting the potential novelty of the metabolites derived from these predicted gene clusters or existing compounds for which the modules could not be elucidated.

As for unknown BGCs, *cluster-5* represented high similar to lipopeptides (J. H. Li et al., 2021) which predicted chemical structure and module organization were shown in Figure 17. The hybrid T1PKS (Type I Polyketide Synthase) and NRPS (Non-Ribosomal Peptide Synthase) identified in *clusters-14* were previously discovered in the above study. Genes within these clusters include Type I polyketide synthase, transposase, non-ribosomal peptide synthase/polyketide synthase, and transposase, IS1 family transposase, tyrosine-type recombinase/integrase, three hypothetical proteins, universal stress protein UspE, FNR family transcription factor, dimethyl sulfoxide reductase anchor subunit, pyridoxal-dependent decarboxylase, TauD/TfdA family dioxygenase, class I SAM-dependent methyltransferase, and MFS transporter. Lastly, *cluster-20*, characterized as a hybrid NRPS+T1PKS, exhibited a 60% similarity with the putrebactin biosynthetic gene cluster from *X. budapestensis* which could be a novel analog due to the genes identified in *X. stockiae* strain RT25.5 showed significant differences from the reference strain.

Table 17 Secondary metabolite gene clusters annotated in *X. stockiae* strain RT25.5 using antiSMASH and our in-house database

The gene clusters included 13 nonribosomal peptide synthetases (NRPSs), 4 hybrids, 1 terpene and 3 other gene clusters.

Cluster	Type	From	To	Identified gene clusters	Approach	MiBIG ID/References
1	NRPS-like	463,189	504,807	ATred	manual	(Tietze et al., 2020)
2	Other	581,475	625,089	Aryl polyenes	antiSMASH (100%)	BGC0002008
3	Other	642,212	652,970	Butyrolactone	antiSMASH (100%)	Blin et al., 2021
4	Hybrid	1,421,197	1,485,269	Fabclavine Ia	antiSMASH (100%)	BGC0001872
5	NRPS	1,485,429	1,527,914	Unknown - lipopeptides	manual	NA
6	NRPS	1,678,984	1,690,725	Bovienimide A	manual	(Shi et al., 2022)
7	Hybrid	1,709,083	1,767,762	Acinetobactin	manual	BGC0000294
8	NRPS	1,897,190	1,915,359	Xenematide	manual	BGC0001826
9	NRPS	1,934,250	1,956,644	Xenobactin	manual	(Grundmann et al., 2013)
10	NRPS	2,014,205	2,076,576	PAX peptides	manual	Dreyer et al., 2019
11	NRPS	2,192,855	2,197,015	Nematophin	manual	BGC0001434
12	NRPS	2,197,503	2,211,741	Rhabdopeptide/xenortide-like peptides (RXPs)	manual	BGC0000416
13	NRPS	2,220,964	2,236,638	GameXpeptide	manual	BGC0002716
14	Hybrid	2,252,638	2,281,381	Unknown	manual	NA
15	Terpene	2,323,962	2,461,175	Carotenoid	antiSMASH (50%)	BGC0000640
16	NRPS	2,343,886	2,368,454	Cuidadopeptide	manual	Inhouse database
17	NRPS	2,398,339	2,401,344	ATred	manual	(Tietze et al., 2020)
18	NRPS	2,434,403	2,441,629	Pyrrolizixenamide	manual	BGC0001873
19	NRPS	2,793,938	2,877,007	Xenoamicin	manual	BGC0000464
20	Hybrid	3,464,983	3,522,468	Unknown	manual	NA
21	Other	3,717,582	3,743,022	Betalactone	antiSMASH (100%)	Blin et al., 2021

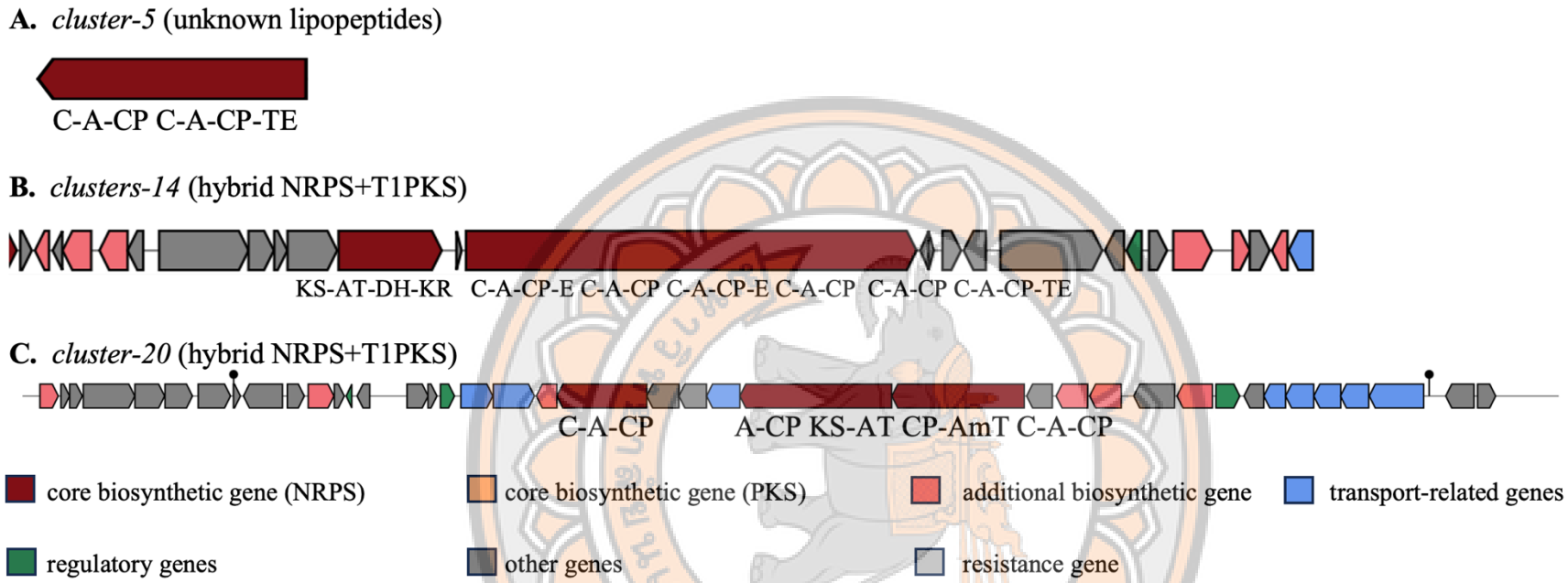

Figure 16 Summary of the domain composition and organization of the unidentified clusters

Detection of secondary metabolites produced using LC-MSMS analysis

The culture of strain RT25.5 was examined for bioactive compounds, leading to the identification of several compounds of interest. These included GameXPeptides A and C, Pyrrolo[1,2-a]pyrazine-1,4-dione, hexahydro-3-(phenylmethyl), PE(16:1/0:0) ([M+H]+ C21H43N1O7P1), PE(18:1/0:0) ([M+H]+ C23H47N1O7P1), xenobactins, Pyrrolizixenamides A (N-(1-oxo-5,6,7,7a-tetrahydropyrrolizin-3-yl)hexanamide, Pyrrolizixenamides B N-(1-oxo-5,6,7,7a-tetrahydropyrrolizin-3-yl)heptanamide). and 5S-hydroxynorvaline-S-Ile and N-(Indol-3-ylethyl)-2-hydroxy-3-methylpe, as shown in Figure 22.

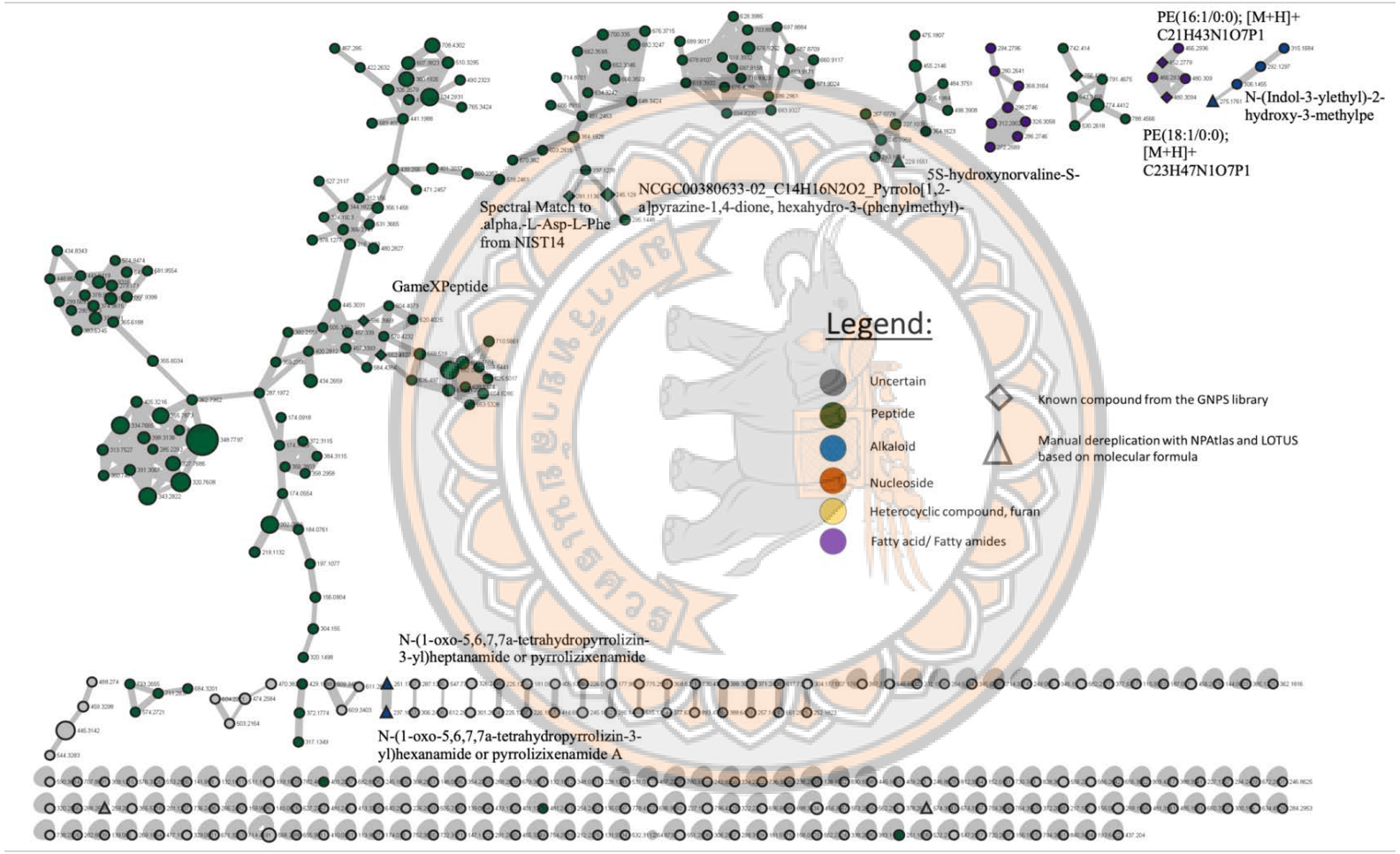

Figure 17 Detection of secondary metabolites produced by the *X. stockiae* strain RT25.5

Isolation the natural product from the *X. stockiae* strain RT25.5 using the easy Promoter Activation and Compound Identification (easyPACId) approach

The creation of the Δ*hfq* mutant was successfully verified by colony PCR. Compared to the culture of *X. stockiae* wild type (Figure 19A), the Δ*hfq* mutant (Figure 19B) appears colorless due to the absence of its secondary metabolite pigments, aryl polyenes—yellow pigments commonly found in Gram-negative bacteria. HPLC-MS analysis of the culture supernatants confirmed the absence of most secondary metabolite in the Δ*hfq* strains compared to the wild type, as illustrated by base peak chromatograms (BPC) of NPs (Figure 19C). However, HPLC-MS analysis of targeted BGCs production in *Xenorhabdus* Δ*hfq* mutants showed no significant difference when compared to non-induced conditions.

***X. stockiae* RT25.5 wild type**	***X. stockiae* RT25.5 Δ*hfq***
Yellow colony	*Colorless Colony*
A.	**B.**
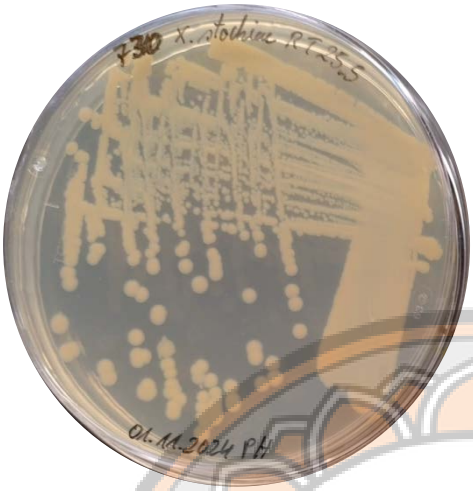	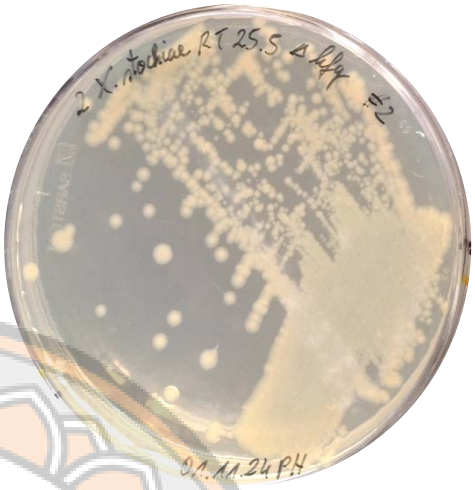
Many peaks of bioactive compunds	Less peaks of bioactive compounds

C.

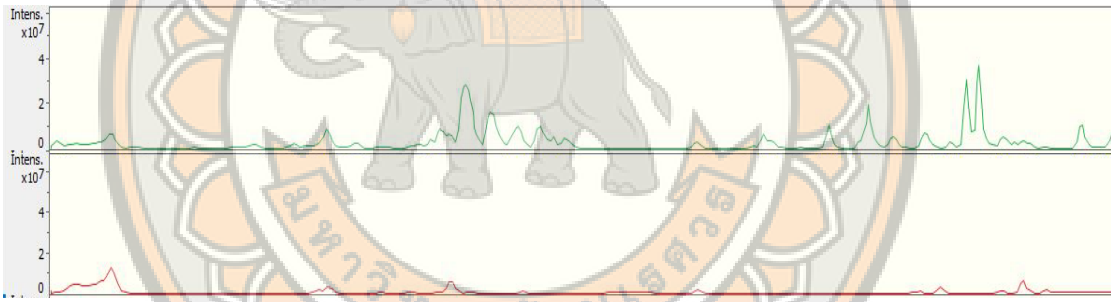

Figure 18 Comparative characteristics of *X. stockiae* wild type and *X. stockiae hfq* deletion

(A) *Xenorhabdus stockiae* wild type (B) *Xenorhabdus stockiae* Δ*hfq* (C) HPLC-MS analysis compare between *X. stockiae* WT (green line) and *X. stockiae* Δ*hfq* (red line)

Bacterial strains and their antimicrobial activities

The crude extract of *X. stockiae* strain RT 25.5 exhibited antimicrobial activity against both Gram-positive and Gram-negative bacteria in a rapid screening using the disk diffusion method. This included *A. baumannii*, *S. aureus*, *E. coli*, *E. faecalis*,

and *K. pneumoniae*. Notably, the extract showed potent activity against an extensively drug-resistant (XDR) strain of *A. baumannii*, a bacterium for which the development of novel antibiotics is urgently needed (Clarke, 2016; Luísa et al., 2014), with a zone of inhibition of 8 mm. In comparison, the antibiotic control had a zone of inhibition of 12 mm. Therefore, the minimum inhibitory concentration (MIC) and minimum bactericidal concentration (MBC) of the crude extract were determined against *A. baumannii* strain AB320. The results showed MIC and MBC values of the crude extract of 3.90 mg/mL and 7.81 mg/mL, respectively. By contrast, the MIC and MBC of the antibiotic control were 0.0024 mg/mL and 0.0049 mg/mL, respectively. The time kill curve results revealed that the viable count of *A. baumannii* strain AB320 (XDR) gradually decreased from 1 to 6 hours after-exposure to the crude extract, while those of the controls displayed remained unchanged over 24 hours (Figure 20). These findings suggest that the bacterial crude extract was a potential resource for discovering effective antimicrobial agents, particularly against challenging bacterial infections such as *A. baumannii*.

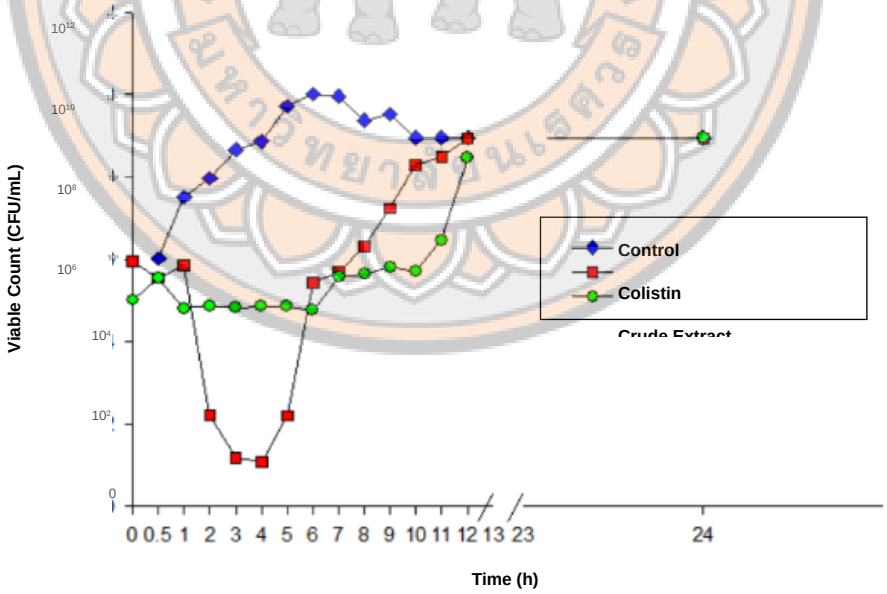

Figure 19 The time-kill curves of the 1X MIC of the extract against *A. baumannii* strain AB320 (XDR)

To observe morphological and ultrastructural changes in the bacterial cells before and after treatment with the extract, we then employed electron microscopy technique. The results illustrated that the cell wall and cell membrane of *A. baumannii* treated with the crude extract at 1X MIC exhibited substantial ultrastructural damage compared to the controls (Figure 21). These damages included condensation of the nucleoid and distortion of the cell surface with numerous clumps and blebs. In addition, cells treated with the extract exhibited cytoplasmic changes, including vacuolization and nucleoid aggregation, along with increased permeability and corresponding membrane destabilization that could eventually lead to cell lysis.

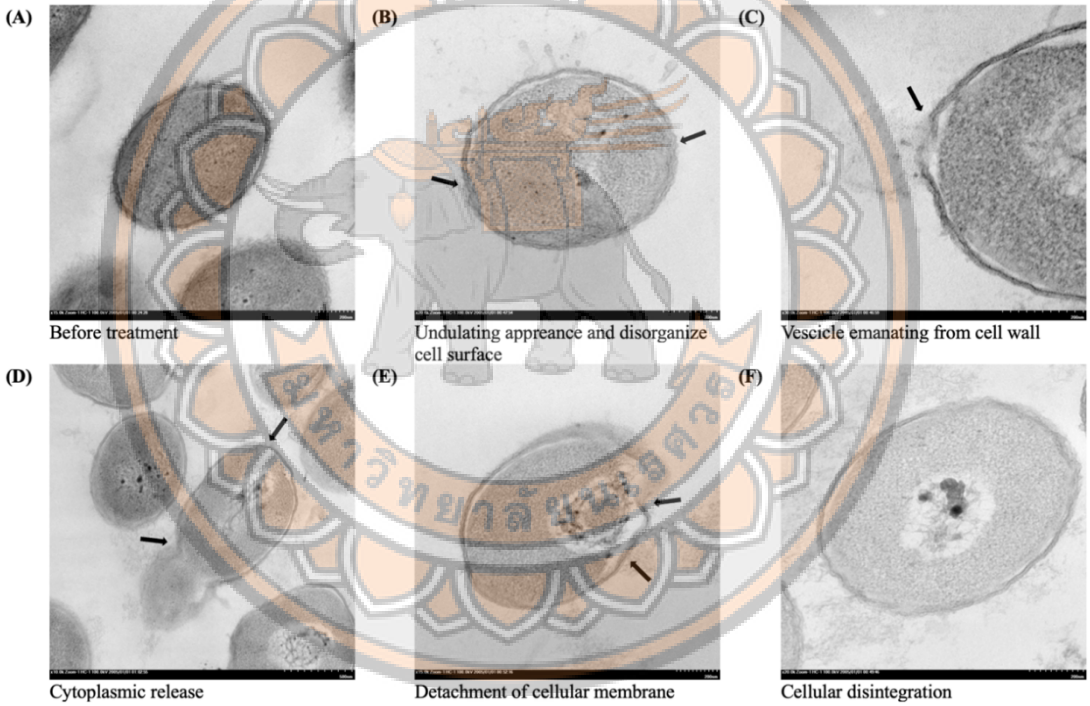

Figure 20 TEM images of *A. baumannii* strain AB320 (XDR)

Before (A) and after (B–F) exposure to crude extract of *X. stockiae* strain RT25.5 for 4 hours. Figure 4B-F shows ultrastructural damage in bacterial cells induced by the bioactive compounds.

Differential protein expressions in *Acinetobacter baylyi* treated with crude extract of *X. stockiae* strain RT25.5

A proteomic assay was performed to identify differentially expressed proteins in *Acinetobacter baylyi*, which was used as a model organism instead of *A. baumannii* strain AB320. This substitution was due to biosafety limitations, as *A. baylyi* is a non-pathogenic strain. The assay was conducted under both treated and untreated conditions with the crude extract of *X. stockiae* strain RT25.5. Proteins were considered upregulated if the log2 fold change exceeded 0.6 and downregulated if it was below 0.6. Statistically significant proteins were defined by a p-value < 0.05 (Inmaculada et al., 2023). Information on the identified proteins, including names, accession numbers, and abundances, was retrieved from the UniProt database ("UniProt: The Universal Protein Knowledgebase in 2023," 2023). A volcano plot in Figure 22 demonstrated the differential alterations in protein abundance between treated and untreated samples (Table 18), based on the specified fold change criteria. A total of 229 proteins consistently up regulated in *Acinetobacter* treated group compared to the untreated group. Among these proteins, notable examples include putative monooxygenase (Flavin-binding family), aldehyde dehydrogenase, metal-dependent hydrolase, putative short-chain dehydrogenase, lipase, type VI secretion system tube protein Hcp, zinc metalloprotease, alcohol dehydrogenase, p-hydroxybenzoate hydroxylase, and putative RND efflux membrane fusion protein. Functional analysis showed that the upregulated proteins involved numerous essential metabolic and biological processes, for examples, enzymatic degradation of antibacterial agents, alterations in bacterial proteins that serve as targets for antimicrobial agents binding, and changes in membrane permeability to the agents. These biological processes revealed that multiple immune-related pathways were involved in bacterial host responses. In contrast, the *Acinetobacter* treated group exhibited a significant decrease in the expressions of 147 proteins, including heme oxygenase, putative receptor protein, putative transcriptional regulator (AraC family) (Nitrilase regulator), YbdD/YjiX family protein, l-carnitine dehydrogenase, 30S ribosomal protein S12, NAD (+) diphosphatase, putative acetyltransferase, putative acetyl-CoA hydrolase/transferase, and putative ferric siderophore receptor protein (Table 18). These expressions indicated a significant impact, leading to the reduction of heme de-cyclizing activity, cellular component proteins, DNA-binding transcription

factor activity, alpha-methyl acyl-CoA racemase activity, tRNA binding, NAD+ diphosphatase activity, acyltransferase activity (transferring groups other than amino-acyl groups), acetate CoA-transferase activity, and siderophore-iron transmembrane transporter activity.

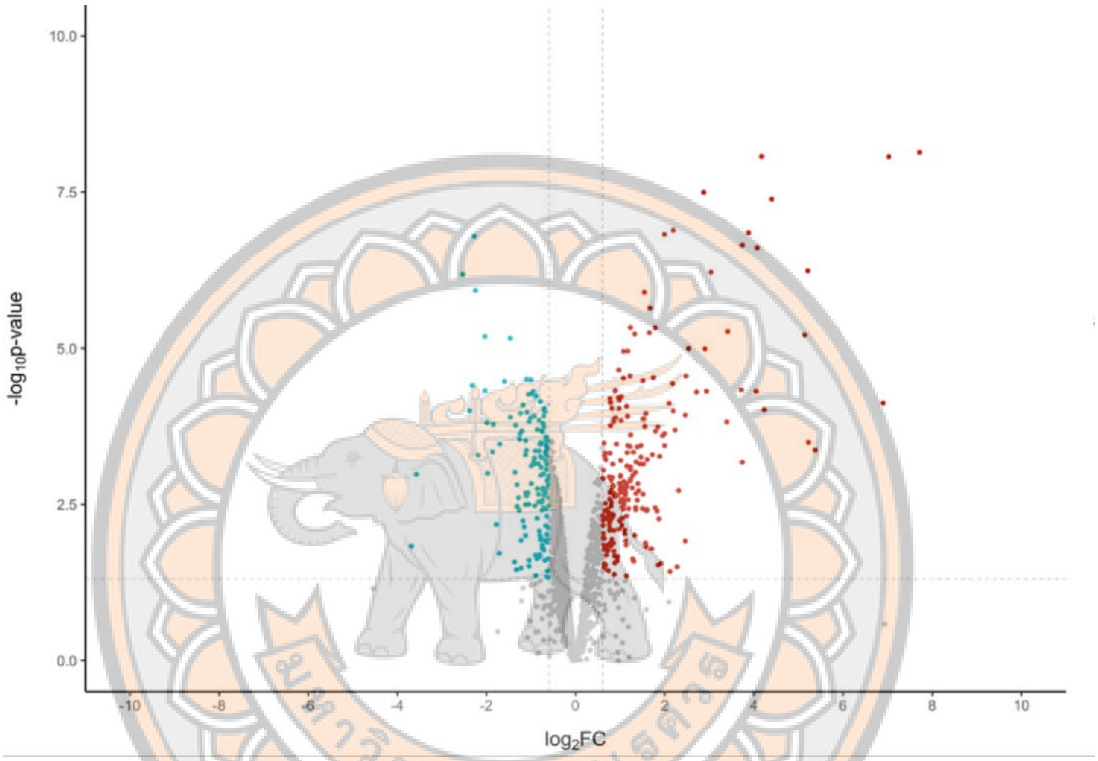

Figure 21 Protein profiling was conducted on *A. baylyi* treated with the crude extract of *X. stockiae* strain RT25.5 and compared to an untreated control group

The y-axis represents the statistical significance of gene expression differences, while the x-axis indicates the magnitude of these differences. Downregulated proteins are shown in blue, non-significant proteins in grey, and upregulated proteins in red.

Table 18 The altered protein expressions in *Acinetobacter*-treated with *X. stockiae* strain RT25.5 extract

No.	proteinDescription	Gene symbol	pval	log2fc	padj	diffexpressed
1	Putative monooxygenase (Flavin-binding family)	ACIAD2794	7.28E-09	7.715546498	8.137931381	UP
2	Aldehyde dehydrogenase	calB	8.48E-09	4.17105034	8.071352713	UP
3	Metal-dependent hydrolase	ACIAD0640	8.56E-09	7.023171355	8.067676988	UP
4	Putative short-chain dehydrogenase	ACIAD3555	3.19E-08	2.871085121	7.495675255	UP
5	Lipase	ACIAD3309	4.08E-08	4.397051078	7.389451785	UP
6	Type VI secretion system tube protein Hcp	ACIAD2689	1.29E-07	2.188816011	6.890214262	UP
7	Zinc metalloprotease	ACIAD1377	1.42E-07	3.87736158	6.849137274	UP
8	Alcohol dehydrogenase	adhA	1.50E-07	1.99143151	6.823354776	UP
9	p-hydroxybenzoate hydroxylase	pobA	2.24E-07	3.736154839	6.649303585	UP
10	Putative RND efflux membrane fusion protein	ACIAD3625	2.47E-07	4.07152987	6.607321351	UP
11	Probable FAD-binding monooxygenase AlmA	almA	5.76E-07	5.206550363	6.239527921	UP
12	Type VI secretion system tip protein VgrG	ACIAD3427	6.06E-07	3.035360981	6.217435944	UP
13	Putative alcohol dehydrogenase	ACIAD2015	1.27E-06	1.539003418	5.895908767	UP
14	Hydroxybenzaldehyde dehydrogenase	hcaB	2.27E-06	1.668649539	5.644334402	UP
15	Putative RND type efflux pump involved in aminoglycoside resistance (AdeT)	ACIAD0008	4.66E-06	1.22733417	5.331403521	UP

Table 18 (Cont.)

No.	proteinDescription	Gene symbol	pval	log2fc	padj	diffexpressed
16	Putative FMN oxidoreductase	ACIAD1143	4.70E-06	1.784414093	5.327905233	UP
17	Putative transcriptional regulator putative detoxification transcriptional regulator	ACIAD3599	5.40E-06	3.409919902	5.267655593	UP
18	Putative 3-hydroxybutyryl-CoA epimerase	ACIAD2989	5.64E-06	1.653459596	5.24884653	UP
19	Acetaldehyde dehydrogenase 2 (Acetaldehyde dehydrogenase II) (ACDH-II)	acoD	5.91E-06	1.324798017	5.228096397	UP
20	Putative carboxymethylenebutenolidase (Dienelactone hydrolase) (DLH)	ACIAD2677	6.13E-06	5.13828439	5.21277764	UP
21	Nodulation protein	nolG	1.01E-05	2.533203756	4.997299325	UP
22	Putative oxidoreductase, short-chain dehydrogenase/reductase family	ACIAD2676	1.02E-05	2.898074572	4.990510515	UP
23	Putative transcriptional regulator (TetR family)	ACIAD2793	1.11E-05	1.164987693	4.955894212	UP
24	3-dehydroshikimate dehydratase	quiC	1.12E-05	1.071285304	4.951600012	UP
25	Protocatechuate 3,4-dioxygenase alpha chain	pcaG	2.23E-05	0.966483963	4.651572167	UP
26	Metallo-beta-lactamase domain-containing protein	ACIAD1678	2.77E-05	1.218289291	4.557984176	UP
27	Anthranilate 1,2-dioxygenase electron transfer component	antC	2.78E-05	2.473418686	4.555800173	UP

Table 18 (Cont.)

No.	proteinDescription	Gene symbol	pval	log2fc	padj	diffexpressed
28	Glycine zipper 2TM domain-containing protein	ACIAD2419	2.95E-05	1.741512275	4.530164262	UP
29	Putative alcohol dehydrogenase	ACIAD2929	3.00E-05	1.066798215	4.522577046	UP
30	Uncharacterized protein	ACIAD3114	3.30E-05	1.507940716	4.480970289	UP
31	DUF4105 domain-containing protein	ACIAD0513	3.68E-05	2.17284065	4.433693434	UP
32	Citrate transporter	citN	4.64E-05	3.716392188	4.333018151	UP
33	Putative bifunctional protein (SpoT)	ACIAD3326	4.78E-05	0.883401516	4.320466877	UP
34	ABC3 transporter permease protein domain-containing protein	ACIAD1059	4.89E-05	2.936002569	4.310619278	UP
35	Uncharacterized protein	ACIAD1492	4.90E-05	4.050007447	4.30982383	UP
36	Serine aminopeptidase S33 domain-containing protein	ACIAD2795	5.02E-05	2.71137442	4.299373536	UP
37	SCP2 domain-containing protein	ACIAD2928	5.97E-05	1.017507985	4.224114738	UP
38	DNA repair protein RadA	radA	6.23E-05	0.958877199	4.205239424	UP
39	NA	NA	6.41E-05	0.770524794	4.193014408	UP
40	Phenol degradation protein meta	ACIAD2673	6.76E-05	0.97785342	4.169966116	UP
41	Protocatechuate 3,4-dioxygenase beta chain	pcaH	7.52E-05	0.781338013	4.123787009	UP
42	Fatty acid hydroxylase domain-containing protein	ACIAD3405	7.55E-05	6.896846289	4.121806333	UP
43	Putative integral membrane protein, possible transporter	ACIAD3184	7.59E-05	2.095749289	4.11982007	UP

Table 18 (Cont.)

No.	proteinDescription	Gene symbol	pval	log2fc	padj	diffexpressed
44	Transglycosylase SLT domain-containing protein	ACIAD1663	8.44E-05	1.140392988	4.07352057	UP
45	Beta-lactamase-related domain-containing protein	ACIAD0400	9.12E-05	0.816533579	4.040124377	UP
46	3-oxoadipate enol-lactonase 1	pcaD	9.16E-05	0.968724028	4.038290657	UP
47	Putative oxidoreductase	ACIAD2790	9.65E-05	4.231112948	4.015438759	UP
48	Uncharacterized protein	ACIAD2031	0.000100902	2.186971573	3.996101861	UP
49	Cellulose synthase regulatory subunit	ACIAD1177	0.000111332	1.57225412	3.953381452	UP
50	Putative membrane protein	ACIAD0147	0.000117309	2.457258716	3.930666883	UP
51	D-amino acid dehydrogenase	dadA	0.000123304	1.161322612	3.909021384	UP
52	3-hydroxyacyl-[acyl-carrier-protein] dehydratase FabZ	fabZ	0.000130423	0.899103571	3.884646301	UP
53	3-carboxy-cis,cis-muconate cycloisomerase	pcaB	0.000134991	1.507888467	3.869695505	UP
54	Small-conductance mechanosensitive channel	ACIAD0750	0.000135578	1.531031048	3.867810543	UP
55	Putative transporter	ACIAD0702	0.00013689	0.857837439	3.863626715	UP
56	Type I secretion system permease/ATPase	ACIAD1488	0.000142694	1.017397398	3.845595768	UP
57	D-alanyl-D-alanine endopeptidase, penicillin-binding protein 7 and penicillin-binding protein 8	pbpG	0.000149519	0.852404192	3.825303015	UP

Table 18 (Cont.)

No.	proteinDescription	Gene symbol	pval	log2fc	padj	diffexpressed
58	Acyl coenzyme A dehydrogenase	fadE	0.000151985	3.388565553	3.818198993	UP
59	PGAP1-like protein	ACIAD3425	0.000173434	0.780988081	3.760864771	UP
60	Anthranilate 1,2-dioxygenase small subunit	antB	0.000179076	1.552574955	3.746963582	UP
61	VanK	vanK	0.000183449	1.842466983	3.736484251	UP
62	Putative transport of long-chain fatty acids	ACIAD2788	0.000204828	2.229640505	3.688610715	UP
63	Putative hemagglutinin protein (FhaB)	ACIAD2784	0.000213862	1.791500603	3.669865905	UP
64	tRNA(Ile)-lysidine synthase	tilS	0.000232854	1.996155614	3.632915695	UP
65	NA	NA	0.000244002	1.230115489	3.612607117	UP
66	Uncharacterized protein	ACIAD2949	0.000251891	1.946065306	3.598786703	UP
67	Putative flavin-binding monooxygenase	ACIAD2339	0.000321394	5.220000966	3.492962118	UP
68	Polyketide cyclase / dehydrase and lipid transport	ACIAD2349	0.000331335	0.634638548	3.479732452	UP
69	Paraquat-inducible protein	pqiB	0.000343191	0.916922211	3.46446471	UP
70	Sodium/proline symporter	putP	0.000360538	1.465426462	3.443048401	UP
71	Putative very-long-chain acyl-CoA synthetase	ACIAD0437	0.000361009	1.167228058	3.442482384	UP
72	Putative transport protein (MFS superfamily)	ACIAD2822	0.000362842	1.99544581	3.440282485	UP

Table 18 (Cont.)

No.	proteinDescription	Gene symbol	pval	log2fc	padj	diffexpressed
73	Putative UDP-glucose lipid carrier transferase/glucose-1-phosphate transferase in colanic acid gene cluster (WcaJ)	ACIAD0098	0.000375421	1.218439994	3.425481151	UP
74	Acyl-coenzyme A dehydrogenase	ACIAD2277	0.00038029	1.379642602	3.419884849	UP
75	Putative efflux transporter causing drug resistance (Acr family)	ACIAD3624	0.000426407	5.373668598	3.370175948	UP
76	DUF2171 domain-containing protein	ACIAD0005	0.00046307	1.293201048	3.334353038	UP
77	Putative transport protein (ABC superfamily, ATP_bind)	ACIAD1873	0.000470337	1.154513656	3.32759115	UP
78	Xenobiotic reductase	xenB	0.00047679	0.656713945	3.321672587	UP
79	OmpW family protein	ACIAD2272	0.000480761	0.767270981	3.318070633	UP
80	Putative acyl-CoA dehydrogenase	ACIAD3262	0.00050858	1.71902847	3.293640436	UP
81	DUF4411 domain-containing protein	ACIAD3428	0.000523295	0.647799771	3.281253314	UP
82	Putative transporter with mechanosensitive ion channel	ACIAD1869	0.000540287	1.88356797	3.2673754	UP
83	Efflux pump membrane transporter	ACIAD2944	0.000555388	1.463959401	3.255403432	UP
84	Putative permease (PerM family)	ACIAD2633	0.000606391	1.603901046	3.217247312	UP
85	PNPLA domain-containing protein	ACIAD1335	0.000608339	0.677169808	3.215854314	UP
86	Type VI secretion system tip protein VgrG	ACIAD3115	0.00062633	1.008797353	3.203196907	UP

Table 18 (Cont.)

No.	proteinDescription	Gene symbol	pval	log2fc	padj	diffexpressed
87	Thiol:disulfide interchange protein	dsbD	0.000662046	1.355864486	3.179111514	UP
88	MAPEG family protein	ACIAD0237	0.000668488	3.734161154	3.174906367	UP
89	Xanthine dehydrogenase, large subunit	xdhB	0.000712358	1.439361204	3.147301573	UP
90	Putative aldehyde dehydrogenase	ACIAD0998	0.000714925	1.519338903	3.145739509	UP
91	Putative thiolase putative acyl-CoA thiolase	ACIAD2988	0.000716105	0.829794166	3.145023543	UP
92	Glutathione-regulated potassium-efflux system protein (K(+)/H(+) antiporter)	kef	0.000769577	1.146382011	3.113748081	UP
93	4-hydroxybenzoate transporter PcaK	pcaK	0.000792616	1.226099079	3.100937357	UP
94	Type VI secretion system tip protein VgrG	ACIAD1788	0.000877855	1.226921632	3.056577117	UP
95	Preprotein translocase subunit SecA	ACIAD0896	0.000899147	0.621779068	3.046169406	UP
96	J domain-containing protein	ACIAD2412	0.000969822	1.339768252	3.013307783	UP
97	Cytochrome bo(3) ubiquinol oxidase subunit 3	cyoC	0.001085915	1.280207346	2.964204156	UP
98	NADH-quinone oxidoreductase subunit A	nuoA	0.001090415	1.005184371	2.962408072	UP
99	Metal-dependent hydrolase	ACIAD0886	0.001134679	1.003174685	2.945126861	UP
100	2,4-dienoyl-CoA reductase	fadH	0.00114623	0.751397524	2.94072816	UP
101	Putative 3-oxoacyl-[acyl-carrier-protein] synthase III	ACIAD2101	0.00117077	0.821431446	2.931528372	UP
102	Putative pilus assembly protein (FilE)	ACIAD0671	0.001210046	0.615542778	2.917198076	UP

Table 18 (Cont.)

No.	proteinDescription	Gene symbol	pval	log2fc	padj	diffexpressed
103	2,4-dienoyl-CoA reductase [NADPH] (2,4-dienoyl coenzyme A reductase)	fadH	0.001259731	1.229026122	2.899722196	UP
104	CDP-diacylglycerol--glycerol-3-phosphate 3-phosphatidyltransferase (Phosphatidylglycerophosphate synthase) (PGP synthase)	pgsA	0.001291029	0.792475703	2.889064019	UP
105	Uncharacterized protein	ACIAD0907	0.001345378	1.219730739	2.871155726	UP
106	4-carboxymuconolactone decarboxylase	pcaC	0.001362979	1.081891102	2.86551078	UP
107	50S ribosomal protein L2	rplB	0.001450855	0.982414716	2.838375881	UP
108	Quinate/shikimate dehydrogenase (quinone)	quiA	0.001456698	1.129754988	2.836630547	UP
109	Putative amino acid transport protein (ABC superfamily, ATP_bind and membrane)	ACIAD3488	0.001476894	1.39342968	2.830650764	UP
110	Phosphate transporter	pit	0.001536023	0.99998037	2.81360237	UP
111	Putative general stress protein 26	ACIAD1776	0.001551834	0.827455065	2.809154638	UP
112	Pyruvate dehydrogenase (Cytochrome)	poxB	0.001605824	0.842641214	2.79430204	UP
113	Penicillin-binding protein 1B	mrcB	0.001607052	0.847414738	2.79397001	UP
114	Ubiquinol oxidase subunit I, cyanide insensitive	cioA	0.001636444	1.148470783	2.786098934	UP
115	Divalent metal cation transporter	ACIAD2521	0.001659805	1.099414695	2.779942824	UP

Table 18 (Cont.)

No.	proteinDescription	Gene symbol	pval	log2fc	padj	diffexpressed
116	Small-conductance mechanosensitive channel	ACIAD3026	0.0016988	0.817707098	2.769857864	UP
117	Starvation-induced protein involved in peptide utilization during carbon starvation	cstA	0.001708667	1.070289693	2.767342555	UP
118	Small ribosomal subunit biogenesis GTPase RsgA	rsgA	0.001726046	1.26945655	2.762947649	UP
119	EAL domain-containing protein	ACIAD2209	0.001805759	1.017687274	2.743340251	UP
120	Intermembrane phospholipid transport system permease protein MlaE	ttg2B	0.001835923	0.988595848	2.736145623	UP
121	Apolipoprotein N-acyltransferase	lnt	0.001856849	1.107533177	2.731223477	UP
122	Elongation factor 4	lepA	0.001859316	1.000325791	2.730646772	UP
123	DUF4850 domain-containing protein	ACIAD0814	0.001894958	0.802561866	2.722400458	UP
124	NADH-quinone oxidoreductase subunit M	nuoM	0.001896908	2.309738858	2.721953824	UP
125	Cytochrome bo(3) ubiquinol oxidase subunit 1	cyoB	0.00190249	1.412201911	2.720677717	UP
126	Protein-export membrane protein SecF	secF	0.001962643	0.807688084	2.7071587	UP
127	Putative fatty acid desaturase	ACIAD1208	0.002018771	1.002866299	2.694912895	UP
128	Putative secretion protein (HlyD family)	ACIAD3109	0.002030681	0.764534227	2.692358398	UP
129	Coenzyme A biosynthesis bifunctional protein CoaBC	dfp	0.002032092	1.11924892	2.692056717	UP

Table 18 (Cont.)

No.	proteinDescription	Gene symbol	pval	log2fc	padj	diffexpressed
130	Putative transporter	ACIAD1243	0.002035007	1.022604306	2.691434095	UP
131	Membrane protein insertase YidC	yidC	0.002100745	0.863866025	2.677626724	UP
132	Formate/nitrite transporter family protein	ACIAD3593	0.002113448	0.858382216	2.675008465	UP
133	ADP-dependent (S)-NAD(P)H-hydrate dehydratase	nnrD	0.002116433	1.352032781	2.674395512	UP
134	Polyribonucleotide nucleotidyltransferase	pnp	0.002153003	0.844657339	2.666955276	UP
135	PNPLA domain-containing protein	ACIAD0806	0.002175943	1.510051901	2.662352518	UP
136	Sodium/glutamate symporter	gltS	0.002236415	1.111493767	2.650447663	UP
137	DNA-directed RNA polymerase subunit beta'	rpoC	0.002311507	0.92761127	2.636104873	UP
138	Glucose dehydrogenase [pyrroloquinoline-quinone] (Quinoprotein glucose DH)	gcd	0.002352546	0.879845056	2.628461853	UP
139	Cytochrome d terminal oxidase, polypeptide subunit I	cydA	0.002603461	1.028697977	2.584448996	UP
140	30S ribosomal protein S3	rpsC	0.002604441	0.765448692	2.584285403	UP
141	Type VI secretion system baseplate subunit TssF	ACIAD2687	0.002676359	1.179742282	2.572455688	UP

Table 18 (Cont.)

No.	proteinDescription	Gene symbol	pval	log2fc	padj	diffexpressed
142	D-alanine/D-serine/glycine transport protein (APC family)	cycA	0.002706116	1.076769269	2.567653625	UP
143	Probable potassium transport system protein Kup	kup	0.002719498	1.37938219	2.565511227	UP
144	DUF445 domain-containing protein	ACIAD1103	0.002880845	0.996713237	2.540480056	UP
145	Transketolase	tkt	0.002940342	0.804128763	2.531602199	UP
146	Soluble pyridine nucleotide transhydrogenase (NAD(P)(+) transhydrogenase [B-specific])	sthA	0.003061625	0.662653958	2.514047978	UP
147	Ribosomal RNA large subunit methyltransferase K/L	rlmL	0.003063402	1.084132021	2.513796	UP
148	Putative uracil transport protein (NCS2 family)	ACIAD3628	0.003211668	1.079023388	2.493269409	UP
149	Putative bifunctional protein (MaeB)	ACIAD2287	0.00335817	0.791969507	2.473897318	UP
150	Chromosome partition protein Smc	smc	0.003462107	1.039205936	2.460659484	UP
151	NADH-quinone oxidoreductase subunit N	nuoN	0.003549407	1.343169944	2.449844199	UP
152	Benzoate transport protein	benK	0.003576105	1.781536501	2.446589694	UP
153	Putative transcriptional regulator (TetR-family)	ACIAD0757	0.003691088	1.49962029	2.432845585	UP
154	APC family, D-serine/D-alanine/glycine transport protein	cycA	0.003701211	1.187729601	2.431656166	UP

Table 18 (Cont.)

No.	proteinDescription	Gene symbol	pval	log2fc	padj	diffexpressed
155	NADH-quinone oxidoreductase subunit H	nuoH	0.003771975	1.06535822	2.423431191	UP
156	50S ribosomal subunit assembly factor BipA	typA	0.003797162	0.714417041	2.420540853	UP
157	histidine kinase	pilS	0.003836669	1.601534247	2.416045626	UP
158	histidine kinase	ACIAD0727	0.003849605	1.346302001	2.414583852	UP
159	UvrABC system protein C	uvrC	0.003939306	1.602627578	2.404580322	UP
160	mannose-1-phosphate guanylyltransferase	epsM	0.003991776	0.655773423	2.398833787	UP
161	Putative transport protein	ACIAD1191	0.003994468	1.583317917	2.398541079	UP
162	Lysine-specific permease	lysP	0.00405775	1.826114428	2.39171476	UP
163	LprI domain-containing protein	ACIAD0315	0.004392704	0.766093946	2.357268044	UP
164	Ubiquinol oxidase subunit 2	cyoA	0.004439216	0.733462307	2.352693677	UP
165	Penicillin-binding protein 1A	ponA	0.004620517	0.831028164	2.335309386	UP
166	UPF0761 membrane protein ACIAD3168	ACIAD3168	0.004691315	0.841068936	2.328705443	UP
167	PDZ domain-containing protein	ACIAD1186	0.004776102	0.604826464	2.320926436	UP
168	Quinone-dependent D-lactate dehydrogenase	dld	0.004781197	0.801098033	2.320463336	UP
169	Phosphotransferase system, fructose-specific IIBC component	fruA	0.004879598	1.144376215	2.311615979	UP
170	Phospho-N-acetylmuramoyl-pentapeptide-transferase	mraY	0.004886077	0.755829445	2.311039725	UP

Table 18 (Cont.)

No.	proteinDescription	Gene symbol	pval	log2fc	padj	diffexpressed
171	ATP-dependent lipid A-core flippase	msbA	0.005165548	0.81566256	2.286883623	UP
172	Probable malate:quinone oxidoreductase	mqo	0.005241937	0.677298333	2.280508185	UP
173	Small-conductance mechanosensitive channel	ACIAD3477	0.005282423	1.039188598	2.277166804	UP
174	Putative adenylate or guanylate cyclase	ACIAD1397	0.005418629	1.866390399	2.266110607	UP
175	CBS domain-containing protein	ACIAD0230	0.005599375	0.73997491	2.251860415	UP
176	Probable proton/glutamate-aspartate symporter	gltP	0.005632808	0.745637536	2.249275066	UP
177	DNA topoisomerase 4 subunit A	parC	0.005694421	0.98979197	2.244550406	UP
178	Protein translocase subunit SecY	secY	0.005700799	0.618881058	2.244064297	UP
179	Putative arginine/lysine/ornithine decarboxylase	ACIAD3341	0.005722007	0.76889202	2.242451647	UP
180	cyclic pyranopterin monophosphate synthase	moaCB	0.005764933	0.761740293	2.239205718	UP
181	Putative glutamate synthase	ACIAD1934	0.005768741	0.775878825	2.238918968	UP
182			0.005801445	0.985461422	2.236463837	UP
183	Putative integral membrane protein	lolC	0.006634394	0.751395443	2.178198735	UP
184	NADH-quinone oxidoreductase subunit K	nuoK	0.006832733	1.035268485	2.165405527	UP
185	Acetolactate synthase	ilvI	0.006885834	0.614064563	2.162043478	UP

Table 18 (Cont.)

No.	proteinDescription	Gene symbol	pval	log2fc	padj	diffexpressed
186	4-hydroxycinnamoyl CoA hydratase/lyase	hcaA	0.007702933	0.761941243	2.113343906	UP
187	ATP synthase subunit c	atpE	0.007912295	0.968426084	2.101697541	UP
188	Uncharacterized protein	ACIAD2009	0.008169704	1.101233939	2.087793669	UP
189	Serine aminopeptidase S33 domain-containing protein	ACIAD3141	0.008305885	0.853010498	2.080614078	UP
190	tRNA uridine 5-carboxymethylaminomethyl modification enzyme MnmG	mnmG	0.008323566	0.759511456	2.079690572	UP
191	Cyanophycinase	ACIAD1280	0.009259127	0.619751826	2.033429956	UP
192	Peptidoglycan D,D-transpeptidase FtsI	ftsI	0.009369741	1.100275127	2.028272397	UP
193	L-lactate permease	lldP	0.009947102	1.324163656	2.002303435	UP
194	Tyrosine-protein kinase, autophosphorylates	ptk	0.01084067	0.614442535	1.964943878	UP
195	Putative transport protein (ABC superfamily, atp_bind)	ACIAD0007	0.011131835	0.640640429	1.953433232	UP
196	Protein translocase subunit SecD	secD	0.011507577	0.812546177	1.93901612	UP
197	ATP-dependent DNA helicase RecG	recG	0.012203803	1.119571636	1.913504796	UP
198	Alkane 1-monooxygenase	alkB	0.012319307	2.457478377	1.909413734	UP
199	DNA mismatch repair protein MutS	mutS	0.013239314	0.842734616	1.878134526	UP
200	Peptidase M48 domain-containing protein	ACIAD1324	0.013251019	0.771122886	1.877750739	UP

Table 18 (Cont.)

No.	proteinDescription	Gene symbol	pval	log2fc	padj	diffexpressed
201	Putative transcriptional regulator (AraC family)	ACIAD2012	0.013252713	1.565314865	1.877695198	UP
202	23S rRNA (uracil(1939)-C(5))-methyltransferase RlmD	rlmD	0.013990452	0.735234367	1.854168242	UP
203	Putative transport protein (MFS superfamily)	ACIAD3450	0.014173324	1.128831364	1.848528297	UP
204	Putative suppressor of F exclusion of phage T7 (FxsA)	ACIAD2040	0.014332938	0.63390144	1.843664793	UP
205	DUF4062 domain-containing protein	ACIAD3256	0.014693453	0.78425764	1.83287613	UP
206	Putative permease (MFS superfamily)	ACIAD2100	0.015115166	1.580135613	1.820587075	UP
207	Putative membrane protein	ACIAD2331	0.01531919	0.681965095	1.814764203	UP
208	Putative transport protein (MFS superfamily)	ACIAD0233	0.016309185	1.70053247	1.787567745	UP
209	C4-dicarboxylate transport protein	dctA	0.016633764	0.644171919	1.779009455	UP
210	Putative ferrous iron transport protein B (FeoB)	ACIAD0268	0.017373127	0.721904434	1.760122004	UP
211	Permease	ACIAD0255	0.017770335	0.851590494	1.750304389	UP
212	DNA helicase	ACIAD0495	0.020506576	0.687649829	1.688106844	UP
213	Dicarboxylic acid transport protein alpha-ketoglutarate permease (MFS superfamily)	pcaT	0.021216552	0.87032703	1.673325202	UP
214	PRS2 protein	ACIAD2266	0.02178912	0.94494127	1.661760305	UP

Table 18 (Cont.)

No.	proteinDescription	Gene symbol	pval	log2fc	padj	diffexpressed
215	Osmo-dependent choline transporter BetT2	betT2	0.023607195	1.279855312	1.626955608	UP
216	Putative glycosyl transferase family 2 (Rhamnosyl transferase)	ACIAD0082	0.025541131	0.923180981	1.592759884	UP
217	pH adaptation potassium efflux system transmembrane protein	phaAB	0.025827142	1.300180605	1.58792365	UP
218	Putative bifunctional protein	ACIAD0799	0.027488915	0.876829689	1.560842402	UP
219	AI-2E family transporter	ACIAD3289	0.027814304	1.914022865	1.555731802	UP
220	Putative glycosyl transferase family 1	ACIAD0090	0.028409883	0.641866886	1.546530549	UP
221	RcnB family protein	ACIAD0618	0.029600706	0.671127634	1.528697937	UP
222	Peptidase C13 family protein	ACIAD0681	0.029649491	1.845267244	1.527982755	UP
223	Putative transporter	ACIAD2214	0.031816124	2.275362138	1.497352731	UP
224	DNA topoisomerase 4 subunit B	parE	0.032029946	0.637999068	1.4944438	UP
225	Undecaprenyl-diphosphatase 3	uppP3	0.034165727	0.639585197	1.466409336	UP
226	Phosphatidylglycerol--prolipoprotein diacylglyceryl transferase	lgt	0.036527214	0.732836138	1.437383448	UP
227	NADH dehydrogenase I chain L	nuoL	0.037784407	2.116245958	1.422687395	UP
228	Microcin B17 transport protein (ABC superfamily, atp_bind and membrane)	sbmA	0.042013521	0.866310359	1.376610924	UP
229	AMP-dependent synthetase/ligase domain-containing protein	ACIAD0571	0.044423491	1.133654586	1.352387316	UP

Table 18 (Cont.)

No.	proteinDescription	Gene symbol	pval	log2fc	padj	diffexpressed
230	Heme oxygenase	hemO	1.61E-07	-2.280355017	6.793760618	DOWN
231	Putative receptor protein	ACIAD1472	6.56E-07	-2.53279883	6.182983934	DOWN
232	Putative transcriptional regulator (AraC family) (Nitrilase regulator)	ACIAD1622	1.19E-06	-2.250935121	5.923534292	DOWN
233	YbdD/YjiX family protein	ACIAD2204	6.45E-06	-2.038335399	5.190153255	DOWN
234	L-carnitine dehydrogenase	caiB	6.90E-06	-1.470697484	5.161169436	DOWN
235	30S ribosomal protein S12	rpsL	3.12E-05	-1.107084408	4.506176168	DOWN
236	NAD(+) diphosphatase	ACIAD1135	3.17E-05	-1.006396503	4.498649313	DOWN
237	Putative acetyltransferase	ACIAD0864	3.40E-05	-1.600132046	4.468073561	DOWN
238	Putative acetyl-CoA hydrolase/transferase	ACIAD3390	3.94E-05	-2.323932877	4.404372548	DOWN
239	Putative ferric siderophore receptor protein	ACIAD1163	4.78E-05	-2.033142298	4.320740389	DOWN
240	Gluconokinase	gntK	4.94E-05	-0.950502477	4.305856379	DOWN
241	Putative ferric siderophore receptor protein	ACIAD1240	5.10E-05	-0.959092343	4.292689216	DOWN
242	Putative ferric siderophore receptor protein	ACIAD2049	5.45E-05	-1.057828053	4.263301204	DOWN
243	HAD family hydrolase	ACIAD1038	5.50E-05	-0.925843542	4.259791827	DOWN
244	Nucleoside-specific channel-forming protein	tsx	5.86E-05	-0.884251146	4.231787341	DOWN
245	Putative ferric siderophore receptor protein	ACIAD2116	7.18E-05	-0.796726695	4.144141005	DOWN
246	Putative L-asparaginase I (AnsA)	ACIAD0476	8.11E-05	-1.184749739	4.091188109	DOWN

Table 18 (Cont.)

No.	proteinDescription	Gene symbol	pval	log2fc	padj	diffexpressed
247	Putative acetyltransferase (WeeI)	ACIAD0094	9.26E-05	-0.711406101	4.033187522	DOWN
248	Uncharacterized protein	ACIAD1474	9.95E-05	-2.385045109	4.002353502	DOWN
249	Twitching motility protein	pilU	0.000103271	-0.693090652	3.986021798	DOWN
250	ComB	comB	0.000105259	-1.101668986	3.977739326	DOWN
251	FilA	ACIAD0780	0.00011009	-1.241523538	3.958253603	DOWN
252	Putative aspartate racemase	ACIAD0318	0.000121988	-0.718552738	3.913682702	DOWN
253	Esterase	aesT	0.0001225	-0.929204609	3.911863527	DOWN
254	Fatty acyl-CoA reductase	acr1	0.000127976	-1.469316749	3.892871441	DOWN
255	Putative acyl-CoA dehydrogenase	ACIAD1821	0.000129596	-1.0113898	3.88740983	DOWN
256	7,8-dihydroneopterin aldolase	folB	0.00014187	-0.82446029	3.84810858	DOWN
257	Putative ferrichrome-iron receptor protein	ACIAD0973	0.000149228	-1.044307475	3.826148584	DOWN
258	Putative hemolysin activator protein (FhaC)	ACIAD2785	0.00015721	-1.98963171	3.803519957	DOWN
259	Arginine succinyltransferase	astA	0.000160192	-0.73418767	3.795359949	DOWN
260	Glycosyltransferase 2-like domain-containing protein	ACIAD0572	0.00016678	-1.8505046	3.777855676	DOWN
261	Putative ferric siderophore receptor protein	ACIAD0745	0.000171268	-1.346013657	3.766323618	DOWN
262	Succinylglutamate desuccinylase	astE	0.000183712	-0.711573257	3.735862293	DOWN
263	AcuG	acuG	0.000200651	-0.862974202	3.697559505	DOWN
264	Cyanophycin synthetase	cphA	0.000207187	-0.762842236	3.683637948	DOWN

Table 18 (Cont.)

No.	proteinDescription	Gene symbol	pval	log2fc	padj	diffexpressed
265	Putative long-chain fatty acid transport protein	ACIAD0835	0.000211139	-1.208702474	3.675430945	DOWN
266	tRNA-cytidine(32) 2-sulfurtransferase	ttcA	0.000218649	-0.751984621	3.660252964	DOWN
267	Putative transcriptional regulator (IcIR family)	ACIAD1822	0.000237047	-1.248396302	3.625166275	DOWN
268	Putative enoyl-CoA hydratase	ACIAD1820	0.000261615	-0.666633126	3.582337957	DOWN
269	Uncharacterized protein	ACIAD0779	0.00028572	-1.262262768	3.544059561	DOWN
270	Uncharacterized protein	ACIAD2741	0.000292328	-0.665168448	3.534129435	DOWN
271	Putative flavoprotein oxidoreductase	ACIAD3522	0.000302472	-1.124376707	3.51931505	DOWN
272	Acetoacetyl-CoA transferase, beta subunit	atoA	0.000308448	-0.628341338	3.510817898	DOWN
273	Putative transcriptional regulator (LysR family)	ACIAD1230	0.000318281	-0.66544699	3.497189911	DOWN
274	Uncharacterized protein	ACIAD1290	0.000330932	-0.790477644	3.480261672	DOWN
275	AcuC	acuC	0.000341408	-1.705486778	3.466726817	DOWN
276	HTH-type transcriptional regulator BenM	benM	0.000347345	-0.801051952	3.459238353	DOWN
277	Putative transcriptional regulator (LysR family)	ACIAD0323	0.000348904	-0.671406613	3.457293705	DOWN
278	N-succinylarginine dihydrolase	astB	0.000383824	-0.643854405	3.415867421	DOWN
279	Alanine racemase	alr	0.000431964	-1.105383668	3.364551959	DOWN
280	Putative fatty acid desaturase	ACIAD0630	0.000440671	-0.909159779	3.355885131	DOWN

Table 18 (Cont.)

No.	proteinDescription	Gene symbol	pval	log2fc	padj	diffexpressed
281	Twitching motility protein	pilI	0.000442353	-0.820758987	3.354230879	DOWN
282	Thioesterase	ACIAD1951	0.000452128	-0.672905645	3.344738302	DOWN
283	Putative flavoprotein oxidoreductase	ACIAD1827	0.000456836	-1.86510397	3.340239432	DOWN
284	Rad50/SbcC-type AAA domain-containing protein	ACIAD0378	0.000474837	-0.683645955	3.323455425	DOWN
285	Perosamine synthetase (WeeJ)	per	0.000509865	-1.128462413	3.292544911	DOWN
286	Putative transcriptional regulator (AraC family)	ACIAD1576	0.000518714	-2.191427185	3.285071988	DOWN
287	DUF2846 domain-containing protein	ACIAD0189	0.000525835	-0.653356153	3.279150606	DOWN
288	Putative two-component system sensor protein (ColR-like)	ACIAD1634	0.000545154	-0.792719457	3.263480958	DOWN
289	Putative ferric siderophore receptor protein	ACIAD1054	0.000567225	-0.762326584	3.246244956	DOWN
290	IrrE N-terminal-like domain-containing protein	ACIAD3429	0.000573011	-0.925309145	3.241836998	DOWN
291	DUF490 domain-containing protein	ACIAD2402	0.000642895	-0.671020668	3.191859959	DOWN
292	Uncharacterized protein	ACIAD0777	0.00065581	-0.945838575	3.183221902	DOWN
293	CBS domain-containing protein	ACIAD2305	0.000681654	-0.6297683	3.166436255	DOWN
294	Outer membrane lipoprotein carrier protein LolA	ACIAD0576	0.000705022	-0.838668244	3.151797097	DOWN
295	Porin	ACIAD0139	0.000705941	-0.909141023	3.151231319	DOWN

Table 18 (Cont.)

No.	proteinDescription	Gene symbol	pval	log2fc	padj	diffexpressed
296	Alkanesulfonate monooxygenase	ssuD	0.000728287	-0.64589299	3.137697448	DOWN
297	Uncharacterized protein	ACIAD1267	0.00076791	-1.00053437	3.114689571	DOWN
298	Putative ferric siderophore receptor protein	ACIAD2325	0.000813858	-0.772305686	3.089451172	DOWN
299	[Ribosomal protein S18]-alanine N-acetyltransferase	rimI	0.000872255	-0.657250828	3.05935637	DOWN
300	Putative acetyltransferase (GNAT family)	ACIAD1002	0.000967829	-1.363064849	3.014201418	DOWN
301	DUF2750 domain-containing protein	ACIAD2303	0.001012129	-1.97880788	2.994764043	DOWN
302	Putative substrate binding protein (ABC superfamily, peri_bind)	ACIAD2524	0.001027869	-0.718553914	2.988062207	DOWN
303	Putative glucose-6-phosphate 1-epimerase	ACIAD0191	0.001043653	-3.576514437	2.981444033	DOWN
304	FilD	filD	0.001084397	-0.782808318	2.964811744	DOWN
305	Uncharacterized protein	ACIAD2191	0.00111132	-0.602347692	2.95416084	DOWN
306	Sulfate transport protein (ABC superfamily, peri_bind)	cysP	0.001249231	-0.624745624	2.903357076	DOWN
307	Big-1 domain-containing protein	ACIAD3144	0.001319018	-0.644263441	2.879749354	DOWN
308	Penicillin-binding protein activator	ACIAD1131	0.001476621	-0.998623837	2.830730968	DOWN
309	Uncharacterized protein	ACIAD2256	0.001501798	-0.618149696	2.823388589	DOWN
310	Restriction endonuclease type IV Mrr domain-containing protein	ACIAD1480	0.001525849	-1.317536715	2.816488327	DOWN

Table 18 (Cont.)

No.	proteinDescription	Gene symbol	pval	log2fc	padj	diffexpressed
311	2-C-methyl-D-erythritol 2,4-cyclodiphosphate synthase	ispF	0.001720312	-0.630230916	2.764392891	DOWN
312	Phytanoyl-CoA dioxygenase	ACIAD3482	0.001729668	-0.737829998	2.76203714	DOWN
313	ComF	comF	0.001774309	-0.865492743	2.750970718	DOWN
314	Thioesterase	ACIAD0290	0.001872651	-0.733747078	2.727543125	DOWN
315	Putative glutathione S-transferase	ACIAD3130	0.002064118	-1.071597253	2.685265568	DOWN
316	tRNA-dihydrouridine synthase B	dusB	0.002070376	-0.672032121	2.683950806	DOWN
317	Putative monooxygenase	ACIAD1830	0.002071035	-1.1215932	2.683812566	DOWN
318	Putative transcriptional regulator, luxR family	ACIAD1165	0.002188238	-0.83368399	2.659905454	DOWN
319	Putative acetyl-CoA synthetase/AMP-(Fatty) acid ligase	ACIAD1611	0.002256863	-0.711785809	2.646494859	DOWN
320	Putative tonB-dependent ferric siderophore receptor protein	ACIAD1780	0.002319743	-1.10725883	2.634560113	DOWN
321	Uncharacterized protein	ACIAD0489	0.002490898	-1.28480816	2.603643986	DOWN
322	Putative transcriptional regulator (ArsR family)	ACIAD1865	0.002496676	-0.608859899	2.602637835	DOWN
323	Putative glutathione S-transferase	ACIAD0017	0.002730641	-0.745017673	2.563735467	DOWN
324	proton-translocating NAD(P)(+) transhydrogenase	pntA-1	0.002788924	-0.761656174	2.554563338	DOWN

Table 18 (Cont.)

No.	proteinDescription	Gene symbol	pval	log2fc	padj	diffexpressed
325	Thioesterase	ACIAD2585	0.002899436	-0.837148069	2.537686473	DOWN
326	Stringent starvation protein A	sspA	0.002906218	-0.815425242	2.53667183	DOWN
327	Regulator of ribonuclease activity B domain-containing protein	ACIAD0716	0.002918844	-0.765192054	2.534789052	DOWN
328	Adenosylmethionine-8-amino-7-oxononanoate aminotransferase	bioA	0.00315992	-1.05438144	2.500323864	DOWN
329	4-hydroxybenzoyl-CoA thioesterase	ACIAD0575	0.003190749	-1.128552191	2.496107422	DOWN
330	Putative ferric siderophore receptor protein	ACIAD2082	0.003361296	-0.920126616	2.473493227	DOWN
331	DUF1176 domain-containing protein	ACIAD0815	0.003364732	-0.602713274	2.473049475	DOWN
332	Putative transcriptional regulator	ACIAD2672	0.003433099	-1.316323575	2.464313634	DOWN
333	Uncharacterized protein	ACIAD1136	0.003578489	-0.722774828	2.446300336	DOWN
334	Uncharacterized protein	ACIAD1192	0.003648591	-0.685150224	2.437874768	DOWN
335	Outer membrane protein assembly factor BamB	bamB	0.003708967	-0.66620048	2.430747038	DOWN
336	Putative bifunctional protein	ACIAD2236	0.003896681	-0.757623936	2.409305105	DOWN
337	Putative sulfonate monooxygenase (MsuD)	ACIAD3471	0.003943818	-1.271490575	2.40408311	DOWN
338	Putative ferric siderophore receptor protein	ACIAD1764	0.004911775	-0.650747749	2.308761528	DOWN
339	Putative transcriptional regulator	ACIAD3490	0.005298	-0.86803622	2.275888022	DOWN

Table 18 (Cont.)

No.	proteinDescription	Gene symbol	pval	log2fc	padj	diffexpressed
340	Zinc finger/thioredoxin putative domain-containing protein	ACIAD2444	0.005806946	-1.183665263	2.236052209	DOWN
341	DUF2520 domain-containing protein	ACIAD1273	0.006667239	-1.783142734	2.176053959	DOWN
342	Putative acetyltransferase	ACIAD2293	0.006929262	-0.670787489	2.15931302	DOWN
343	Putative enoyl-CoA hydratase (PaaG-like)	ACIAD1829	0.007262868	-1.154241162	2.13889184	DOWN
344	UDP-N-acetylenolpyruvoylglucosamine reductase	murB	0.007476406	-0.615171748	2.126307137	DOWN
345	Adenylate kinase	ACIAD2987	0.008470169	-0.817630623	2.07210794	DOWN
346	Putative intracellular sulfur oxidation protein (DsrE-like)	ACIAD1892	0.009505911	-0.641429143	2.022006272	DOWN
347	Uncharacterized protein	ACIAD0333	0.009658196	-0.655304497	2.015103987	DOWN
348	Putative pseudouridylate synthase	ACIAD2377	0.010026848	-1.126336975	1.998835585	DOWN
349	Outer membrane protein	czcC	0.010121067	-0.801879026	1.994773699	DOWN
350	S6PP domain-containing protein	ACIAD1961	0.01160187	-0.766295208	1.935472021	DOWN
351	SEC-C motif domain protein	ACIAD0231	0.011686868	-0.791611671	1.932301879	DOWN
352	Uncharacterized protein	ACIAD1962	0.01182082	-0.60557196	1.927352402	DOWN
353	Phosphofructokinase	fruK	0.011955914	-0.688328921	1.92241723	DOWN
354	SCP2 domain-containing protein	ACIAD1406	0.011974811	-1.229259251	1.921731342	DOWN
355	PEGA domain-containing protein	ACIAD3559	0.012758697	-0.645836571	1.894193672	DOWN

Table 18 (Cont.)

No.	proteinDescription	Gene symbol	pval	log2fc	padj	diffexpressed
356	Putative alkylphosphonate uptake protein (PhnA) in phosphonate metabolism	ACIAD0719	0.014380422	-0.75137943	1.842228365	DOWN
357	Putative short-chain dehydrogenase/reductase SDR protein	ACIAD1828	0.01477857	-3.685008007	1.830367576	DOWN
358	Malonyl-[acyl-carrier protein] O-methyltransferase	bioC	0.01525527	-0.742746411	1.816580099	DOWN
359	Putative transcriptional regulator (AraC family)	ACIAD0160	0.015865611	-0.754603917	1.799543189	DOWN
360	protein-tyrosine-phosphatase	ptp	0.017073678	-0.715131791	1.767672913	DOWN
361	Putative aldolase	ACIAD1293	0.019329703	-1.712165176	1.713774826	DOWN
362	RNA pyrophosphohydrolase	rppH	0.020106253	-0.807612142	1.69666885	DOWN
363	Glutamate/aspartate transport protein (ABC superfamily, atp_bind)	gltL	0.0206344	-0.907202258	1.685408144	DOWN
364	EH_Signature domain-containing protein	ACIAD3456	0.021656183	-0.804021619	1.664418078	DOWN
365	pH adaptation potassium efflux system E transmembrane protein	phaE	0.023436671	-0.868793157	1.630104074	DOWN
366	Putative transcriptional regulator (LysR family)	ACIAD1543	0.023442552	-0.620493467	1.629995111	DOWN
367	HTH-type transcriptional regulator AlkR	alkR	0.024862027	-1.045645725	1.604463458	DOWN

Table 18 (Cont.)

No.	proteinDescription	Gene symbol	pval	log2fc	padj	diffexpressed
368	ABC transporter substrate-binding protein PnrA-like domain-containing protein	ACIAD0198	0.025052029	-0.693329671	1.6011571	DOWN
369	Type IV pilus biogenesis protein	pilJ	0.02648438	-1.373718162	1.577010182	DOWN
370	FilA	filA	0.030911027	-1.048476582	1.509886564	DOWN
371	Exported protein	ACIAD0269	0.033187018	-1.226685928	1.479031763	DOWN
372	Putative oxidoreductase, short-chain dehydrogenase/reductase	ACIAD1824	0.035331892	-1.329407806	1.451833105	DOWN
373	Cyclopropane-fatty-acyl-phospholipid synthase	ACIAD1632	0.036831252	-0.629628463	1.433783513	DOWN
374	DcaE	dcaE	0.044113816	-0.898093733	1.355425377	DOWN
375	Protein PsiE	ACIAD0621	0.045408393	-0.659662466	1.342863872	DOWN
376	Uncharacterized protein	ACIAD2716	0.046624097	-0.613243968	1.331389562	DOWN

CHAPTER V

DISCUSSION

The average genome size of 13 entomopathogenic bacterial strains was approximately 4.6 Mb, with an average of 24 biosynthetic gene clusters (BGCs). This is consistent with previous reports that found an average of 22 BGCs across 45 strains of these bacteria (Yi-Ming, Merle, Yan-Ni, Shabbir, et al., 2022), which is two-to tenfold higher than the average BGC levels observed in other Enterobacteria. For example, *Serratia* was found to have an average of 17.8 BGCs, *Yersinia* had 13.7, and *Proteus* had 8.4 (Omkar et al., 2022). The greater genome size of *Xenorhabdus* and *Photorhabdus* appears to have a linear relationship with the number of BGCs, indicating a greater potential for producing bioactive compounds and secondary metabolites (Kazuya et al., 2014; Shi et al., 2022) These findings are supported by pan-core genome analysis conducted using the Anvi'o platform (Eren et al., 2015). Which core genes are shared by all species. In contrast, accessory genes are present in some species, while singleton genes are found in only one species. The results revealed that *Xenorhabdus* and *Photorhabdus* share a conserved set of core genes that are essential for fundamental cellular functions and relatively stable in sequence and function (Tettelin et al., 2005). However, notable distinctions exist between the two genera was found in accessory and singleton region (Figure 13). Each genus possesses a unique set of genes, which shape their distinct characteristics and lifestyles (Yi-Ming, Merle, Yan-Ni, & Helge, 2022). Interestingly, although BGCs are prolific in all genomes, most of their BGCs are distributed across the accessory and singleton regions. These findings reflect adaptations to diverse ecological niches, including regulatory elements and the production of secondary metabolites, including antibiotics and toxins, which are rarely found in other organisms (Jordan et al., 2001).

NRPS were the most abundant BGCs in both genera genomes, consistent with findings by Shi et al. (2022a), highlighting their potential ecological significance. The "others" group ranked second, possibly aiding in specific bacterial functions, while hybrid PKS/NRPS clusters showed moderate enrichment. In contrast, PKS, RiPPs, and terpene BGCs were relatively scarce.

Certain widely shared clusters resembled known BGCs for betalactone production (Yi-Ming, Merle, Yan-Ni, Shabbir, et al., 2022), followed by GameXpeptides (Nollmann et al., 2015b) and photoxenobactin-associated clusters (Yi-Ming, Merle, Yan-Ni, Shabbir, et al., 2022). The products of betalactone and Gxps clusters have been identified as playing a role in insect immune suppression, while photoxenobactin has been shown to possess insecticidal properties (Shi et al., 2022). Other clusters exhibited similarities to various types of bioactive compounds with antibacterial, insecticidal, antiprotozoal, antifungal, and antiparasitic properties (Bode et al., 2017; Nicholas et al., 2017; Yi-Ming & Helge, 2018), as well as broad-spectrum compounds like fabclavine (Wenski et al., 2019). However, some clusters were strain-specific, such as acinetobactin, ATred, butyrolactone, cuidadopeptide, PAX peptides, and RXPs in *X. stockiae* genomes. Unique discoveries included althiomycin in *X. indica* strain KK26.2, andrimid in *P. temperata* strain MW27.4, and malonomycin in *P. akhurstii* strain NN168.5.

To prioritize candidate strains from extensive genomic data, further characterization of BGCs was performed using BiG-SCAPE-COROSON. The tools offer a framework for natural product discovery by grouping similar BGCs, predicting their potential functions, and enabling researchers to explore the diversity of biosynthetic pathways. The analysis revealed significant BGC diversity across the two genera, identifying a total of 181 biosynthetic clusters (Table 14). Among these, 145 clusters matched known BGCs, while 36 were classified as unknown, suggesting the potential novelty of the associated metabolites. This finding aligns with previous discoveries of novel compounds using similar approaches, such as detoxin or rimosamide analogs from actinobacteria (Jorge et al., 2020). Other studies have successfully linked phylogenetic trees to BGC-guided genome mining, uncovering aryl polyenes from *Escherichia coli* (Pablo et al., 2016), arseno-organic metabolites from *Streptomyces lividans* (Pablo et al., 2016), corbomycin from *Streptomyces* sp. WAC01529 (Culp et al., 2020), and cepacin A from *Burkholderia ambifaria* (Alex et al., 2019).

Given these insights, strains *X. stockiae* RT25.5, *X. stockiae* SBRx11.1, *X. japonica* MW12.3, *X. indica* KK26.2, *X. miraniensis* MH16.1, *P. akhurstii* NN168.5, *P. temperata* MW27.4, and *P. hainanensis* NN169.4 emerge as promising candidates

for further exploration in the discovery of novel compounds. Among them, *X. stockiae* RT25.5, *X. stockiae* SBRx11.1, *X. indica* KK26.2, *P. temperata* MW27.4, and *P. akhurstii* NN168.5 stand out as strong candidates for experimental natural product discovery due to their richness in unique and unknown clusters. We subsequently selected then *X. stockiae* RT25.5 for further studies due to an intriguing orphan cluster containing genes related to transcription regulation and transport. Previous research has emphasized the significance of transcription regulation and transport mechanisms in the biosynthesis of antibiotics such as oleandomycin (Dyson, 2009) and spiramycin (Nguyen et al., 2010).

The strain *X. stockiae* RT25.5 underwent high-throughput whole genome sequencing, assembly, and annotation, followed by bioinformatics analyses. AntiSMASH and manual refinements identified 21 BGCs. Remarkably, cluster-2 showed homology with aryl polyenes (Gina et al., 2019), part of a widely distributed category of bacterial pigmented polyketides. Cluster-4 exhibited high similarity to fabclavine biosynthesis clusters, known for their broad-spectrum activity against bacteria, fungi, and eukaryotic cells (Fuchs et al., 2014) (Wenski et al., 2019). Cluster-6, an NRPS cluster, shared similarity with bovienimide, previously shown to suppress insect immune responses and potentially cause fatal immunosuppressive conditions (Yi-Ming, Merle, Yan-Ni, Shabbir, et al., 2022). The conservativeness of this biosynthetic gene cluster in *Xenorhabdus* spp. has been acknowledged by the Crawford laboratory (J.-H. Li et al., 2021). Cluster-7 was likely related to Acinetobactin, an NRP-siderophore involved in iron acquisition. Clusters-8 and 9 resembled xenematide and xenobactin, respectively, with xenematide exhibiting moderate antibacterial and weak insecticidal activity (Crawford et al., 2011), and xenobactin showing potent antiprotozoal and specific antibiotic activity (Grundmann et al., 2013). Cluster-10, identified as a Peptide-Antimicrobial-Xenorhabdus (PAX) cluster, shared 73% gene similarity with *X. innexi* strain HGB1681 and 28% with *X. bovienii* CS03 (Dreyer et al., 2019; Gualtieri et al., 2009). The most significant difference lied in the last amino acid (Gln vs. Ser) (Figure 18). We inferred that the structures and functions of compounds originating from *X. stockiae* strain RT25.5 may differ from those found in the published clusters. Cluster-11 was similar to nematophin biosynthesis, known for nematocidal and antifungal activity (Cai et al., 2017). Cluster-12 was linked to

Rhabdopeptide/Xenortide-like peptides, confirmed through manual verification, with antiprotozoal activity. Cluster-13 resembled, with antibacterial activity (Fu et al., 2012). Cluster-15 was classified as a carotenoid, essential for photoprotection and oxidative stress defense (Takashi, 2020). Cluster-16 was like cuidadopeptide, while cluster-17 resembled ATred (Andreas et al., 2020). Cluster-18 was linked to pyrrolizixenamide, a plant alkaloid with potent toxicity, and cluster-19 showed similarity to xenoamicin from *X. doucetiae*, with antiprotozoal activity (Qiuqin et al., 2013). Notably, among the unknown BGCs, there is one intertesting hybrid T1PKS-NRPS clusters (cluster-14) were identified. The hybrid cluster included genes encoding a drug-resistance transporter (EmrB/QacA efflux family protein), with transport-related genes located near the hybrid-encoding BGC. This suggests a mechanism to protect the producing organism from the metabolite's potentially harmful effects (Ellis et al., 2019). Several bioactive compounds such as griselimycin (Angela et al., 2015), salinosporamide A (Andrew et al., 2011), and platensimycin (Ryan et al., 2014), have been identified using resistance-guided genome mining, emphasizing the utility of such strategies in discovering new natural products.

Mass spectrometry data from LC-MSMS combined with molecular network analysis using the GNPS database led to the detection of several bioactive compounds in *X. stockiae* strain RT25.5 culture. GameXPeptides A and C are known for their broad spectrum of antimicrobial, antifungal, and insecticidal activities, with potential efficacy against various microorganisms. These peptides may also exhibit additional biological properties, such as immunomodulatory effects or interactions with host organisms, depending on their structure (Friederike et al., 2015). Pyrrolo[1,2-a]pyrazine-1,4-dione, hexahydro-3 (phenylmethyl), a natural compound found in organisms like *Streptomyces antioxidans*, *Streptomyces xiamenensis*, and *Vibrio anguillarum*, has been identified as an antibiotic against multidrug-resistant *Staphylococcus aureus* (MDRSA) (George Seghal et al., 2018). Spectroscopic analysis confirmed its identity and showed it possesses non-hemolytic behavior and antioxidant properties, emphasizing its bioactivity potential. Meanwhile, PE(16:1/0:0) and PE(18:1/0:0), identified through the GNPS database, were not associated with any reported biological activities, similar to Alpha-L-Asp-L-Phe from NIST14, which also lacked known activities. Xenobactins, on the other hand, are known to modulate host immune

responses (Dreyer et al., 2019; Grundmann et al., 2013; Tobias et al., 2017). Pyrrolizixenamide A and B, found in *X. szentirmaii* and *X. stockiae*, are pyrrolizidine alkaloids (PAs) with diverse pharmacological activities, some of which have antibacterial and antitumor properties. While most PAs originate from plants, a few bacterial PAs have been identified, suggesting they may influence the immune response of symbiotic hosts like nematodes, potentially promoting stable symbiosis with *Xenorhabdus* bacteria (Fang et al., 2021; Schimming et al., 2015).

Integrating *in silico* and *in vitro* approaches revealed a gap in the compounds detected by both methods. *In vitro* analysis failed to detect compounds such as fabclavine, bovienimide A, acinetobactin, xenematide, PAX peptides, nematophin, rhabdopeptide/xenortide-like peptides (RXPs), and xenoamicin. While, *in silico* analysis cannot predict the presence of Pyrrolo[1,2-a]pyrazine-1,4-dione, hexahydro-3-(phenylmethyl), which could correspond to one of the unknown clusters. These findings highlight the need for further characterization of unknown clusters to fully understand secondary metabolite production in *X. stockiae* strain RT25.5. Genome analysis provided a foundation for predicting biosynthetic pathways, while *in vitro* detection shown the presence of specific compounds. This integrated approach not only validated genetic predictions but also facilitated the further exploration of potential applications and the discovery of new compounds that may have been overlooked.

To unveil the unknown clusters, easyPACId (Edna et al., 2019; Edna et al., 2023), an efficient tool for specialized metabolite production, which allows direct bioactivity testing, was employed. The *X. stockiae* strain RT25.5 Δ*hfq* mutant was successfully created. The mutant was colorless and exhibited an absence of most natural products (NPs), as shown in base peak chromatograms (BPC). However, targeting NP production in the Δ*hfq* mutants was unsuccessful. This limitation may arise from the nature of biosynthetic gene clusters, which often consist of multiple separated transcription units. Activating only one transcription unit may result in partial BGC activation, leading to incomplete or no NP production. To fully activate the BGC and achieve complete compound production, serveral promoters must be activated simultaneously (Sebnem Hazal et al., 2022). Further investigations are needed to overcome this challenge and optimize NP production.

The antimicrobial activities of *X. stockiae* strain RT25.5 were comprehensively examined through various biological approaches, demonstrating its potential as a valuable source for antimicrobial agent discovery, particularly against challenging bacterial infections such as *Acinetobacter baumannii*. Antibacterial susceptibility tests, including MIC and MBC assays, highlighted the potency and spectrum of the RT25.5 extract. To investigate its specific impact on bacterial cells, electron microscopy revealed morphological changes in *A. baumannii* treated with the extract, such as cytoplasmic vacuolization, nucleoid aggregation, increased membrane permeability, and eventual cell lysis. These findings suggest that the extract disrupted cell membrane integrity, leading to ribonucleic acid loss but sparing deoxyribonucleic acid, potentially implying a transcription-inhibition mode of action (Mareike et al., 2010). Proteomic analysis further revealed significant changes in protein expression within *A. baylyi* treated with the RT25.5 extract. A total of 229 proteins showed increased expression, linked to critical biological processes such as enzymatic degradation of antimicrobial agents, modifications of bacterial proteins targeted by antimicrobials, and alterations in membrane permeability. These findings suggest the involvement of multiple immune-related pathways in bacterial host responses. Conversely, 147 proteins exhibited reduced expression, including those involved in essential cellular processes such as heme de-cyclizing activity, transcriptional regulation, tRNA binding, and siderophore-iron transmembrane transport. These findings supported our hypothesis, highlighting the impact of the treatment on protein expressions, particularly in crucial cellular processes and transcriptional regulatory mechanisms. These results provide valuable insights into the antimicrobial mechanisms of the RT25.5 extract and its potential applications in combating multidrug-resistant pathogens.

Genome analysis provided a foundation for predicting biosynthetic pathways, while in vitro detection confirmed the presence of specific bioactive compounds. This integrated approach not only validated genetic predictions but also enabled the discovery of novel compounds that may have been previously overlooked. The observed antimicrobial activity of *X. stockiae* strain RT25.5 highlights its potential as a valuable resource for developing effective antimicrobial agents, particularly against multidrug-resistant bacterial infections. Proteomic analysis further revealed significant

changes in protein expression in *A. baylyi* treated with the crude extract, offering key insights into the antimicrobial mechanisms of strain RT25.5. These findings emphasize the importance of genome mining as a powerful tool for identifying bioactive compound-producing strains and expanding the repertoire of potential therapeutic agents. Future research should focus on characterizing the specific bioactive molecules responsible for the antimicrobial effects, optimizing their production, and evaluating their efficacy in clinical applications, paving the way for the development of next-generation antibiotics.

REFERENCES

Ahmadi Badi, S., Moshiri, A., Fateh, A., Rahimi Jamnani, F., Sarshar, M., Vaziri, F., & Siadat, S. D. (2017). Microbiota-derived extracellular vesicles as new systemic regulators. *Frontiers in Microbiology*, *8*, 1610. https://doi.org/https://doi.org/10.3389/fmicb.2017.01610

Ajiboye, T. O., Skiebe, E., & Wilharm, G. (2018). Contributions of ferric uptake regulator Fur to the sensitivity and oxidative response of *Acinetobacter baumannii* to antibiotics. *Microbial Pathogenesis*, *119*, 35-41.

Akhurst, R. J. (1980). Morphological and functional dimorphism in *Xenorhabdus* spp., bacteria symbiotically associated with the insect pathogenic nematodes *Neoaplectana* and *Heterorhabditis*. *Microbiology*, *121*(2), 303-309.

Akhurst, R. J. (1982). Antibiotic Activity of *Xenorhabdus* spp., Bacteria Symbiotically Associated with Insect Pathogenic Nematodes of the Families *Heterorhabditidae* and *Steinernematidae*. *Microbiology*, *128*(12), 3061-3065. https://doi.org/https://doi.org/10.1099/00221287-128-12-3061

Alex, J. M., James, A. H. M., Matthew, J. B., Matthew, J., Cerith, J., Gordon, W., Angharad, E. G., Daniel, R. N., Thomas, R. C., & Julian, P. (2019). Genome mining identifies cepacin as a plant-protective metabolite of the biopesticidal bacterium Burkholderia ambifaria. *Nature Microbiology*, *4*(6), 996-1005.

Alexandre, L., Karl, G., Shiyuyun, T., & Mark, B. (2018). Modeling leaderless transcription and atypical genes results in more accurate gene prediction in prokaryotes. *Genome Research*, *28*(7), 1079-1089.

Ali, H. M., Salem, M. Z., El-Shikh, M. S., Megeed, A. A., Alogaibi, Y. A., & Talea, I. A. (2017). Investigation of the virulence factors and molecular characterization of the clonal relations of multidrug-resistant *Acinetobacter baumannii* isolates. *Journal of AOAC International*, *100*(1), 152-158.

Ambler, R. P. (1980). The structure of ß-lactamases Philosophical. *Transactions of the Royal Society*, *289*, 321-331.

Ambrosi, C., Scribano, D., Aleandri, M., Zagaglia, C., Di Francesco, L., Putignani, L., & Palamara, A. T. (2017). *Acinetobacter baumannii* virulence traits: a

comparative study of a novel sequence type with other Italian endemic international clones. *Frontiers in Microbiology*, *8*, 1977.

Andreas, T., Yan-Ni, S., Max, K., & Helge, B. B. (2020). Nonribosomal peptides produced by minimal and engineered synthetases with terminal reductase domains. *ChemBioChem*, *21*(19), 2750-2754.

Andrew, J. K., Ryan, P. M., Anna, L., & Bradley, S. M. (2011). Bacterial self-resistance to the natural proteasome inhibitor salinosporamide A. *ACS Chemical Biology*, *6*(11), 1257-1264.

Andrey, P., Dmitry, A., Dmitry, M., Alla, L., & Anton, K. (2020). Using SPAdes de novo assembler. *Current Protocols in Bioinformatics*, *70*(1), e102.

Angela, K., Peer, L., Deepak, V. A., Armin, B., Evelyne, F., Sylvie, S., Nestor, Z., Jennifer, H., Silke, C. W., & Claudia, K. (2015). Targeting DnaN for tuberculosis therapy using novel griselimycins. *Science*, *348*(6239), 1106-1112.

Antunes, L. C., Imperi, F., Carattoli, A., & Visca, P. (2011). Deciphering the multifactorial nature of *Acinetobacter baumannii* pathogenicity. *PloS One*, *6*(8), e22674.

Aranda, J., Bardina, C., Beceiro, A., Rumbo, S., Cabral, M. P., Barbé, J., & Bou, G. (2011). *Acinetobacter baumannii* RecA protein in repair of DNA damage, antimicrobial resistance, general stress response, and virulence. *Journal of Bacteriology*, *193*(15), 3740-3747. https://doi.org/10.1128/jb.00389-11

Arroyo, L. A., Herrera, C. M., Fernandez, L., Hankins, J. V., Trent, M. S., & Hancock, R. E. (2011). The pmrCAB operon mediates polymyxin resistance in *Acinetobacter baumannii* ATCC 17978 and clinical isolates through phosphoethanolamine modification of lipid A. *Antimicrobial Agents and Chemotherapy*, *55*(8), 3743-3751.

Ayoub Moubareck, C., & Hammoudi Halat, D. (2020). Insights into *Acinetobacter baumannii*: A Review of Microbiological, Virulence, and Resistance Traits in a Threatening Nosocomial Pathogen. *Antibiotics (Basel)*, *9*(3), 119. https://doi.org/10.3390/antibiotics9030119

Azar, Z. S., Kary, N. E., & Mohammadi, D. (2025). Characterization of two novel isolates of Photorhabdus and Xenorhabdus: Molecular identification, growth

rate, virulence, and antibacterial susceptibility. *International Journal of Tropical Insect Science*, 1-13. https://doi.org/https://doi.org/10.1007/s42690-024-01396-1

Babitzke, P., & Romeo, T. (2007). CsrB sRNA family: sequestration of RNA-binding regulatory proteins. *Current Opinion in Microbiology*, *10*(2), 156-163.

Baek, C. H., Wang, S., Roland, K. L., & Curtiss, R. (2009). Leucine-responsive regulatory protein (Lrp) acts as a virulence repressor in *Salmonella enterica* serovar Typhimurium. *Journal of Bacteriology*, *191*(4), 1278-1292.

Bager, R., Roghanian, M., Gerdes, K., & Clarke, D. J. (2016). Alarmone (p)ppGpp regulates the transition from pathogenicity to mutualism in *Photorhabdus luminescens*. *Molecular Microbiology*, *100*(4), 735-747.

Barbara, R. T., Kai, B., Jorge, C. N.-M., Nicole, E. A., Marc, G. C., Susan, E., Sanghoon, L., David, M., Michael, J. J. R., & Zachary, L. R. (2023). MIBiG 3.0: a community-driven effort to annotate experimentally validated biosynthetic gene clusters. *Nucleic Acids Research*, *51*(D1), D603-D610.

Basler, M., Ho, B., & Mekalanos, J. (2013). Tit-for-tat: type VI secretion system counterattack during bacterial cell-cell interactions. *Cell*, *152*(4), 884-894.

Beceiro, A., Llobet, E., Aranda, J., Bengoechea, J. A., Doumith, M., Hornsey, M., Dhanji, H., Chart, H., Bou, G., & Livermore, D. M. (2011). Phosphoethanolamine modification of lipid A in colistin-resistant variants of *Acinetobacter baumannii* mediated by the pmrAB two-component regulatory system. *Antimicrobial Agents and Chemotherapy*, *55*(7), 3370-3379.

Beemelmanns, C., Guo, H., Rischer, M., & Poulsen, M. (2016). Natural products from microbes associated with insects. *Beilstein Journal of Organic Chemistry*, *12*(1), 314-327.

Benmahmod, A. B., Said, H. S., & Ibrahim, R. H. (2019). Prevalence and mechanisms of carbapenem resistance among *Acinetobacter baumannii* clinical isolates in Egypt. *Microbial Drug Resistance*, *25*(4), 480-488.

Bentancor, L. V., Routray, A., Bozkurt-Guzel, C., Camacho-Peiro, A., Pier, G. B., & Maira-Litrán, T. (2012). Evaluation of the trimeric autotransporter Ata as a vaccine candidate against *Acinetobacter baumannii* infections. *Infection and Immunity*, *80*(10), 3381-3388. https://doi.org/10.1128/iai.06096-11

Bhargava, N., Sharma, P., & Capalash, N. (2010). Quorum sensing in Acinetobacter: an emerging pathogen. *Critical Reviews in Microbiology*, *36*(4), 349-360.

Bhuiyan, M. S., Ellett, F., Murray, G. L., Kostoulias, X., Cerqueira, G. M., Schulze, K. E., Mahamad Maifiah, M. H., Li, J., Creek, D. J., Lieschke, G. J., & Peleg, A. Y. (2016). *Acinetobacter baumannii* phenylacetic acid metabolism influences infection outcome through a direct effect on neutrophil chemotaxis. *Proceedings of the National Academy of Sciences*, *113*(34), 9599-9604. https://doi.org/10.1073/pnas.1523116113

Bird, A. F., & Akhurst, R. J. (1983). The nature of the intestinal vesicle in nematodes of the family Steinernematidae. *International Journal for Parasitology*, *13*(6), 599-606.

Bock, C. H., Shapiro-Ilan, D. I., Wedge, D. E., & Cantrell, C. L. (2014). Identification of the antifungal compound, trans-cinnamic acid, produced by *Photorhabdus luminescens*, a potential biopesticide against pecan scab. *Journal of Pest Science*, *87*(1), 155-162.

Bode, E., Brachmann, A. O., Kegler, C., Simsek, R., Dauth, C., Zhou, Q., Kaiser, M., Klemmt, P., & Bode, H. B. (2015). Simple "on-demand" production of bioactive natural products. *ChemBioChem*, *16*(7), 1115-1119.

Bode, E., He, Y., Vo, T. D., Schultz, R., Kaiser, M., & Bode, H. B. (2017). Biosynthesis and function of simple amides in Xenorhabdus doucetiae. *Environmental Microbiology*, *19*(11), 4564-4575.

Bode, H. B. (2009). Entomopathogenic bacteria as a source of secondary metabolites. *Current Opinion in Chemical Biology*, *13*(2), 224-230.

Boemare, N. (2002). *Biology, taxonomy and systematics of Photorhabdus and Xenorhabdus.* CABI Press.

Boemare, N., & Tailliez, P. (2009). Molecular approaches and techniques for the study of entomopathogenic bacteria. In *Insect pathogens: Molecular approaches and techniques* (pp. 32-49). CABI Wallingford UK.

Boemare, N. E., Akhurst, R. J., & Mourant, R. G. (1993). DNA relatedness between *Xenorhabdus* spp.(Enterobacteriaceae), symbiotic bacteria of entomopathogenic nematodes, and a proposal to transfer *Xenorhabdus*

luminescens to a new genus, *Photorhabdus* gen. nov. *International Journal of Systematic and Evolutionary Microbiology*, *43*(2), 249-255.

Bogaerts, P., Naas, T., El Garch, F., Cuzon, G., Deplano, A., Delaire, T., Huang, T.-D., Lissoir, B., Nordmann, P., & Glupczynski, Y. (2010). GES extended-spectrum β-lactamases in Acinetobacter baumannii isolates in Belgium. *Antimicrobial Agents and Chemotherapy*, *54*(11), 4872-4878. https://doi.org/10.1128/aac.00871-10

Boll, J. M., Tucker, A. T., Klein, D. R., Beltran, A. M., Brodbelt, J. S., Davies, B. W., & Trent, M. S. (2015). Reinforcing lipid A acylation on the cell surface of *Acinetobacter baumannii* promotes cationic antimicrobial peptide resistance and desiccation survival. *MBio*, *6*(3). https://doi.org/https://doi.org/10.1128/mbio.00478-15

Borgeaud, S., Metzger, L. C., Scrignari, T., & Blokesch, M. (2015). The type VI secretion system of *Vibrio cholerae* fosters horizontal gene transfer. *Science*, *347*(6217), 63-67.

Böszörményi, E., Érsek, T., Fodor, A., Fodor, A., Földes, L. S., Hevesi, M., Hogan, J., Katona, Z., Klein, M., & Kormány, A. (2009). Isolation and activity of *Xenorhabdus* antimicrobial compounds against the plant pathogens *Erwinia amylovora* and *Phytophthora nicotianae*. *Journal of Applied Microbiology*, *107*(3), 746-759.

Bou, G., Cerveró, G., Dominguez, M. A., Quereda, C., & Martínez-Beltrán, J. (2000). Characterization of a nosocomial outbreak caused by a multiresistant *acinetobacter baumannii* strain with a carbapenem-hydrolyzing enzyme: high-level carbapenem resistance in *A. baumannii* Is Not Due solely to the presence of β-lactamases. *Journal of Clinical Microbiology*, *38*(9), 3299-3305.

Bowden, S. D., Eyres, A., Chung, J. C., Monson, R. E., Thompson, A., Salmond, G. P., Spring, D. R., & Welch, M. (2013). Virulence in *Pectobacterium atrosepticum* is regulated by a coincidence circuit involving quorum sensing and the stress alarmone,(p)ppGpp. *Molecular Microbiology*, *90*(3), 457-471.

Brachmann, A. O., Brameyer, S., Kresovic, D., Hitkova, I., Kopp, Y., Manske, C., Schubert, K., Bode, H. B., & Heermann, R. (2013). Pyrones as bacterial signaling molecules. *Nature Chemical biology*, *9*(9), 573-578.

Brachmann, A. O., Forst, S., Furgani, G. M., Fodor, A., & Bode, H. B. (2006). Xenofuranones A and B: phenylpyruvate dimers from *Xenorhabdus szentirmaii*. *Journal of Natural Products*, *69*(12), 1830-1832.

Brachmann, A. O., Joyce, S. A., Jenke-Kodama, H., Schwär, G., Clarke, D. J., & Bode, H. B. (2007). A Type II Polyketide Synthase is Responsible for Anthraquinone Biosynthesis in *Photorhabdus luminescens*. *ChemBioChem*, *8*(14), 1721-1728. https://doi.org/10.1002/cbic.200700300

Brachmann, A. O., Kirchner, F., Kegler, C., Kinski, S. C., Schmitt, I., & Bode, H. B. (2012). Triggering the production of the cryptic blue pigment indigoidine from *Photorhabdus luminescens*. *J Biotechnol*, *157*(1), 96-99. https://doi.org/10.1016/j.jbiotec.2011.10.002

Brinkman, A. B., Ettema, T. J., De Vos, W. M., & Van Der Oost, J. (2003). The Lrp family of transcriptional regulators. *Molecular Microbiology*, *48*(2), 287-294.

Brock, D. A., Douglas, T. E., Queller, D. C., & Strassmann, J. E. (2011). Primitive agriculture in a social amoeba. *Nature*, *469*(7330), 393-396.

Brown, A., Fernández, I. S., Gordiyenko, Y., & Ramakrishnan, V. (2016). Ribosome-dependent activation of stringent control. *Nature*, *534*(7606), 277-280.

Bush, K., Jacoby, G. A., & Medeiros, A. A. (1995). A functional classification scheme for beta-lactamases and its correlation with molecular structure. *Antimicrobial Agents and Chemotherapy*, *39*(6), 1211-1233.

Butaye, P., Cloeckaert, A., & Schwarz, S. (2003). Mobile genes coding for efflux-mediated antimicrobial resistance in Gram-positive and Gram-negative bacteria. *International Journal of Antimicrobial Agents*, *22*(3), 205-210.

Camacho, M. I., Alvarez, A. F., Chavez, R. G., Romeo, T., Merino, E., & Georgellis, D. (2015). Effects of the global regulator CsrA on the BarA/UvrY two-component signaling system. *Journal of Bacteriology*, *197*(5), 983-991.

Camarena, L., Bruno, V., Euskirchen, G., Poggio, S., & Snyder, M. (2010). Molecular mechanisms of ethanol-induced pathogenesis revealed by RNA-sequencing.

PLoS Pathog, *6*(4), e1000834. https://doi.org/https://doi.org/10.1371/journal.ppat.1000834

Carruthers, M. D., Nicholson, P. A., Tracy, E. N., & Munson Jr, R. S. (2013). *Acinetobacter baumannii* utilizes a type VI secretion system for bacterial competition. *PloS One*, *8*(3), e59388. https://doi.org/https://doi.org/10.1371/journal.pone.0059388

Castillo-Juarez, I., Lopez-Jacome, L. E., Soberón-Chávez, G., Tomás, M., Lee, J., Castañeda-Tamez, P., Hernández-Bárragan, I. Á., Cruz-Muñiz, M. Y., Maeda, T., & Wood, T. K. (2017). Exploiting quorum sensing inhibition for the control of P*seudomonas aeruginosa* and *Acinetobacter baumannii* biofilms. *Current Topics in Medicinal Chemistry*, *17*(17), 1915-1927.

Catel-Ferreira, M., Coadou, G., Molle, V., Mugnier, P., Nordmann, P., Siroy, A., Jouenne, T., & Dé, E. (2011). Structure–function relationships of CarO, the carbapenem resistance-associated outer membrane protein of *Acinetobacter baumannii*. *Journal of Antimicrobial Chemotherapy*, *66*(9), 2053-2056.

Catel-Ferreira, M., Marti, S., Guillon, L., Jara, L., Coadou, G., Molle, V., Bouffartigues, E., Bou, G., Shalk, I., & Jouenne, T. (2016). The outer membrane porin OmpW of *Acinetobacter baumannii* is involved in iron uptake and colistin binding. *FEBS Letters*, *590*(2), 224-231.

Celmer, W. D., & Solomons, I. (1955). The structures of thiolutin and aureothricin, antibiotics containing a unique pyrrolinonodithiole nucleus. *Journal of the American Chemical Society*, *77*(10), 2861-2865.

Cerqueira, G. M., Kostoulias, X., Khoo, C., Aibinu, I., Qu, Y., Traven, A., & Peleg, A. Y. (2014). A Global Virulence Regulator in *Acinetobacter baumanni*i and Its Control of the Phenylacetic Acid Catabolic Pathway. *The Journal of Infectious Diseases*, *210*(1), 46-55. https://doi.org/10.1093/infdis/jiu024

Chalabaev, S., Turlin, E., Bay, S., Ganneau, C., Brito-Fravallo, E., Charles, J.-F., Danchin, A., & Biville, F. (2008). Cinnamic acid, an autoinducer of its own biosynthesis, is processed via Hca enzymes in Photorhabdus luminescens. *Applied and Environmental Microbiology*, *74*(6), 1717-1725.

Challinor, V. L., & Bode, H. B. (2015). Bioactive natural products from novel microbial sources. *Annals of the New York Academy of Sciences*, *1354*(1), 82-97. https://doi.org/10.1111/nyas.12954

Chaston, J. M., Suen, G., Tucker, S. L., Andersen, A. W., Bhasin, A., Bode, E., Bode, H. B., Brachmann, A. O., Cowles, C. E., & Cowles, K. N. (2011). The entomopathogenic bacterial endosymbionts *Xenorhabdus* and *Photorhabdus*: convergent lifestyles from divergent genomes. *PloS One*, *6*(11), e27909. https://doi.org/https://doi.org/10.1371/journal.pone.0027909

Chen, G. (1996). *Antimicrobial activity of the nematode symbionts, Xenorhabdus and Photorhabdus (Enterobacteriaceae), and the discovery of two groups of antimicrobial substances, nematophin and xenorxides* [Doctoral dissertation, Dept. of Biological Sciences)/Simon Fraser University]. https://summit.sfu.ca/_flysystem/fedora/sfu_migrate/7145/b18292021.pdf

Chen, H., Cao, J., Zhou, C., Liu, H., Zhang, X., & Zhou, T. (2017). Biofilm formation restrained by subinhibitory concentrations of tigecyclin in *Acinetobacter baumannii* is associated with downregulation of efflux pumps. *Chemotherapy*, *62*(2), 128-133.

Chin, C. Y., Gregg, K. A., Napier, B. A., Ernst, R. K., & Weiss, D. S. (2015). A PmrB-regulated deacetylase required for lipid A modification and polymyxin resistance in *Acinetobacter baumannii*. *Antimicrobial Agents and Chemotherapy*, *59*(12), 7911-7914.

Choi, C. H., Lee, E. Y., Lee, Y. C., Park, T. I., Kim, H. J., Hyun, S. H., Kim, S. A., Lee, S. K., & Lee, J. C. (2005). Outer membrane protein 38 of *Acinetobacter baumannii* localizes to the mitochondria and induces apoptosis of epithelial cells. *Cellular Microbiology*, *7*(8), 1127-1138.

Choi, C. H., Lee, J. S., Lee, Y. C., Park, T. I., & Lee, J. C. (2008). *Acinetobacter baumannii* invades epithelial cells and outer membrane protein A mediates interactions with epithelial cells. *BMC Microbiology*, *8*(1), 216. https://doi.org/10.1186/1471-2180-8-216

Chopra, I., & Roberts, M. (2001). Tetracycline antibiotics: mode of action, applications, molecular biology, and epidemiology of bacterial resistance. *Microbiology and Molecular Biology Reviews*, *65*(2), 232-260.

Ciche, T. A., Blackburn, M., Carney, J. R., & Ensign, J. C. (2003). Photobactin: a catechol siderophore produced by *Photorhabdus luminescens*, an entomopathogen mutually associated with *Heterorhabditis bacteriophora* NC1 nematodes. *Applied and Environmental Microbiology*, *69*(8), 4706-4713.

Cisneros, J. M., & Rodríguez-Baño, J. (2002). Nosocomial bacteremia due to *Acinetobacter baumannii:* epidemiology, clinical features and treatment. *Clinical Microbiology and Infection*, *8*(11), 687-693.

Clarke, D. J. (2016). The regulation of secondary metabolism in *Photorhabdus*. In *The Molecular Biology of Photorhabdus Bacteria* (pp. 81-102). Springer.

Cowles, K. N., Cowles, C. E., Richards, G. R., Martens, E. C., & Goodrich-Blair, H. (2007). The global regulator Lrp contributes to mutualism, pathogenesis and phenotypic variation in the bacterium *Xenorhabdus nematophila*. *Cellular Microbiology*, *9*(5), 1311-1323.

Coyne, S., Courvalin, P., & Périchon, B. (2011). Efflux-mediated antibiotic resistance in *Acinetobacter* spp. *Antimicrobial Agents and Chemotherapy*, *55*(3), 947-953.

Cramton, S. E., Gerke, C., Schnell, N. F., Nichols, W. W., & Götz, F. (1999). The intercellular adhesion (ica) locus is present in *Staphylococcus aureus* and is required for biofilm formation. *Infection and Immunity*, *67*(10), 5427-5433.

Crawford, J. M., Kontnik, R., & Clardy, J. (2010). Regulating alternative lifestyles in entomopathogenic bacteria. *Current Biology*, *20*(1), 69-74.

Crawford, J. M., Mahlstedt, S. A., Malcolmson, S. J., Clardy, J., & Walsh, C. T. (2011). Dihydrophenylalanine: a prephenate-derived *Photorhabdus luminescens* antibiotic and intermediate in dihydrostilbene biosynthesis. *Chemistry & Biology*, *18*(9), 1102-1112. https://doi.org/10.1016/j.chembiol.2011.07.009

Crawford, J. M., Portmann, C., Zhang, X., Roeffaers, M. B., & Clardy, J. (2012). Small molecule perimeter defense in entomopathogenic bacteria. *Proceedings of the National Academy of Sciences*, *109*(27), 10821-10826.

Davies, J. A., Harrison, J. J., Marques, L. L., Foglia, G. R., Stremick, C. A., Storey, D. G., Turner, R. J., Olson, M. E., & Ceri, H. (2007). The GacS sensor kinase controls phenotypic reversion of small colony variants isolated from biofilms of *Pseudomonas aeruginosa* PA14. *FEMS Microbiology Ecology*, *59*(1), 32-46.

de Breij, A., Dijkshoorn, L., Lagendijk, E., van der Meer, J., Koster, A., Bloemberg, G., Wolterbeek, R., van den Broek, P., & Nibbering, P. (2010). Do biofilm formation and interactions with human cells explain the clinical success of *Acinetobacter baumannii*? *PloS One*, *5*(5), e10732. https://doi.org/https://doi.org/10.1371/journal.pone.0010732

del Mar Tomás, M., Beceiro, A., Pérez, A., Velasco, D., Moure, R., Villanueva, R., Martínez-Beltrán, J., & Bou, G. (2005). Cloning and functional analysis of the gene encoding the 33-to 36-kilodalton outer membrane protein associated with carbapenem resistance in *Acinetobacter baumannii*. *Antimicrobial Agents and Chemotherapy*, *49*(12), 5172-5175.

Derzelle, S., Duchaud, E., Kunst, F., Danchin, A., & Bertin, P. (2002). Identification, characterization, and regulation of a cluster of genes involved in carbapenem biosynthesis in *Photorhabdus luminescens*. *Applied and Environmental Microbiology*, *68*(8), 3780-3789.

Dreyer, J., Marina, R., Booysen, E., Staden, A. D. V., Deane, S. M., & Dicks, L. M. T. (2019). Xenorhabdus khoisanae SB10 produces Lys-rich PAX lipopeptides and a Xenocoumacin in its antimicrobial complex. *BMC Microbiology*, *19*, 1-11.

Dubois, D., Prasadarao, N. V., Mittal, R., Bret, L., Roujou-Gris, M., & Bonnet, R. (2009). CTX-M β-lactamase production and virulence of *Escherichia coli* K1. *Emerging Infectious Diseases*, *15*(12), 1988.

Duchaud, E., Rusniok, C., Frangeul, L., Buchrieser, C., Givaudan, A., Taourit, S., Bocs, S., Boursaux-Eude, C., Chandler, M., & Charles, J.-F. (2003). The

genome sequence of the entomopathogenic bacterium *Photorhabdus luminescens*. *Nature Biotechnology*, *21*(11), 1307-1313.

Dudnik, A., Bigler, L., & Dudler, R. (2013). Heterologous expression of a *Photorhabdus luminescens* syrbactin-like gene cluster results in production of the potent proteasome inhibitor glidobactin A. *Microbiol Res*, *168*(2), 73-76. https://doi.org/10.1016/j.micres.2012.09.006

Dupont, M., Pagès, J.-M., Lafitte, D., Siroy, A., & Bollet, C. (2005). Identification of an OprD Homologue in *Acinetobacter baumannii*. *Journal of Proteome Research*, *4*(6), 2386-2390.

Dyson, P. (2009). *Streptomyces* (3rd th ed.). Academic Press. https://doi.org/https://doi.org/10.1016/B978-012373944-5.00037-7

Easom, C. A., & Clarke, D. J. (2012). HdfR is a regulator in *Photorhabdus luminescens* that modulates metabolism and symbiosis with the nematode *Heterorhabditis*. *Environmental Microbiology*, *14*(4), 953-966.

Edna, B., Antje, K. H., Merle, H., Desalegne, A., Yan-Ni, S., Tien Duy, V., Frank, W., Yi-Ming, S., Peter, G., & Svenja, S. (2019). Promoter activation in Δhfq mutants as an efficient tool for specialized metabolite production enabling direct bioactivity testing. *Angewandte Chemie*, *131*(52), 19133-19139.

Edna, B., Daniela, A., Petra, H., Elmar, M., Karin, M., Nicole, R., & Helge, B. B. (2023). easyPACId, a simple method for Induced Production, isolation, identification, and testing of Natural products from Proteobacteria. *Bio-Protocol*, *13*(3), 1-13.

Elhosseiny, N. M., Amin, M. A., Yassin, A. S., & Attia, A. S. (2015). *Acinetobacter baumannii* universal stress protein A plays a pivotal role in stress response and is essential for pneumonia and sepsis pathogenesis. *International Journal of Medical Microbiology*, *305*(1), 114-123. https://doi.org/https://doi.org/10.1016/j.ijmm.2014.11.008

Elhosseiny, N. M., El-Tayeb, O. M., Yassin, A. S., Lory, S., & Attia, A. S. (2016). The secretome of *Acinetobacter baumannii* ATCC 17978 type II secretion system reveals a novel plasmid encoded phospholipase that could be implicated in lung colonization. *International Journal of Medical Microbiology*, *306*(8), 633-641.

Ellis, C. O. N., Michelle, S., Charles, B. L., & Natalie, M.-A. (2019). Targeted antibiotic discovery through biosynthesis-associated resistance determinants: Target directed genome mining. *Critical Reviews in Microbiology*, *45*(3), 255-277. https://doi.org/https://doi.org/10.1080/1040841X.2019.1590307

Eren, A. M., Özcan, C. E., Christopher, Q., Joseph, H. V., Hilary, G. M., Mitchell, L. S., & Tom, O. D. (2015). Anvi'o: an advanced analysis and visualization platform for 'omics data. *PeerJ*, *3*, e1319. https://doi.org/https://doi.org/10.7717/peerj.1319

Espinal, P., Pantel, A., Rolo, D., Marti, S., López-Rojas, R., Smani, Y., Pachón, J., Vila, J., & Lavigne, J.-P. (2019). Relationship between different resistance mechanisms and virulence in *Acinetobacter baumannii*. *Microbial Drug Resistance*, *25*(5), 752-760.

Ettlinger, L., Gäumann, E., Hütter, R., Keller-Schierlein, W., Kradolfer, F., Neipp, L., Prelog, V., Reusser, P., & Zähner, H. (1959). Stoffwechselprodukte von Actinomyceten, XVI. Cinerubine. *Chemische Berichte*, *92*(8), 1867-1879.

Fernández-Cuenca, F., Smani, Y., Gómez-Sánchez, M. C., Docobo-Pérez, F., Caballero-Moyano, F. J., Domínguez-Herrera, J., Pascual, A., & Pachón, J. (2011). Attenuated virulence of a slow-growing pandrug-resistant *Acinetobacter baumannii* is associated with decreased expression of genes encoding the porins CarO and OprD-like. *International Journal of Antimicrobial Agents*, *38*(6), 548-549.

Fiester, S. E., Arivett, B. A., Schmidt, R. E., Beckett, A. C., Ticak, T., Carrier, M. V., Ghosh, R., Ohneck, E. J., Metz, M. L., & Sellin Jeffries, M. K. (2016). Iron-regulated phospholipase C activity contributes to the cytolytic activity and virulence of *Acinetobacter baumannii*. *PloS One*, *11*(11), e0167068. https://doi.org/https://doi.org/10.1371/journal.pone.0167068

Friederike, I. N., Christina, D., Geraldine, M., Carsten, K., Marcel, K., Nick, R. W., & Helge, B. B. (2015). Insect-specific production of new GameXPeptides in Photorhabdus luminescens TTO1, widespread natural products in entomopathogenic bacteria. *ChemBioChem*, *16*(2), 205-208.

Fu, J., Bian, X., Hu, S., Wang, H., Huang, F., Seibert, P. M., Plaza, A., Xia, L., Müller, R., & Stewart, A. F. (2012). Full-length RecE enhances linear-linear

homologous recombination and facilitates direct cloning for bioprospecting. *Nature Biotechnology*, *30*(5), 440-446.

Fuchs, S. W., Grundmann, F., Kurz, M., Kaiser, M., & Bode, H. B. (2014). Fabclavines: Bioactive Peptide–Polyketide-Polyamino Hybrids from *Xenorhabdus*. *ChemBioChem*, *15*(4), 512-516.

Fuchs, S. W., Proschak, A., Jaskolla, T. W., Karas, M., & Bode, H. B. (2011). Structure elucidation and biosynthesis of lysine-rich cyclic peptides in *Xenorhabdus nematophila*. *Organic & Biomolecular Chemistry*, *9*(9), 3130-3132.

Fukruksa, C., Yimthin, T., Suwannaroj, M., Muangpat, P., Tandhavanant, S., Thanwisai, A., & Vitta, A. (2017). Isolation and identification of Xenorhabdus and Photorhabdus bacteria associated with entomopathogenic nematodes and their larvicidal activity against Aedes aegypti. *Parasites & Vectors*, *10*(1), 440. https://doi.org/10.1186/s13071-017-2383-2

Gaca, A. O., Colomer-Winter, C., & Lemos, J. A. (2015). Many means to a common end: the intricacies of (p) ppGpp metabolism and its control of bacterial homeostasis. *Journal of Bacteriology*, *197*(7), 1146-1156.

Gaca, A. O., Kudrin, P., Colomer-Winter, C., Beljantseva, J., Liu, K., Anderson, B., Wang, J. D., Rejman, D., Potrykus, K., & Cashel, M. (2015). From (p)ppGpp to (pp)pGpp: characterization of regulatory effects of pGpp synthesized by the small alarmone synthetase of *Enterococcus faecalis*. *Journal of Bacteriology*, *197*(18), 2908-2919.

Gaddy, J. A., Arivett, B. A., McConnell, M. J., López-Rojas, R., Pachón, J., & Actis, L. A. (2012). Role of acinetobactin-mediated iron acquisition functions in the interaction of *Acinetobacter baumannii* strain ATCC 19606T with human lung epithelial cells, *Galleria mellonella* caterpillars, and mice. *Infection and Immunity*, *80*(3), 1015-1024.

Gaddy, J. A., Tomaras, A. P., & Actis, L. A. (2009). The *Acinetobacter baumannii* 19606 OmpA protein plays a role in biofilm formation on abiotic surfaces and in the interaction of this pathogen with eukaryotic cells. *Infection and Immunity*, *77*(8), 3150-3160.

Gallego, L., & Towner, K. J. (2001). Carriage of class 1 integrons and antibiotic resistance in clinical isolates of *Acinetobacter baumannii* from Northern Spain. *Journal of Medical Microbiology*, *50*(1), 71-77. https://doi.org/https://doi.org/10.1099/0022-1317-50-1-71

Gebhardt, M. J., Gallagher, L. A., Jacobson, R. K., Usacheva, E. A., Peterson, L. R., Zurawski, D. V., & Shuman, H. A. (2015). Joint transcriptional control of virulence and resistance to antibiotic and environmental stress in *Acinetobacter baumannii*. *MBio*, *6*(6), e01660-01615. https://doi.org/10.1128/mBio.01660-15

Gehrlein, M., Leying, H., Cullmann, W., Wendt, S., & Opferkuch, W. (1991). Imipenem resistance in *Acinetobacter baumanii* is due to altered penicillin-binding proteins. *Chemotherapy*, *37*(6), 405-412.

Geisinger, E., Huo, W., Hernandez-Bird, J., & Isberg, R. R. (2019). *Acinetobacter baumannii*: envelope determinants that control drug resistance, virulence, and surface variability. *Annual Review of Microbiology*, *73*, 481-506.

Geisinger, E., & Isberg, R. R. (2015). Antibiotic modulation of capsular exopolysaccharide and virulence in *Acinetobacter baumannii*. *PLoS Pathog*, *11*(2), e1004691. https://doi.org/https://doi.org/10.1371/journal.ppat.1004691

George Seghal, K., Sethu, P., Arya, S., Amrudha, R., & Joseph, S. (2018). An antibiotic agent pyrrolo 1, 2-a pyrazine-1, 4-dione, hexahydro isolated from a marine bacteria Bacillus tequilensis MSI45 effectively controls multi-drug resistant Staphylococcus aureus. *RSC Advances*, *8*, 17837-17846.

Gina, L. C. G., Maximilian, S., Kudratullah, K., Yi-Ming, S., Tim, A. S. n., Nicholas, J. T., Nina, M., Michael, G., & Helge, B. B. (2019). An uncommon type II PKS catalyzes biosynthesis of aryl polyene pigments. *Journal of the American Chemical Society*, *141*(42), 16615-16623.

Glare, T., Jurat-Fuentes, J.-L., & O'callaghan, M. (2017). Basic and applied research: entomopathogenic bacteria. In *Microbial control of insect and mite pests* (pp. 47-67). Elsevier.

Goodrich-Blair, H., & Clarke, D. J. (2007). Mutualism and pathogenesis in *Xenorhabdus* and *Photorhabdus*: two roads to the same destination. *Molecular Microbiology*, *64*(2), 260-268.

Gordon, N. C., & Wareham, D. W. (2010). Multidrug-resistant Acinetobacter baumannii: mechanisms of virulence and resistance. *International Journal of Antimicrobial Agents*, *35*(3), 219-226.

Grant, J. R., & Stothard, P. (2008). The CGView Server: a comparative genomics tool for circular genomes. *Nucleic Acids Research*, *36*(suppl_2), W181-W184.

Grundmann, F., Kaiser, M., Kurz, M., Schiell, M., Batzer, A., & Bode, H. B. (2013). Structure determination of the bioactive depsipeptide xenobactin from *Xenorhabdus* sp. PB30. 3. *RSC Advances*, *3*(44), 22072-22077.

Gualtieri, M., Aumelas, A., & Thaler, J.-O. (2009). Identification of a new antimicrobial lysine-rich cyclolipopeptide family from *Xenorhabdus nematophila*. *The Journal of Antibiotics*, *62*(6), 295-302.

Harding, C. M., Hennon, S. W., & Feldman, M. F. (2018). Uncovering the mechanisms of *Acinetobacter baumannii* virulence. *Nature Reviews Microbiology*, *16*(2), 91-102.

Harding, C. M., Kinsella, R. L., Palmer, L. D., Skaar, E. P., & Feldman, M. F. (2016). Medically relevant *Acinetobacter* species require a type II secretion system and specific membrane-associated chaperones for the export of multiple substrates and full virulence. *PLoS Pathogens*, *12*(1), e1005391. https://doi.org/https://doi.org/10.1371/journal.ppat.1005391

Hart, B. R., & Blumenthal, R. M. (2011). Unexpected coregulator range for the global regulator Lrp of *Escherichia coli* and *Proteus mirabilis*. *Journal of Bacteriology*, *193*(5), 1054-1064.

Haseley, S. R., Pantophlet, R., Brade, L., Holst, O., & Brade, H. (1997). Structural and serological characterisation of the O-antigenic polysaccharide of the lipopolysaccharide from *Acinetobacter junii* strain 65. *European Journal of Biochemistry*, *245*(2), 477-481.

Hauryliuk, V., Atkinson, G. C., Murakami, K. S., Tenson, T., & Gerdes, K. (2015). Recent functional insights into the role of (p) ppGpp in bacterial physiology. *Nature Reviews Microbiology*, *13*(5), 298-309.

Heather, S. K., & Randy, G. (2009). *Entomopathogenic nematode and bacteria mutualism*. CRC Press.

Heeb, S., & Haas, D. (2001). Regulatory Roles of the GacS/GacA Two-Component System in Plant-Associated and Other Gram-Negative Bacteria. *Molecular Plant-Microbe Interactions*, *14*(12), 1351-1363. https://doi.org/10.1094/mpmi.2001.14.12.1351

Herbert, E. E., & Goodrich-Blair, H. (2007). Friend and foe: the two faces of *Xenorhabdus nematophila*. *Nature Reviews Microbiology*, *5*(8), 634-646.

Hesketh, A., Chen, W. J., Ryding, J., Chang, S., & Bibb, M. (2007). The global role of ppGpp synthesis in morphological differentiation and antibiotic production in *Streptomyces coelicolor* A3 (2). *Genome Biology*, *8*(8), R161. https://doi.org/https://doi.org/10.1186/gb-2007-8-8-r161

Hood, M. I., Jacobs, A. C., Sayood, K., Dunman, P. M., & Skaar, E. P. (2010). *Acinetobacter baumannii* increases tolerance to antibiotics in response to monovalent cations. *Antimicrobial Agents and Chemotherapy*, *54*(3), 1029-1041.

Hood, M. I., Mortensen, B. L., Moore, J. L., Zhang, Y., Kehl-Fie, T. E., Sugitani, N., Chazin, W. J., Caprioli, R. M., & Skaar, E. P. (2012). Identification of an *Acinetobacter baumannii* zinc acquisition system that facilitates resistance to calprotectin-mediated zinc sequestration. *PLoS Pathog*, *8*(12), e1003068. https://doi.org/https://doi.org/10.1371/journal.ppat.1003068

Hu, K., Li, J., Li, B., Webster, J. M., & Chen, G. (2006). A novel antimicrobial epoxide isolated from larval *Galleria mellonella* infected by the nematode symbiont, *Photorhabdus luminescens* (Enterobacteriaceae). *Bioorganic & Medicinal Chemistry*, *14*(13), 4677-4681.

Hu, K., Li, J., Wang, W., Wu, H., Lin, H., & Webster, J. M. (1998). Comparison of metabolites produced *in vitro* and *in vivo* by *Photorhabdus luminescens*, a bacterial symbiont of the entomopathogenic nematode *Heterorhabditis megidis*. *Canadian Journal of Microbiology*, *44*(11), 1072-1077. https://doi.org/10.1139/w98-098

Hu, K., Li, J., & Webster, J. M. (1996). 3, 5-Dihydroxy-4-isopropylstilbene: a selective nematicidal compound from the culture filtrate of *Photorhabdus luminescens*. *Canadian Journal of Plant Pathology*, *18*, 104.

Huang, W., Wang, S., Yao, Y., Xia, Y., Yang, X., Long, Q., Sun, W., Liu, C., Li, Y., & Ma, Y. (2015). OmpW is a potential target for eliciting protective immunity against *Acinetobacter baumannii* infections. *Vaccine, 33*(36), 4479-4485.

Huang, W., Yao, Y., Wang, S., Xia, Y., Yang, X., Long, Q., Sun, W., Liu, C., Li, Y., & Chu, X. (2016). Immunization with a 22-kDa outer membrane protein elicits protective immunity to multidrug-resistant *Acinetobacter baumannii*. *Scientific Reports*, *6*(1), 1-12.

Hussa, E. A., Casanova-Torres, Á. M., & Goodrich-Blair, H. (2015). The global transcription factor Lrp controls virulence modulation in *Xenorhabdus nematophila*. *Journal of Bacteriology*, *197*(18), 3015-3025.

Imai, Y., Meyer, K. J., Iinishi, A., Favre-Godal, Q., Green, R., Manuse, S., Caboni, M., Mori, M., Niles, S., & Ghiglieri, M. (2019). A new antibiotic selectively kills Gram-negative pathogens. *Nature, 576*(7787), 459-464.

Inmaculada, G., Manuel Carlos, L., Adriana, E., Génesis, P., Bartolomé, C., Celia, B., Marina, S., Manuel, S., Emma, C., & Thomas, M. C. (2023). Differential expression profile of genes involved in the immune response associated to progression of chronic Chagas disease. *PLOS Neglected Tropical Diseases, 17*(7), e0011474. https://doi.org/https://doi.org/10.1371/journal.pntd.0011474

Iwashkiw, J. A., Seper, A., Weber, B. S., Scott, N. E., Vinogradov, E., Stratilo, C., Reiz, B., Cordwell, S. J., Whittal, R., & Schild, S. (2012). Identification of a general O-linked protein glycosylation system in *Acinetobacter baumannii* and its role in virulence and biofilm formation. *PLoS Pathog*, *8*(6), e1002758. https://doi.org/https://doi.org/10.1371/journal.ppat.1002758

Jacobs, A. C., Hood, I., Boyd, K. L., Olson, P. D., Morrison, J. M., Carson, S., Sayood, K., Iwen, P. C., Skaar, E. P., & Dunman, P. M. (2010). Inactivation of phospholipase D diminishes *Acinetobacter baumannii* pathogenesis. *Infection and Immunity*, *78*(5), 1952-1962.

Jeon, J. H., Lee, J. H., Lee, J. J., Park, K. S., Karim, A. M., Lee, C.-R., Jeong, B. C., & Lee, S. H. (2015). Structural basis for carbapenem-hydrolyzing mechanisms of carbapenemases conferring antibiotic resistance. *International Journal of Molecular Sciences*, *16*(5), 9654-9692.

Ji, D., & Kim, Y. (2004). An entomopathogenic bacterium, *Xenorhabdus nematophila*, inhibits the expression of an antibacterial peptide, cecropin, of the beet armyworm, *Spodoptera exigua*. *Journal of Insect Physiology*, *50*(6), 489-496.

Jianxiong, L., Genhui, C., & John, M. W. (1997). Nematophin, a novel antimicrobial substance produced by Xenorhabdus nematophilus (Enterobactereaceae). *Canadian Journal of Microbiology*, *43*(8), 770-773.

Jianxiong, L., Genhui, C., & Webster, J. M. (1997). Synthesis and antistaphylococcal activity of nematophin and its analogs. *Bioorganic & Medicinal Chemistry Letters*, *7*(10), 1349-1352.

Jin, J. S., Kwon, S.-O., Moon, D. C., Gurung, M., Lee, J. H., Kim, S. I., & Lee, J. C. (2011). *Acinetobacter baumannii* secretes cytotoxic outer membrane protein A via outer membrane vesicles. *PloS One*, *6*(2), e17027. https://doi.org/https://doi.org/10.1371/journal.pone.0017027

Johnson, T. L., Waack, U., Smith, S., Mobley, H., & Sandkvist, M. (2016). *Acinetobacter baumannii* is dependent on the type II secretion system and its substrate LipA for lipid utilization and *in vivo* fitness. *Journal of Bacteriology*, *198*(4), 711-719.

Jones, C. L., Clancy, M., Honnold, C., Singh, S., Snesrud, E., Onmus-Leone, F., McGann, P., Ong, A. C., Kwak, Y., & Waterman, P. (2015). Fatal outbreak of an emerging clone of extensively drug-resistant *Acinetobacter baumannii* with enhanced virulence. *Clinical Infectious Diseases*, *61*(2), 145-154.

Jordan, I. K., Kira, S. M., John, L. S., Yuri, I. W., & Eugene, V. K. (2001). Lineage-specific gene expansions in bacterial and archaeal genomes. *Genome Research*, *11*(4), 555-565.

Jorge, C. N.-M., Nelly, S.-M., Michael, W. M., Satria, A. K., James, H. T., Elizabeth, I. P., Emmanuel, L. C. D. L. S., Marley, Y., Pablo, C.-M., & Sahar, A. (2020). A computational framework to explore large-scale biosynthetic diversity. *Nature Chemical biology*, *16*(1), 60-68.

Joshi, N. A., & Fass, J. N. (2011). *Sickle: A sliding-window, adaptive, quality-based trimming tool for FastQ files (Version 1.33)*. In *GitHub* [Software]. https://github.com/najoshi/sickle

Joyce, S. A., Brachmann, A. O., Glazer, I., Lango, L., Schwär, G., Clarke, D. J., & Bode, H. B. (2008). Bacterial Biosynthesis of a Multipotent Stilbene. *Angewandte Chemie International Edition*, *47*(10), 1942-1945. https://doi.org/10.1002/anie.200705148

Joyce, S. A., & Clarke, D. J. (2003). A *hexA* homologue from *Photorhabdus* regulates pathogenicity, symbiosis and phenotypic variation. *Molecular Microbiology*, *47*(5), 1445-1457.

Joyce, S. A., Lango, L., & Clarke, D. J. (2011). Chapter 1 - The Regulation of Secondary Metabolism and Mutualism in the Insect Pathogenic Bacterium *Photorhabdus luminescens*. In A. I. Laskin, S. Sariaslani, & G. M. Gadd (Eds.), *Advances in Applied Microbiology* (Vol. 76, pp. 1-25). Academic Press. https://doi.org/https://doi.org/10.1016/B978-0-12-387048-3.00001-5

Jun, S. H., Lee, J. H., Kim, B. R., Kim, S. I., Park, T. I., Lee, J. C., & Lee, Y. C. (2013). *Acinetobacter baumannii* outer membrane vesicles elicit a potent innate immune response via membrane proteins. *PloS One*, *8*(8), e71751. https://doi.org/https://doi.org/10.1371/journal.pone.0071751

Juttukonda, L. J., Chazin, W. J., & Skaar, E. P. (2016). *Acinetobacter baumannii* coordinates urea metabolism with metal import to resist host-mediated metal limitation. *MBio*, *7*(5). https://doi.org/https://doi.org/10.1128/mbio.01475-16

Kai, B., Simon, S., Alexander, M. K., Zach, C.-P., Gilles, P. V. W., Marnix, H. M., & Tilmann, W. (2021). antiSMASH 6.0: improving cluster detection and comparison capabilities. *Nucleic Acids Research*, *49*(W1), W29-W35.

Kazuya, Y., Kirk, A. R., Roland, D. K., Katherine, S. R., David, J. G., Victor, N., Pieter, C. D., & Bradley, S. M. (2014). Direct cloning and refactoring of a silent lipopeptide biosynthetic gene cluster yields the antibiotic taromycin A. *Proceedings of the National Academy of Sciences*, *111*(5), 1957-1962.

Kenyon, J. J., & Hall, R. M. (2013). Variation in the complex carbohydrate biosynthesis loci of *Acinetobacter baumannii* genomes. *PloS One*, *8*(4), e62160. https://doi.org/https://doi.org/10.1371/journal.pone.0062160

Kim, S. W., Choi, C. H., Moon, D. C., Jin, J. S., Lee, J. H., Shin, J.-H., Kim, J. M., Lee, Y. C., Seol, S. Y., & Cho, D. T. (2009). Serum resistance of

Acinetobacter baumannii through the binding of factor H to outer membrane proteins. *FEMS Microbiology Letters*, *301*(2), 224-231.

Kim, Y. J., Kim, S. I., Kim, Y. R., Hong, K. W., Wie, S. H., Park, Y. J., Jeong, H., & Kang, M. W. (2012). Carbapenem-resistant *Acinetobacter baumannii*: diversity of resistant mechanisms and risk factors for infection. *Epidemiology & Infection*, *140*(1), 137-145.

Knapp, S., Wieland, C. W., Florquin, S., Pantophlet, R., Dijkshoorn, L., Tshimbalanga, N., Akira, S., & van der Poll, T. (2006). Differential Roles of CD14 and Toll-like Receptors 4and 2 in Murine *Acinetobacter Pneumonia*. *American Journal of Respiratory and Critical Care Medicine*, *173*(1), 122-129.

Koenigs, A., Stahl, J., Averhoff, B., Göttig, S., Wichelhaus, T. A., Wallich, R., Zipfel, P. F., & Kraiczy, P. (2016). CipA of *Acinetobacter baumannii* Is a Novel Plasminogen Binding and Complement Inhibitory Protein. *The Journal of Infectious Diseases*, *213*(9), 1388-1399. https://doi.org/10.1093/infdis/jiv601

Koenigs, A., Zipfel, P. F., & Kraiczy, P. (2015). Translation Elongation Factor Tuf of *Acinetobacter baumannii* Is a Plasminogen-Binding Protein. *PloS One*, *10*(7), e0134418. https://doi.org/10.1371/journal.pone.0134418

Kontnik, R., Crawford, J. M., & Clardy, J. (2010). Exploiting a Global Regulator for Small Molecule Discovery in *Photorhabdus luminescens*. *ACS Chemical Biology*, *5*(7), 659-665. https://doi.org/10.1021/cb100117k

Korotkov, K. V., Sandkvist, M., & Hol, W. G. (2012). The type II secretion system: biogenesis, molecular architecture and mechanism. *Nature Reviews Microbiology*, *10*(5), 336-351.

Krin, E., Chakroun, N., Turlin, E., Givaudan, A., Gaboriau, F., Bonne, I., Rousselle, J.-C., Frangeul, L., Lacroix, C., & Hullo, M.-F. (2006). Pleiotropic role of quorum-sensing autoinducer 2 in P*hotorhabdus luminescens*. *Applied and Environmental Microbiology*, *72*(10), 6439-6451.

Krin, E., Derzelle, S., Bedard, K., Adib-Conquy, M., Turlin, E., Lenormand, P., Hullo, M. F., Bonne, I., Chakroun, N., & Lacroix, C. (2008). Regulatory role of UvrY in adaptation of *Photorhabdus luminescens* growth inside the insect. *Environmental Microbiology*, *10*(5), 1118-1134.

Kuo, S. C., Chang, S. C., Wang, H. Y., Lai, J. F., Chen, P. C., Shiau, Y. R., Huang, I. W., & Lauderdale, T. L. Y. (2012). Emergence of extensively drug-resistant *Acinetobacter baumannii* complex over 10 years: nationwide data from the Taiwan Surveillance of Antimicrobial Resistance (TSAR) program. *BMC Infectious Diseases*, *12*(1), 200. https://doi.org/https://doi.org/10.1186/1471-2334-12-200

Kwon, S. O., Gho, Y. S., Lee, J. C., & Kim, S. I. (2009). Proteome analysis of outer membrane vesicles from a clinical *Acinetobacter baumannii* isolate. *FEMS Microbiology Letters*, *297*(2), 150-156.

Lang, G., Kalvelage, T., Peters, A., Wiese, J., & Imhoff, J. F. (2008). Linear and cyclic peptides from the entomopathogenic bacterium *Xenorhabdus nematophilus*. *Journal of Natural Products*, *71*(6), 1074-1077.

Lango-Scholey, L., Brachmann, A. O., Bode, H. B., & Clarke, D. J. (2013). The expression of *stlA* in *Photorhabdus luminescens* is controlled by nutrient limitation. *PloS One*, *8*(11), e82152. https://doi.org/https://doi.org/10.1371/journal.pone.0082152

Lango, L., & Clarke, D. J. (2010). A metabolic switch is involved in lifestyle decisions in *Photorhabdus luminescens*. *Molecular Microbiology*, *77*(6), 1394-1405.

Lapouge, K., Schubert, M., Allain, F. H. T., & Haas, D. (2008). Gac/Rsm signal transduction pathway of γ-proteobacteria: from RNA recognition to regulation of social behaviour. *Molecular Microbiology*, *67*(2), 241-253.

Lasa, I., & Penadés, J. R. (2006). Bap: a family of surface proteins involved in biofilm formation. *Research in Microbiology*, *157*(2), 99-107.

Lee, C. R., Lee, J. H., Park, M., Park, K. S., Bae, I. K., Kim, Y. B., Cha, C. J., Jeong, B. C., & Lee, S. H. (2017). Biology of Acinetobacter baumannii: Pathogenesis, Antibiotic Resistance Mechanisms, and Prospective Treatment Options [Review]. *Frontiers in Cellular and Infection Microbiology*, *7*(55). https://doi.org/10.3389/fcimb.2017.00055

Lee, J., & Zhang, L. (2015). The hierarchy quorum sensing network in *Pseudomonas aeruginosa*. *Protein Cell*, *6*(1), 26-41. https://doi.org/10.1007/s13238-014-0100-x

Lee, J. S., Choi, C. H., Kim, J. W., & Lee, J. C. (2010). *Acinetobacter baumannii* outer membrane protein A induces dendritic cell death through mitochondrial targeting. *The Journal of Microbiology*, *48*(3), 387-392.

Lees-Miller, R. G., Iwashkiw, J. A., Scott, N. E., Seper, A., Vinogradov, E., Schild, S., & Feldman, M. F. (2013). A common pathway for O-linked protein-glycosylation and synthesis of capsule in *Acinetobacter baumannii*. *Molecular Microbiology*, *89*(5), 816-830.

Li, B., Wever, W. J., Walsh, C. T., & Bowers, A. A. (2014). Dithiolopyrrolones: biosynthesis, synthesis, and activity of a unique class of disulfide-containing antibiotics. *Natural Product Reports*, *31*(7), 905-923.

Li, B., Wever, W. J., Walsh, C. T., & Bowers, A. A. (2015). Correction: Dithiolopyrrolones: biosynthesis, synthesis, and activity of a unique class of disulfide-containing antibiotics. *Natural Product Reports*, *32*(2), 348-349.

Li, F. J., Starrs, L., & Burgio, G. (2018). Tug of war between *Acinetobacter baumannii* and host immune responses. *Pathogens and Disease*, *76*(9), ftz004. https://doi.org/https://doi.org/10.1093/femspd/ftz004

Li, J.-H., Cho, W., Hamchand, R., Oh, J., & Crawford, J. M. (2021). A conserved nonribosomal peptide synthetase in Xenorhabdus bovienii produces citrulline-functionalized lipopeptides. *Journal of Natural Products*, *84*(10), 2692-2699.

Li, J., Chen, G., & Webster, J. M. (1997). Nematophin, a novel antimicrobial substance produced by *Xenorhabdus nematophilus* (Enterobactereaceae). *Canadian journal of microbiology*, *43*(8), 770-773.

Li, J., Chen, G., Webster, J. M., & Czyzewska, E. (1995). Antimicrobial metabolites from a bacterial symbiont. *Journal of Natural Products*, *58*(7), 1081-1086.

Li, J. H., Cho, W., Hamchand, R., Oh, J., & Crawford, J. M. (2021). A Conserved Nonribosomal Peptide Synthetase in Xenorhabdus bovienii Produces Citrulline-Functionalized Lipopeptides. *J Nat Prod*, *84*(10), 2692-2699. https://doi.org/10.1021/acs.jnatprod.1c00573

Li, Z. T., Zhang, R. L., Bi, X. G., Xu, L., Fan, M., Xie, D., Xian, Y., Wang, Y., Li, X. J., & Wu, Z. D. (2015). Outer membrane vesicles isolated from two clinical

Acinetobacter baumannii strains exhibit different toxicity and proteome characteristics. *Microbial Pathogenesis*, *81*, 46-52.

Lin, L., Tan, B., Pantapalangkoor, P., Ho, T., Baquir, B., Tomaras, A., Montgomery, J. I., Barbacci, E. G., Hujer, K., & Bonomo, R. A. (2012). Inhibition of LpxC protects mice from resistant *Acinetobacter baumannii* by modulating inflammation and enhancing phagocytosis. *MBio*, *3*(5). https://doi.org/https://doi.org/10.1128/mbio.00312-12

Lin, M. F., & Lan, C. Y. (2014). Antimicrobial resistance in *Acinetobacter baumannii*: From bench to bedside. *World Journal of Clinical Cases: WJCC*, *2*(12), 787-814.

Lin, W., Kovacikova, G., & Skorupski, K. (2007). The quorum sensing regulator HapR downregulates the expression of the virulence gene transcription factor AphA in *Vibrio cholerae* by antagonizing Lrp-and VpsR-mediated activation. *Molecular Microbiology*, *64*(4), 953-967.

Liu, C. C., Kuo, H. Y., Tang, C. Y., Chang, K. C., & Liou, M. L. (2014). Prevalence and mapping of a plasmid encoding a type IV secretion system in *Acinetobacter baumannii*. *Genomics*, *104*(3), 215-223.

Liu, D., Liu, Z. S., Hu, P., Cai, L., Fu, B. Q., Li, Y. S., Lu, S. Y., Liu, N. N., Ma, X. L., Chi, D., Chang, J., Shui, Y. M., Li, Z. H., Ahmad, W., Zhou, Y., & Ren, H. L. (2016). Characterization of surface antigen protein 1 (SurA1) from *Acinetobacter baumannii* and its role in virulence and fitness. *Veterinary Microbiology*, *186*, 126-138. https://doi.org/https://doi.org/10.1016/j.vetmic.2016.02.018

Liu, M. Y., & Romeo, T. (1997). The global regulator CsrA of *Escherichia coli* is a specific mRNA-binding protein. *Journal of Bacteriology*, *179*(14), 4639-4642.

Loehfelm, T. W., Luke, N. R., & Campagnari, A. A. (2008). Identification and characterization of an *Acinetobacter baumannii* biofilm-associated protein. *Journal of Bacteriology*, *190*(3), 1036-1044.

Luísa, C. S. A., Paolo, V., & Kevin, J. T. (2014). Acinetobacter baumannii: evolution of a global pathogen. *Pathogens and Disease*, *71*(3), 292-301.

Luke, N. R., Sauberan, S. L., Russo, T. A., Beanan, J. M., Olson, R., Loehfelm, T. W., Cox, A. D., Michael, F. S., Vinogradov, E. V., & Campagnari, A. A. (2010). Identification and characterization of a glycosyltransferase involved in *Acinetobacter baumannii* lipopolysaccharide core biosynthesis. *Infection and Immunity*, *78*(5), 2017-2023.

Mack, D., Fischer, W., Krokotsch, A., Leopold, K., Hartmann, R., Egge, H., & Laufs, R. (1996). The intercellular adhesin involved in biofilm accumulation of *Staphylococcus epidermidis* is a linear beta-1, 6-linked glucosaminoglycan: purification and structural analysis. *Journal of Bacteriology*, *178*(1), 175-183.

Maira-Litrán, T., Kropec, A., Abeygunawardana, C., Joyce, J., Mark III, G., Goldmann, D. A., & Pier, G. B. (2002). Immunochemical properties of the staphylococcal poly-N-acetylglucosamine surface polysaccharide. *Infection and Immunity*, *70*(8), 4433-4440.

Mak, J. K., Kim, M.-J., Pham, J., Tapsall, J., & White, P. A. (2009). Antibiotic resistance determinants in nosocomial strains of multidrug-resistant *Acinetobacter baumannii*. *Journal of Antimicrobial Chemotherapy*, *63*(1), 47-54.

Mareike, H., Marina, B., Jacques, H., Mohammad Fotouhi, A., Dagmar, G., & Anne, S. U. (2010). Damage of the bacterial cell envelope by antimicrobial peptides gramicidin S and PGLa as revealed by transmission and scanning electron microscopy. *Antimicrobial Agents and Chemotherapy*, *54*(8), 3132-3142.

McConnell, M. J., Actis, L., & Pachón, J. (2013). *Acinetobacter baumannii*: human infections, factors contributing to pathogenesis and animal models. *FEMS Microbiology Reviews*, *37*(2), 130-155. https://doi.org/10.1111/j.1574-6976.2012.00344.x

McInerney, B. V., Taylor, W. C., Lacey, M. J., Akhurst, R. J., & Gregson, R. P. (1991). Biologically active metabolites from *Xenorhabdus* spp., Part 2. Benzopyran-1-one derivatives with gastroprotective activity. *Journal of Natural Products*, *54*(3), 785-795.

McQueary, C. N., Kirkup, B. C., Si, Y., Barlow, M., Actis, L. A., Craft, D. W., & Zurawski, D. V. (2012). Extracellular stress and lipopolysaccharide modulate

Acinetobacter baumannii surface-associated motility. *Journal of Microbiology*, *50*(3), 434-443.

Mendes, R. E., Farrell, D. J., Sader, H. S., & Jones, R. N. (2010). Comprehensive assessment of tigecycline activity tested against a worldwide collection of *Acinetobacter* spp.(2005–2009). *Diagnostic Microbiology and Infectious Disease*, *68*(3), 307-311.

Moffatt, J. H., Harper, M., Harrison, P., Hale, J. D., Vinogradov, E., Seemann, T., Henry, R., Crane, B., Michael, F. S., & Cox, A. D. (2010). Colistin resistance in *Acinetobacter baumannii* is mediated by complete loss of lipopolysaccharide production. *Antimicrobial Agents and Chemotherapy*, *54*(12), 4971-4977.

Moon, D. C., Choi, C. H., Lee, J. H., Choi, C.-W., Kim, H.-Y., Park, J. S., Kim, S. I., & Lee, J. C. (2012). *Acinetobacter baumannii* outer membrane protein A modulates the biogenesis of outer membrane vesicles. *The Journal of Microbiology*, *50*(1), 155-160.

Moore, J. L., Becker, K. W., Nicklay, J. J., Boyd, K. L., Skaar, E. P., & Caprioli, R. M. (2014). Imaging mass spectrometry for assessing temporal proteomics: analysis of calprotectin in *Acinetobacter baumannii* pulmonary infection. *Proteomics*, *14*(7-8), 820-828.

Morikawa, M., Kagihiro, S., Haruki, M., Takano, K., Branda, S., Kolter, R., & Kanaya, S. (2006). Biofilm formation by a Bacillus subtilis strain that produces γ-polyglutamate. *Microbiology*, *152*(9), 2801-2807.

Morris, F. C., Dexter, C., Kostoulias, X., Uddin, M. I., & Peleg, A. (2019). The mechanisms of disease caused by *Acinetobacter baumannii*. *Frontiers in Microbiology*, *10*, 1601.

Moubareck, C., Brémont, S., Conroy, M.-C., Courvalin, P., & Lambert, T. (2009). GES-11, a Novel Integron-Associated GES Variant in Acinetobacter baumannii. *Antimicrobial Agents and Chemotherapy*, *53*(8), 3579-3581. https://doi.org/10.1128/aac.00072-09

Mougous, J. D., Cuff, M. E., Raunser, S., Shen, A., Zhou, M., Gifford, C. A., Goodman, A. L., Joachimiak, G., Ordoñez, C. L., & Lory, S. (2006). A

virulence locus of *Pseudomonas aeruginosa* encodes a protein secretion apparatus. *Science, 312*(5779), 1526-1530.

Mussi, M. A., Limansky, A. S., & Viale, A. M. (2005). Acquisition of resistance to carbapenems in multidrug-resistant clinical strains of *Acinetobacter baumannii*: natural insertional inactivation of a gene encoding a member of a novel family of β-barrel outer membrane proteins. *Antimicrobial Agents and Chemotherapy, 49*(4), 1432-1440.

Nairn, B. L., Lonergan, Z. R., Wang, J., Braymer, J. J., Zhang, Y., Calcutt, M. W., Lisher, J. P., Gilston, B. A., Chazin, W. J., & de Crécy-Lagard, V. (2016). The response of *Acinetobacter baumannii* to zinc starvation. *Cell Host & Microbe, 19*(6), 826-836.

Nelson, L. K., Stanton, M. M., Elphinstone, R. E., Helwerda, J., Turner, R. J., & Ceri, H. (2010). Phenotypic diversification *in vivo*: *Pseudomonas aeruginosa gacS*− strains generate small colony variants *in vivo* that are distinct from in vitro variants. *Microbiology, 156*(12), 3699-3709.

Nemec, A., Dolzani, L., Brisse, S., van den Broek, P., & Dijkshoorn, L. (2004). Diversity of aminoglycoside-resistance genes and their association with class 1 integrons among strains of pan-European *Acinetobacter baumannii* clones. *Journal of Medical Microbiology, 53*(12), 1233-1240. https://doi.org/https://doi.org/10.1099/jmm.0.45716-0

Newman, D. J., & Cragg, G. M. (2012). Natural products as sources of new drugs over the 30 years from 1981 to 2010. *Journal of Natural Products, 75*(3), 311-335.

Nguyen, H. C., Karray, F., Lautru, S., Gagnat, J., Lebrihi, A., Ho Huynh, T. D., & Pernodet, J. L. (2010). Glycosylation steps during spiramycin biosynthesis in Streptomyces ambofaciens: involvement of three glycosyltransferases and their interplay with two auxiliary proteins. *Antimicrob Agents Chemother, 54*(7), 2830-2839. https://doi.org/https://doi.org/10.1128/aac.01602-09

Nicholas, J. T., Antje, K. H., Helena, E., Patrick, R. W., Nick, N., Rolf, B., & Helge, B. B. (2017). Photorhabdus-nematode symbiosis is dependent on hfq-mediated regulation of secondary metabolites. *Environmental Microbiology, 19*(1), 119-129.

Niu, C., Clemmer, K. M., Bonomo, R. A., & Rather, P. N. (2008). Isolation and characterization of an autoinducer synthase from *Acinetobacter baumannii*. *Journal of Bacteriology*, *190*(9), 3386-3392.

Nollmann, F. I., Dauth, C., Mulley, G., Kegler, C., Kaiser, M., Waterfield, N. R., & Bode, H. B. (2015). Insect-specific production of new GameXPeptides in *Photorhabdus luminescens* TTO1, widespread natural products in entomopathogenic bacteria. *ChemBioChem*, *16*(2), 205-208.

Nollmann, F. I., Dowling, A., Kaiser, M., Deckmann, K., Grösch, S., & Bode, H. B. (2012). Synthesis of szentiamide, a depsipeptide from entomopathogenic *Xenorhabdus szentirmaii* with activity against *Plasmodium falciparum*. *Beilstein Journal of Organic Chemistry*, *8*(1), 528-533.

Ohlendorf, B., Simon, S., Wiese, J., & Imhoff, J. F. (2011). Szentiamide, an N-formylated cyclic depsipeptide from *Xenorhabdus szentirmaii* DSM 16338T. *Natural Product Communications*, *6*(9). https://doi.org/https://doi.org/10.1177/1934578X1100600909

Olivia, S., Victoria, L. C., Nicholas, J. T., Hélène, A., Peter, G., Laura, P., Christian, R., Harald, S., & Helge, B. B. (2015). Structure, biosynthesis, and occurrence of bacterial pyrrolizidine alkaloids. *Angewandte Chemie International Edition*, *54*(43), 12702-12705.

Omkar, S. M., Colton, J. L., Jonathan, M. M., Tilmann, W., & Bernhard, O. P. (2022). Pangenome analysis of Enterobacteria reveals richness of secondary metabolite gene clusters and their associated gene sets. *Synthetic and Systems Biotechnology*, *7*(3), 900-910.

Pablo, C.-M., Johannes Florian, K., Christian, M.-G., Luis Alfonso, Y.-G., Nelly, S.-M., Hilda, R.-A., Jörg, F., & Francisco, B.-G. (2016). Phylogenomic analysis of natural products biosynthetic gene clusters allows discovery of arseno-organic metabolites in model streptomycetes. *Genome Biology and Evolution*, *8*(6), 1906-1916.

Palma, L., Frizzo, L., Kaiser, S., Berry, C., Caballero, P., Bode, H. B., & Del Valle, E. E. (2024). Genome Sequence Analysis of Native Xenorhabdus Strains Isolated from Entomopathogenic Nematodes in Argentina. *Toxins*, *16*(2), 108. https://www.mdpi.com/2072-6651/16/2/108

Park, D., Ciezki, K., Van Der Hoeven, R., Singh, S., Reimer, D., Bode, H. B., & Forst, S. (2009). Genetic analysis of xenocoumacin antibiotic production in the mutualistic bacterium *Xenorhabdus nematophila*. *Molecular Microbiology*, *73*(5), 938-949.

Park, H. B., & Crawford, J. M. (2015). Lumiquinone A, an α-aminomalonate-derived aminobenzoquinone from *Photorhabdus luminescens*. *Journal of Natural Products*, *78*(6), 1437-1441.

Patricia Stock, S., Campbell, J. F., & Nadler, S. A. (2001). Phylogeny of Steinernema Travassos, 1927 (Cephalobina: Steinernematidae) inferred from ribosomal DNA sequences and morphological characters. *Journal of Parasitology*, *87*(4), 877-889.

Paul, S., Andrew, M., Owen, O., Nitin, S. B., Jonathan, T. W., Daniel, R., Nada, A., Benno, S., & Trey, I. (2003). Cytoscape: a software environment for integrated models of biomolecular interaction networks. *Genome Research*, *13*(11), 2498-2504.

Paul, V. J., Frautschy, S., Fenical, W., & Nealson, K. H. (1981). Isolation and structure assignment of several new antibacterial compounds from the insect-symbiotic bacteria *Xenorhabdus* spp. *Journal of Chemical Ecology*, *7*, 589-597.

Pelletier, M. R., Casella, L. G., Jones, J. W., Adams, M. D., Zurawski, D. V., Hazlett, K. R., Doi, Y., & Ernst, R. K. (2013). Unique structural modifications are present in the lipopolysaccharide from colistin-resistant strains of *Acinetobacter baumannii*. *Antimicrobial Agents and Chemotherapy*, *57*(10), 4831-4840.

Penwell, W. F., Arivett, B. A., & Actis, L. A. (2012). The *Acinetobacter baumannii entA* gene located outside the acinetobactin cluster is critical for siderophore production, iron acquisition and virulence. *PloS One*, *7*(5). https://doi.org/https://doi.org/10.1371/journal.pone.0036493

Pereira, C. S., Thompson, J. A., & Xavier, K. B. (2013). AI-2-mediated signalling in bacteria. *FEMS Microbiology Reviews*, *37*(2), 156-181.

Pérez, A., Merino, M., Rumbo-Feal, S., Álvarez-Fraga, L., Vallejo, J. A., Beceiro, A., Ohneck, E. J., Mateos, J., Fernández-Puente, P., Actis, L. A., Poza, M., &

Bou, G. (2017). The FhaB/FhaC two-partner secretion system is involved in adhesion of *Acinetobacter baumannii* AbH12O-A2 strain. *Virulence*, *8*(6), 959-974. https://doi.org/10.1080/21505594.2016.1262313

Pernestig, A.-K., Georgellis, D., Romeo, T., Suzuki, K., Tomenius, H., Normark, S., & Melefors, Ö. (2003). The *Escherichia coli* BarA-UvrY two-component system is needed for efficient switching between glycolytic and gluconeogenic carbon sources. *Journal of Bacteriology*, *185*(3), 843-853.

Piel, J. (2009). Metabolites from symbiotic bacteria. *Natural Product Reports*, *26*(3), 338-362.

Pires, S., & Parker, D. (2019). Innate immune responses to *Acinetobacter baumannii* in the airway. *Journal of Interferon & Cytokine Research*, *39*(8), 441-449.

Poinar, G. O. (1966). The presence of *Achromobacter nematophilus* in the infective stage of a Neoaplectana sp.(Steinernematidae: Nematoda). *Nematologica*, *12*(1), 105-108.

Poinar, G. O. (1975). Description and biology of a new insect parasitic rhabditoid, *Heterorhabditis bacteriophora* n. gen., n. sp.(Rhabditida; Heterorhabditidae n. fam.). *Nematologica*, *21*(4), 463-470.

Poinar, G. O., Gaugler, R., & Kaya, H. K. (1990). Entomopathogenic nematodes in biological control. *Taxonomy and Biology of Steinernematidae and Heterorhabditidae. CRC Press, Boca Raton, Florida*, 23-74.

Poinar, G. O., Hess, R. T., Lanier, W., Kinney, S., & White, J. H. (1989). Preliminary observations of a bacteriophage infecting *Xenorhabdus luminescens* (Enterobacteriaceae). *Experientia*, *45*(2), 191-192.

Poinar, G. O., & Thomas, G. M. (1966). Significance of *Achromobacter nematophilus* Poinar and Thomas (Achromobacteraceae: Eubacteriales) in the development of the nematode, DD-136 (Neoaplectana sp. Steinernematidae). *Parasitology*, *56*(2), 385-390.

Poinar Jr, G., Hess, R., & Thomas, G. (1980). Isolation of defective bacteriophages from *Xenorhabdus* spp.(Enterobacteriaceae). *IRCS Medical Science: Microbiology, Parasitology and Infectious Diseases*, *8*(3-4). https://www.cabidigitallibrary.org/doi/full/10.5555/19800869444

Poinar Jr, G. O., & Grewal, P. (2012). History of entomopathogenic nematology. *Journal of Nematology*, *44*(2), 153.

Poinar Jr, G. O., & Leutenegger, R. (1968). Anatomy of the infective and normal third-stage juveniles of *Neoaplectana carpocapsae* Weiser (Steinernematidae: Nematoda). *The Journal of Parasitology*, *54*(2), 340-350.

Poinar Jr, G. O., Thomas, G., Haygood, M., & Nealson, K. H. (1980). Growth and luminescence of the symbolic bacteria associated with the terrestrial nematode, *Heterorphabditis bacteriophora*. *Soil Biology and Biochemistry*, *12*(1), 5-10.

Poinar Jr, G. O., & Thomas, G. M. (1967). The nature of *Achromobacter nematophilus* as an insect pathogen. *Journal of Invertebrate Pathology*, *9*(4), 510-514.

Proschak, A., Schultz, K., Herrmann, J., Dowling, A. J., Brachmann, A. O., ffrench-Constant, R., Müller, R., & Bode, H. B. (2011). Cytotoxic fatty acid amides from *Xenorhabdus*. *ChemBioChem*, *12*(13), 2011-2015.

Proschak, A., Zhou, Q., Schöner, T., Thanwisai, A., Kresovic, D., Dowling, A., Proschak, E., & Bode, H. B. (2014). Biosynthesis of the insecticidal xenocyloins in *Xenorhabdus bovienii*. *ChemBioChem*, *15*(3), 369-372.

Půža, V., & Machado, R. A. R. (2024). Systematics and phylogeny of the entomopathogenic nematobacterial complexes Steinernema–Xenorhabdus and Heterorhabditis–Photorhabdus. *Zoological Letters*, *10*(1), 13. https://doi.org/10.1186/s40851-024-00235-y

Qin, Z., Huang, S., Yu, Y., & Deng, H. (2013). Dithiolopyrrolone natural products: isolation, synthesis and biosynthesis. *Marine Drugs*, *11*(10), 3970-3997.

Qiuqin, Z., Florian, G., Marcel, K., Matthias, S., Sophie, G., Andreas, B., Michael, K., & Helge, B. B. (2013). Structure and biosynthesis of xenoamicins from entomopathogenic Xenorhabdus. *Chemistry–A European Journal*, *19*, 16772-16779.

Quale, J., Bratu, S., Landman, D., & Heddurshetti, R. (2003). Molecular epidemiology and mechanisms of carbapenem resistance in *Acinetobacter baumannii* endemic in New York City. *Clinical Infectious Diseases*, *37*(2), 214-220.

Queenan, A. M., & Bush, K. (2007). Carbapenemases: the Versatile β-Lactamases. *Clinical Microbiology Reviews*, *20*(3), 440-458. https://doi.org/10.1128/cmr.00001-07

Reimer, D. (2013). *Identification and characterization of selected secondary metabolite biosynthetic pathways from Xenorhabdus nematophila* [Doctoral dissertation, Ph. D. thesis, Johann Wolfgang Groethe-Universität, Frankfurt,

Reimer, D., Cowles, K., Proschak, A., Nollmann, F., Dowling, A., & Kaiser, M. (2013). R. ffrench-Constant, H. Goodrich-Blair and HB Bode. *ChemBioChem*, *14*, 1991-1997.

Reimer, D., Luxenburger, E., Brachmann, A. O., & Bode, H. B. (2009). A new type of pyrrolidine biosynthesis is involved in the late steps of xenocoumacin production in *Xenorhabdus nematophila*. *ChemBioChem*, *10*(12), 1997-2001.

Repizo, G. D., Gagné, S., Foucault-Grunenwald, M.-L., Borges, V., Charpentier, X., Limansky, A. S., Gomes, J. P., Viale, A. M., & Salcedo, S. P. (2015). Differential Role of the T6SS in *Acinetobacter baumannii* Virulence. *PloS One*, *10*(9), e0138265. https://doi.org/10.1371/journal.pone.0138265

Ricardo, A. R. M., Arthur, M., Shimaa, M. G., Aunchalee, T., Sylvie, P., Helge, B. B., Mona, A. H., Kamal, M. K., & Louis, S. T. (2021). Photorhabdus heterorhabditis subsp. aluminescens subsp. nov., Photorhabdus heterorhabditis subsp. heterorhabditis subsp. nov., Photorhabdus australis subsp. thailandensis subsp. nov., Photorhabdus australis subsp. australis subsp. nov., and Photorhabdus aegyptia sp. nov. isolated from Heterorhabditis entomopathogenic nematodes. *International Journal of Systematic and Evolutionary Microbiology*, *71*(1), 004610. https://doi.org/https://doi.org/10.1099/ijsem.0.004610

Richards, G. R., Herbert, E. E., Park, Y., & Goodrich-Blair, H. (2008). *Xenorhabdus nematophila lrhA* is necessary for motility, lipase activity, toxin expression, and virulence in Manduca sexta insects. *Journal of Bacteriology*, *190*(14), 4870-4879.

Richardson, W. H., Schmidt, T. M., & Nealson, K. H. (1988). Identification of an anthraquinone pigment and a hydroxystilbene antibiotic from *Xenorhabdus*

luminescens. *Applied and Environmental Microbiology*, *54*(6), 1602-1605. https://doi.org/10.1128/AEM.54.6.1602-1605.1988

Rill, A., Zhao, L., & Bode, H. B. (2024). Genetic toolbox for Photorhabdus and Xenorhabdus: pSEVA based heterologous expression systems and CRISPR/Cpf1 based genome editing for rapid natural product profiling. *Microbial Cell Factories*, *23*(1), 98. https://doi.org/10.1186/s12934-024-02363-8

Romeo, T. (1998). Global regulation by the small RNA-binding protein CsrA and the non-coding RNA molecule CsrB. *Molecular Microbiology*, *29*(6), 1321-1330.

Ruiz, F. M., Santillana, E., Spínola-Amilibia, M., Torreira, E., Culebras, E., & Romero, A. (2015). Crystal Structure of Hcp from *Acinetobacter baumannii*: A Component of the Type VI Secretion System. *PloS One*, *10*(6), e0129691. https://doi.org/10.1371/journal.pone.0129691

Rumbo, C., Fernández-Moreira, E., Merino, M., Poza, M., Mendez, J. A., Soares, N. C., Mosquera, A., Chaves, F., & Bou, G. (2011). Horizontal transfer of the OXA-24 carbapenemase gene via outer membrane vesicles: a new mechanism of dissemination of carbapenem resistance genes in *Acinetobacter baumannii*. *Antimicrobial Agents and Chemotherapy*, *55*(7), 3084-3090.

Rumbo, C., Tomás, M., Moreira, E. F., Soares, N. C., Carvajal, M., Santillana, E., Beceiro, A., Romero, A., & Bou, G. (2014). The *Acinetobacter baumannii* Omp33-36 porin is a virulence factor that induces apoptosis and modulates autophagy in human cells. *Infection and Immunity*, *82*(11), 4666-4680.

Russo, T. A., Luke, N. R., Beanan, J. M., Olson, R., Sauberan, S. L., MacDonald, U., Schultz, L. W., Umland, T. C., & Campagnari, A. A. (2010). The K1 capsular polysaccharide of *Acinetobacter baumannii* strain 307-0294 is a major virulence factor. *Infection and Immunity*, *78*(9), 3993-4000.

Russo, T. A., MacDonald, U., Beanan, J. M., Olson, R., MacDonald, I. J., Sauberan, S. L., Luke, L. W., & Umland, T. C. (2009). Penicillin-binding protein 7/8 contributes to the survival of *Acinetobacter baumannii in vitro* and *in vivo*.

The Journal of Infectious Diseases, *199*(4), 513-521. https://doi.org/10.1086/596317

Rutherford, S. T., & Bassler, B. L. (2012). Bacterial quorum sensing: its role in virulence and possibilities for its control. *Cold Spring Harbor Perspectives in Medicine*, *2*(11), a012427. https://perspectivesinmedicine.cshlp.org/content/2/11/a012427.short

Ryan, M. P., Tingting, H., Jeffrey, D. R., Michael, J. S., & Ben, S. (2014). Mechanisms of self-resistance in the platensimycin-and platencin-producing Streptomyces platensis MA7327 and MA7339 strains. *Chemistry & Biology*, *21*(3), 389-397.

Saha, R., Saha, N., Donofrio, R. S., & Bestervelt, L. L. (2013). Microbial siderophores: a mini review. *Journal of Basic Microbiology*, *53*(4), 303-317.

Sahly, H., Navon-Venezia, S., Roesler, L., Hay, A., Carmeli, Y., Podschun, R., Hennequin, C., Forestier, C., & Ofek, I. (2008). Extended-spectrum β-lactamase production is associated with an increase in cell invasion and expression of fimbrial adhesins in *Klebsiella pneumoniae*. *Antimicrobial Agents and Chemotherapy*, *52*(9), 3029-3034.

Sajnaga, E., Kazimierczak, W., Karaś, M. A., & Jach, M. E. (2024). Exploring Xenorhabdus and Photorhabdus Nematode Symbionts in Search of Novel Therapeutics. *Molecules*, *29*(21), 5151. https://www.mdpi.com/1420-3049/29/21/5151

Schooling, S. R., & Beveridge, T. J. (2006). Membrane vesicles: an overlooked component of the matrices of biofilms. *Journal of Bacteriology*, *188*(16), 5945-5957.

Sebnem Hazal, G., Evren, T., Edna, B., Harun, C., Hatice, E., Derya, U., Sema, E., Sebastian, L. W., Mustapha, T., & Canan, H. (2022). Antiprotozoal activity of different Xenorhabdus and Photorhabdus bacterial secondary metabolites and identification of bioactive compounds using the easyPACId approach. *Scientific Reports*, *12*(1), 10779. https://doi.org/https://doi.org/10.1038/s41598-022-13722-z

Sechi, L. A., Karadenizli, A., Deriu, A., Zanetti, S., Kolayli, F., Balikci, E., & Vahaboglu, H. (2004). PER-1 type beta-lactamase production in

Acinetobacter baumannii is related to cell adhesion. *Med Sci Monit*, *10*(6), Br180-184.

Septer, A. N., Bose, J. L., Lipzen, A., Martin, J., Whistler, C., & Stabb, E. V. (2015). Bright luminescence of *Vibrio fischeri* aconitase mutants reveals a connection between citrate and the G ac/C sr regulatory system. *Molecular Microbiology*, *95*(2), 283-296.

Shi, H., Zeng, H., Yang, X., Zhao, J., Chen, M., & Qiu, D. (2012). An insecticidal protein from *Xenorhabdus ehlersii* triggers prophenoloxidase activation and hemocyte decrease in *Galleria mellonella*. *Current Microbiology*, *64*(6), 604-610.

Shi, Y.-M., Hirschmann, M., Shi, Y.-N., Ahmed, S., Abebew, D., Tobias, N. J., Grün, P., Crames, J. J., Pöschel, L., & Kuttenlochner, W. (2022). Global analysis of biosynthetic gene clusters reveals conserved and unique natural products in entomopathogenic nematode-symbiotic bacteria. *Nature Chemistry*, *14*(6), 701-712.

Shneider, M. M., Buth, S. A., Ho, B. T., Basler, M., Mekalanos, J. J., & Leiman, P. G. (2013). PAAR-repeat proteins sharpen and diversify the type VI secretion system spike. *Nature*, *500*(7462), 350-353.

Simon, A. (2010). FastQC: a quality control tool for high throughput sequence data. http://www.bioinformatics.babraham.ac.uk/projects/fastqc/

Singh, J. K., Adams, F. G., & Brown, M. H. (2019). Diversity and function of capsular polysaccharide in *Acinetobacter baumannii*. *Frontiers in Microbiology*, *9*, 3301. https://doi.org/https://doi.org/10.3389/fmicb.2018.03301

Siroy, A., Molle, V., Lemaître-Guillier, C., Vallenet, D., Pestel-Caron, M., Cozzone, A. J., Jouenne, T., & Dé, E. (2005). Channel formation by CarO, the carbapenem resistance-associated outer membrane protein of *Acinetobacter baumannii*. *Antimicrobial Agents and Chemotherapy*, *49*(12), 4876-4883.

Smani, Y., Dominguez-Herrera, J., & Pachón, J. (2013). Association of the outer membrane protein Omp33 with fitness and virulence of *Acinetobacter baumannii*. *The Journal of Infectious Diseases*, *208*(10), 1561-1570.

Smani, Y., Fàbrega, A., Roca, I., Sánchez-Encinales, V., Vila, J., & Pachón, J. (2014). Role of OmpA in the multidrug resistance phenotype of *Acinetobacter baumannii*. *Antimicrobial Agents and Chemotherapy*, *58*(3), 1806-1808.

Smani, Y., McConnell, M. J., & Pachón, J. (2012). Role of fibronectin in the adhesion of *Acinetobacter baumannii* to host cells. *PloS One*, *7*(4), e33073. https://doi.org/https://doi.org/10.1371/journal.pone.0033073

Smith, S. G. J., Mahon, V., Lambert, M. A., & Fagan, R. P. (2007). A molecular Swiss army knife: OmpA structure, function and expression. *FEMS Microbiology Letters*, *273*(1), 1-11. https://doi.org/10.1111/j.1574-6968.2007.00778.x

Snyder, H., Stock, S. P., Kim, S.-K., Flores-Lara, Y., & Forst, S. (2007). New Insights into the Colonization and Release Processes of *Xenorhabdus nematophila* and the Morphology and Ultrastructure of the Bacterial Receptacle of Its Nematode Host, *Steinernema carpocapsae*. *Applied and Environmental Microbiology*, *73*(16), 5338-5346. https://doi.org/10.1128/aem.02947-06

Srinivasan, V. B., Vaidyanathan, V., & Rajamohan, G. (2015). AbuO, a TolC-like outer membrane protein of *Acinetobacter baumannii*, is involved in antimicrobial and oxidative stress resistance. *Antimicrobial Agents and Chemotherapy*, *59*(2), 1236-1245.

Stacy, D. M., Welsh, M. A., Rather, P. N., & Blackwell, H. E. (2012). Attenuation of quorum sensing in the pathogen *Acinetobacter baumannii* using non-native N-Acyl homoserine lactones. *ACS Chemical Biology*, *7*(10), 1719-1728.

Stahl, J., Bergmann, H., Göttig, S., Ebersberger, I., & Averhoff, B. (2015). *Acinetobacter baumannii* virulence is mediated by the concerted action of three phospholipases D. *PloS One*, *10*(9), e0138360. https://doi.org/https://doi.org/10.1371/journal.pone.0138360

Stallforth, P., Brock, D. A., Cantley, A. M., Tian, X., Queller, D. C., Strassmann, J. E., & Clardy, J. (2013). A bacterial symbiont is converted from an inedible producer of beneficial molecules into food by a single mutation in the *gacA* gene. *Proceedings of the National Academy of Sciences*, *110*(36), 14528-14533.

Stein, M. L., Beck, P., Kaiser, M., Dudler, R., Becker, C. F. W., & Groll, M. (2012). One-shot NMR analysis of microbial secretions identifies highly potent proteasome inhibitor. *Proceedings of the National Academy of Sciences*, *109*(45), 18367-18371. https://doi.org/10.1073/pnas.1211423109

Steinberger, R., & Holden, P. (2005). Extracellular DNA in single-and multiple-species unsaturated biofilms. *Applied and Environmental Microbiology*, *71*(9), 5404-5410.

Steven, F., Barbara, D., Noel, B., & Erko, S. (1997). Xenorhabdus and Photorhabdus spp.: bugs that kill bugs. *Annual Review of Microbiology*, *51*(1), 47-72

Su, C. H., Wang, J. T., Hsiung, C. A., Chien, L. J., Chi, C. L., Yu, H. T., Chang, F. Y., & Chang, S. C. (2012). Increase of carbapenem-resistant *Acinetobacter baumannii* infection in acute care hospitals in Taiwan: association with hospital antimicrobial usage. *PloS One*, *7*(5), e37788. https://doi.org/https://doi.org/10.1371/journal.pone.0037788

Szittner, R., & Meighen, E. (1990). Nucleotide sequence, expression, and properties of luciferase coded by *lux* genes from a terrestrial bacterium. *The Journal of Biological Chemistry*, *265*(27), 16581-16587.

Tacconelli, E., Magrini, N., Kahlmeter, G., & Singh, N. (2017). Global priority list of antibiotic-resistant bacteria to guide research, discovery, and development of new antibiotics. *World Health Organization*, *27*, 318-327.

Taitt, C. R., Leski, T. A., Stockelman, M. G., Craft, D. W., Zurawski, D. V., Kirkup, B. C., & Vora, G. J. (2014). Antimicrobial resistance determinants in *Acinetobacter baumannii* isolates taken from military treatment facilities. *Antimicrobial Agents and Chemotherapy*, *58*(2), 767-781.

Takashi, M. (2020). Carotenoids as natural functional pigments. *Journal of Natural Medicines*, *74*(1), 1-16.

Takeuchi, K., Yamada, K., & Haas, D. (2012). ppGpp controlled by the Gac/Rsm regulatory pathway sustains biocontrol activity in Pseudomonas fluorescens CHA0. *Molecular Plant-Microbe Interactions*, *25*(11), 1440-1449.

Tang, J., Chen, Y., Wang, X., Ding, Y., Sun, X., & Ni, Z. (2020). Contribution of the AbaI/AbaR Quorum Sensing System to Resistance and Virulence of

Acinetobacter baumannii Clinical Strains. *Infection and Drug Resistance, 13*, 4273.

Tatiana, T., Michael, D., Azat, B., Vyacheslav, C., Eric, P. N., Leonid, Z., Alexandre, L., Kim, D. P., Mark, B., & James, O. (2016). NCBI prokaryotic genome annotation pipeline. *Nucleic Acids Research, 44*(14), 6614-6624.

Tettelin, H., Masignani, V., Cieslewicz, M. J., Donati, C., Medini, D., Ward, N. L., Angiuoli, S. V., Crabtree, J., Jones, A. L., Durkin, A. S., DeBoy, R. T., Davidsen, T. M., Mora, M., Scarselli, M., Margarit y Ros, I., Peterson, J. D., Hauser, C. R., Sundaram, J. P., Nelson, W. C., . . . Fraser, C. M. (2005). Genome analysis of multiple pathogenic isolates of Streptococcus agalactiae: Implications for the microbial "pan-genome". *Proceedings of the National Academy of Sciences, 102*(39), 13950-13955. https://doi.org/doi:10.1073/pnas.0506758102

Theodore, C. M., King, J. B., You, J., & Cichewicz, R. H. (2012). Production of cytotoxic glidobactins/luminmycins by *Photorhabdus asymbiotica* in liquid media and live crickets. *Journal of Natural Products*, *75*(11), 2007-2011. https://doi.org/10.1021/np300623x

Thomas, G. M., & Poinar, G. O. (1979). *Xenorhabdus* gen. nov., a genus of entomopathogenic, nematophilic bacteria of the family Enterobacteriaceae. *International Journal of Systematic and Evolutionary Microbiology, 29*(4), 352-360.

Tietze, A., Shi, Y. N., Kronenwerth, M., & Bode, H. B. (2020). Nonribosomal peptides produced by minimal and engineered synthetases with terminal reductase domains. *ChemBioChem*, *21*(19), 2750-2754.

Tiku, V., Kofoed, E. M., Yan, D., Kang, J., Xu, M., Reichelt, M., Dikic, I., & Tan, M.-W. (2021). Outer membrane vesicles containing OmpA induce mitochondrial fragmentation to promote pathogenesis of *Acinetobacter baumannii*. *Scientific Reports*, *11*(1), 1-16.

Tipton, K. A., & Rather, P. N. (2017). An ompR/envZ two-component system ortholog regulates phase variation, osmotic tolerance, motility, and virulence in *Acinetobacter baumannii strain* AB5075. *Journal of Bacteriology, 199*(3), e00705-00716. https://doi.org/10.1128/jb.00705-16

Tobias, N. J., Mishra, B., Gupta, D. K., Sharma, R., Thines, M., Stinear, T. P., & Bode, H. B. (2016). Genome comparisons provide insights into the role of secondary metabolites in the pathogenic phase of the *Photorhabdus* life cycle. *BMC Genomics, 17*(1), 537.

Tomaras, A. P., Dorsey, C. W., Edelmann, R. E., & Actis, L. A. (2003). Attachment to and biofilm formation on abiotic surfaces by *Acinetobacter baumannii*: involvement of a novel chaperone-usher pili assembly system. *Microbiology, 149*(12), 3473-3484. https://doi.org/https://doi.org/10.1099/mic.0.26541-0

Tomaras, A. P., Flagler, M. J., Dorsey, C. W., Gaddy, J. A., & Actis, L. A. (2008). Characterization of a two-component regulatory system from *Acinetobacter baumannii* that controls biofilm formation and cellular morphology. *Microbiology, 154*(11), 3398-3409. https://doi.org/https://doi.org/10.1099/mic.0.2008/019471-0

Torsten, S. (2014). Prokka: rapid prokaryotic genome annotation. *Bioinformatics, 30*(14), 2068-2069.

Traxler, M. F., Zacharia, V. M., Marquardt, S., Summers, S. M., Nguyen, H. T., Stark, S. E., & Conway, T. (2011). Discretely calibrated regulatory loops controlled by ppGpp partition gene induction across the 'feast to famine'gradient in *Escherichia coli*. *Molecular Microbiology, 79*(4), 830-845.

Turner, P. J., Greenhalgh, J., & Group, M. S. (2003). The activity of meropenem and comparators against *Acinetobacter* strains isolated from European hospitals, 1997–2000. *Clinical Microbiology and Infection, 9*(6), 563-567.

Turton, J. F., Ward, M. E., Woodford, N., Kaufmann, M. E., Pike, R., Livermore, D. M., & Pitt, T. L. (2006). The role of ISAba1 in expression of OXA carbapenemase genes in *Acinetobacter baumannii*. *FEMS Microbiology Letters*, *258*(1), 72-77. https://doi.org/10.1111/j.1574-6968.2006.00195.x

Uppalapati, S. R., Sett, A., & Pathania, R. (2020). The outer membrane proteins OmpA, CarO, and OprD of *Acinetobacter baumannii* confer a two-pronged defense in facilitating its success as a potent human pathogen. *Frontiers in Microbiology, 11*. https://doi.org/https://doi.org/10.3389/fmicb.2020.589234

Vakulskas, C. A., Potts, A. H., Babitzke, P., Ahmer, B. M. M., & Romeo, T. (2015). Regulation of Bacterial Virulence by Csr (Rsm) Systems. *Microbiology and*

Molecular Biology Reviews, *79*(2), 193-224. https://doi.org/10.1128/mmbr.00052-14

Van Dessel, H., Dijkshoorn, L., van der Reijden, T., Bakker, N., Paauw, A., van den Broek, P., Verhoef, J., & Brisse, S. (2004). Identification of a new geographically widespread multiresistant *Acinetobacter baumannii* clone from European hospitals. *Research in Microbiology*, *155*(2), 105-112.

Vercruysse, M., Fauvart, M., Jans, A., Beullens, S., Braeken, K., Cloots, L., Engelen, K., Marchal, K., & Michiels, J. (2011). Stress response regulators identified through genome-wide transcriptome analysis of the (p) ppGpp-dependent response in *Rhizobium etli*. *Genome Biology*, *12*(2), 1-19.

Vidal, R., Dominguez, M., Urrutia, H., Bello, H., Garcia, A., Gonzalez, G., & Zemelman, R. (1997). Effect of imipenem and sulbactam on sessile cells of *Acinetobacter baumannii* growing in biofilm. *Microbios*, *91*(367), 79-87.

Vila, J., Ruiz, J., Goni, P., Marcos, A., & De Anta, T. J. (1995). Mutation in the *gyrA* gene of quinolone-resistant clinical isolates of *Acinetobacter baumannii*. *Antimicrobial Agents and Chemotherapy*, *39*(5), 1201-1203.

Vuong, C., Voyich, J. M., Fischer, E. R., Braughton, K. R., Whitney, A. R., DeLeo, F. R., & Otto, M. (2004). Polysaccharide intercellular adhesin (PIA) protects *Staphylococcus epidermidis* against major components of the human innate immune system. *Cellular Microbiology*, *6*(3), 269-275.

Waack, U., Warnock, M., Yee, A., Huttinger, Z., Smith, S., Kumar, A., Deroux, A., Ginsburg, D., Mobley, H. L. T., Lawrence, D. A., & Sandkvist, M. (2018). CpaA Is a Glycan-Specific Adamalysin-like Protease Secreted by *Acinetobacter baumannii* That Inactivates Coagulation Factor XII. *MBio*, *9*(6), e01606-01618. https://doi.org/10.1128/mBio.01606-18

Wang, N., Ozer, E. A., Mandel, M. J., & Hauser, A. R. (2014). Genome-wide identification of *Acinetobacter baumannii* genes necessary for persistence in the lung. *MBio*, *5*(3). https://doi.org/https://doi.org/10.1128/mbio.01163-14

Waterfield, N. R., Ciche, T., & Clarke, D. (2009). Photorhabdus and a host of hosts. *Annual Review of Microbiology*, *63*(1), 557-574.

Weber, B. S., Miyata, S. T., Iwashkiw, J. A., Mortensen, B. L., Skaar, E. P., Pukatzki, S., & Feldman, M. F. (2013). Genomic and functional analysis of the type VI

secretion system in *Acinetobacter*. *PloS One*, *8*(1), e55142. https://doi.org/https://doi.org/10.1371/journal.pone.0055142

Webster, J., Li, J., & Hu, K. (1999). Nematicidal metabolites produced by *Photorhabdus luminescens* (Enterobacteriaceae), bacterial symbiont of entomopathogenic nematodes. *Nematology*, *1*(5), 457-469.

Webster, J. M., Chen, G., Hu, K., & Li, J. (2002). *Entomopathogenic nematology* (G. R., Ed.). CABI Publishing.

Weilbacher, T., Suzuki, K., Dubey, A. K., Wang, X., Gudapaty, S., Morozov, I., Baker, C. S., Georgellis, D., Babitzke, P., & Romeo, T. (2003). A novel sRNA component of the carbon storage regulatory system of *Escherichia coli*. *Molecular Microbiology*, *48*(3), 657-670.

Wenski, S. L., Kolbert, D., Grammbitter, G. L., & Bode, H. B. (2019). Fabclavine biosynthesis in X. szentirmaii: Shortened derivatives and characterization of the thioester reductase FclG and the condensation domain-like protein FclL. *Journal of Industrial Microbiology and Biotechnology*, *46*(3-4), 565-572.

Whitchurch, C. B., Tolker-Nielsen, T., Ragas, P. C., & Mattick, J. S. (2002). Extracellular DNA required for bacterial biofilm formation. *Science*, *295*(5559), 1487-1487.

World Health Organization. (2020). *Antimicrobial resistance*. https://www.who.int/news-room/fact-sheets/detail/antimicrobial-resistance

Wright, M. S., Haft, D. H., Harkins, D. M., Perez, F., Hujer, K. M., Bajaksouzian, S., Benard, M. F., Jacobs, M. R., Bonomo, R. A., & Adams, M. D. (2014). New insights into dissemination and variation of the health care-associated pathogen *Acinetobacter baumannii* from genomic analysis. *MBio*, *5*(1), 10-1128.

Wu, X., Chavez, J. D., Schweppe, D. K., Zheng, C., Weisbrod, C. R., Eng, J. K., Murali, A., Lee, S. A., Ramage, E., & Gallagher, L. A. (2016). In vivo protein interaction network analysis reveals porin-localized antibiotic inactivation in *Acinetobacter baumannii* strain AB5075. *Nature Communications*, *7*(1), 1-14.

Yi-Ming, S., & Helge, B. B. (2018). Chemical language and warfare of bacterial natural products in bacteria–nematode–insect interactions. *Natural Product Reports*, *35*, 309-335.

Yi-Ming, S., Merle, H., Yan-Ni, S., & Helge, B. B. (2022). Cleavage Off-Loading and Post-assembly-Line Conversions Yield Products with Unusual Termini during Biosynthesis. *ACS Chemical Biology*, *17*(8), 2221-2228.

Yi-Ming, S., Merle, H., Yan-Ni, S., Shabbir, A., Desalegne, A., Nicholas, J. T., Peter, G., Jan, J. C., Laura, P., & Wolfgang, K. (2022). Global analysis of biosynthetic gene clusters reveals conserved and unique natural products in entomopathogenic nematode-symbiotic bacteria. *Nature Chemistry*, *14*(6), 701-712.

Yoon, E.-J., Chabane, Y. N., Goussard, S., Snesrud, E., Courvalin, P., Dé, E., & Grillot-Courvalin, C. (2015). Contribution of resistance-nodulation-cell division efflux systems to antibiotic resistance and biofilm formation in *Acinetobacter baumannii*. *MBio*, *6*(2). https://doi.org/https://doi.org/10.1128/mbio.00309-15

Zarrilli, R. (2016). *Acinetobacter baumannii* virulence determinants involved in biofilm growth and adherence to host epithelial cells. *Virulence*, *7*(4), 367-368.

Zhou, Q., Dowling, A., Heide, H., Wöhnert, J., Brandt, U., Baum, J., Ffrench-Constant, R., & Bode, H. B. (2012). Xentrivalpeptides A–Q: depsipeptide diversification in *Xenorhabdus*. *Journal of Natural Products*, *75*(10), 1717-1722.

Zhou, Q., Grundmann, F., Kaiser, M., Schiell, M., Gaudriault, S., Batzer, A., Kurz, M., & Bode, H. B. (2013). Structure and biosynthesis of xenoamicins from entomopathogenic *Xenorhabdus*. *Chemistry–A European Journal*, *19*(49), 16772-16779.

Zimbler, D. L., Park, T. M., Arivett, B. A., Penwell, W. F., Greer, S. M., Woodruff, T. M., Tierney, D. L., & Actis, L. A. (2012). Stress response and virulence functions of the *Acinetobacter baumannii* NfuA Fe-S scaffold protein. *Journal of Bacteriology*, *194*(11), 2884-2893.

Zoued, A., Brunet, Y. R., Durand, E., Aschtgen, M.-S., Logger, L., Douzi, B., Journet, L., Cambillau, C., & Cascales, E. (2014). Architecture and assembly of the Type VI secretion system. *Biochimica et Biophysica Acta (BBA)-Molecular Cell Research, 1843*(8), 1664-1673.

APPENDIX

APPENDIX A CULTURE MEDIUM AND CHEMICALS PREPARATION

Nutrient bromothymol blue triphenyl tetazolium chioride agar (NBTA) (for bacteria isolation)

Components for 1 L

Nutrient agar (Oxoid, Ltd, England)	28	g
Bromothymol blue	0.025	g
Filtered 0.004% tetrazolium chloride	500	µL (dissolved with 90% alcohol, 0.22 µm filter)
Distilled water	1	L

Preparation

Dissolve all components in distilled water in a flask, then sterilize the flask by placing it in an autoclave at 121°C for 15 minutes. After sterilization, allow the medium in the flask to cool to approximately 50°C, then add tetrazolium chloride. Finally, pour the medium into sterilized petri dishes and let it cool until it solidifies into agar. The NBTA is now ready for use or can be stored in a refrigerator at 4°C.

Luria-Bertani (LB) broth

Components for 1 L

Luria-Bertani broth (LB) powder (Caisson LABS, USA)	25	g
Distilled water	1	L

Preparation

Dissolve LB powder in distilled water in a flask, then sterilize the solution by autoclaving at 121°C for 15 minutes. After sterilization, allow the medium to cool down in the flask. The LB medium is now ready for use or can be stored in a refrigerator at 4°C.

Luria-Bertani (LB) Agar

Components for 1 L

Luria-Bertani broth (LB) powder (Caisson LABS, USA)	25	g
Distilled water	1	L
Agar	1.5	%

Preparation

Dissolve all components in distilled water in a flask, then sterilize the solution by autoclaving at 121°C for 15 minutes. After sterilization, allow the medium to cool down in the flask. The LB medium is now ready for use or can be stored in a refrigerator at 4°C.

Preparation of Muller Hinton Agar (MHA)

Components for 1 L

Muller Hinton Agar (MHA) (Oxoid, Ltd, England)	38	g
Distilled water	1	L

Preparation

Dissolve all the components in 1 liter of distilled water. Sterilize the solution using an autoclave at 121°C for 15 minutes under steam pressure. After sterilization, allow the medium to cool down in the flask. The MHA medium is now ready for use or can be stored in a refrigerator at 4°C.

APPENDIX B BIOINFORMATICS SCRIPTS WRITTEN

AntiSMASH (antibiotics & Secondary Metabolite Shell – loop version)

```
#!/bin/bash

# Define an array of sample names
samples=("sample1" " sample2" " sample3")

# Define the base directory where your input files are located
base_directory="/path/to/your/input/foulder/$sample.gbk"

# Define the directory where you want to store antiSMASH results
output_directory="/path/to/your/output/foulder/$sample_antismash_output"

# Loop through the samples and run antiSMASH
for sample in "${samples[@]}"; do
echo "Running antiSMASH for $sample..."

# Define the input GenBank file path
input_gbk="$base_directory/$sample/$sample.gbk"

# Define the output directory for the current sample
sample_output_dir="$output_directory/$sample"

# Create the sample-specific output directory
mkdir -p "$sample_output_dir"

# Run antiSMASH with specified options
antismash \
--cc-mibig \
--cb-knownclusters \
--cb-subclusters \
```

```
--genefinding-tool prodigal \
--output-dir "$sample_output_dir" \
--output-basename "$sample" \
"$input_gbk"

echo "antiSMASH for $sample completed."
done
echo "All antiSMASH jobs completed."
```

PROKKA (Rapid Prokaryotic Genome Annotation)

```
#!/bin/bash

# Create the output folder if it doesn't exist
mkdir -p "$output_folder"

# Function to run Prokka for a given genome folder or file
function run_prokka() {
local genome_path="$1"
local output_dir="$2"

if [ -d "$genome_path" ]; then
echo "Annotating all .fasta files in $genome_path..."
prokka --outdir "$output_dir" \
--prefix "$(basename "$genome_path")" \
--locustag "$(basename "$genome_path")" \
--cpus 16 \
"$genome_path"/*.fasta
elif [ -f "$genome_path" ]; then
echo "Annotating $genome_path..."
prokka --outdir "$output_dir" \
--prefix "$(basename "$genome_path" .fasta)" \
```

```
--locustag "$(basename "$genome_path" .fasta)" \
--cpus 16 \
"$genome_path"
else
echo "Invalid genome path: $genome_path"
exit 1
fi
}

# Function to check if the input folder contains .fasta files directly
function check_input_folder() {
local genome_folder="$1"

if [[ $(find "$genome_folder" -maxdepth 1 -type f -name "*.fasta" | wc -l) -gt
0 ]]; then
echo "Found .fasta files in $genome_folder."
else
echo "No .fasta files found in $genome_folder."
exit 1
fi
}

# Read the list file line by line and run Prokka for each genome folder
while IFS= read -r genome_name; do
genome_path="$input_folder/$genome_name"
annotation_output="$output_folder/$genome_name"

echo "Checking if $genome_path is a directory or a file..."
run_prokka "$genome_path" "$annotation_output"

echo "Annotation of $genome_name complete."
echo
```

```
done < "$list_file"

echo "All genomes have been annotated."
```

BiG-SCAPE / CORASON

```
#!/bin/bash

# BiG-SCAPE Executable Path
BIGSCAPE_PATH="/path/to/bigscape.py"

# Input folder containing .gbk files
INPUT_FOLDER="/path/to/your/input/folder"

# Output folder for BiG-SCAPE results
OUTPUT_FOLDER="/path/to/output/folder"

# Set optional parameters
CUTOFF=0.30         # Similarity cutoff (default: 0.30)
MODE="hybrids"      # BiG-SCAPE mode: 'all', 'hybrids', 'pfam', etc.
CPU=4               # Number of threads to use
MIN_NR_GCF=1        # Minimum number of GCF members (default: 1)
CLUSTERING="single" # Clustering method: 'single', 'average', or 'complete'

# Run BiG-SCAPE
python3 $BIGSCAPE_PATH \
--inputdir $INPUT_FOLDER \
--outputdir $OUTPUT_FOLDER \
--cutoff $CUTOFF \
--mibig \
--mode $MODE \
--clustering $CLUSTERING \
```

```
--cpu $CPU \
--min_nr_gcf $MIN_NR_GCF

echo "BiG-SCAPE analysis completed. Results are stored in $OUTPUT_FOLDER"

# Save the script to a file, e.g., run_bigscape.sh.
# Make the script executable
chmod +x run_bigscape.sh

#Execute the script:
./run_bigscape.sh

Pangenomics - Anvi'o

#!/bin/bash

# Directory containing genome FASTA files
GENOMES_DIR="/path/to/genomes"

# Directory to store contigs databases
CONTIGS_DIR="/path/to/contigs_db"
mkdir -p $CONTIGS_DIR

# Create contigs databases
for genome in $GENOMES_DIR/*.fasta; do
genome_name=$(basename $genome .fasta)
anvi-gen-contigs-database -f $genome -o $CONTIGS_DIR/$genome_name.db --project-name $genome_name
done

# Directory containing contigs databases
```

```
CONTIGS_DIR="/path/to/contigs_db"

# Annotate each contigs database
for contigs_db in $CONTIGS_DIR/*.db; do
anvi-run-ncbi-cogs -c $contigs_db --num-threads 4
done

# Directory containing contigs databases
CONTIGS_DIR="/path/to/contigs_db"

# Output genomes storage database
GENOMES_STORAGE="genomes-storage.db"

# Create genomes storage
anvi-gen-genomes-storage -c $CONTIGS_DIR/*.db -o $GENOMES_STORAGE
#!/bin/bash

# Input genomes storage database
GENOMES_STORAGE="genomes-storage.db"

# Output pangenome database
PANGENOME_DB="pangenome.db"

# Create pangenome database
anvi-pan-genome -g $GENOMES_STORAGE -o $PANGENOME_DB --minbit 0.5 --mcl-inflation 10 --num-threads 4

# Visualize the Pangenome
anvi-display-pan -p pangenome.db --server-only

#  Export Summary of the Pangenome
anvi-summarize -p pangenome.db -o pangenome_summary
```

APPENDIX C BINDING SITES OF PRIMERS FOR GENE DELETION

Table 19 Binding sites of primers for *hfq* gene deletion. (The *hfq* gene is highlighted in yellow, while the primers are highlighted in blue. P1 and P4 primers also contain overhangs specific to the plasmid pEB17, which are highlighted in grey.)

Primer P5 Forward

GATTCTGCACTGGTTTATCGTGGCATGGATATTGGTACTGCGAAACCGTCCGCAGA

AGAGCAGGCTCAGGCTCCGCATCGTTTGATTGATATTCTGGATCCTGCCGACGTGT

Primer P1 Forward with overhang of plasmid pEB17 (in red alphabets)

ATTCTGCTGCTGATTTCGATCCTCTAGAGTCGACCTGCAGCGTCGCGATGCGCTGG

AACAAATGGCAGAAATTACGGCTGCAGGGAGAATTCCGCTCCTGGTCGGCGGAAC

CATGCTATATTTCAAAGCATTACTGGAAGGGTTATCACCACTACCTTCAGCAGACC

CTGAAGTCAGGGCGGTCATTGAGCAGGAGGCAGAGGAACACGGGTGGGAGGCATT

GCATCAGCAATTGCAGGAGATTGATCCGGTTGCAGCAGCAAGAATCCATCCAAAT

GATCCACAACGTCTTACTCGTGCACTGGAAGTTTTTCGGATTTCGGGTAACACTCTA

ACTACATTGACAGAAACGTCTGGGGAAGTATTGCCTTATCGTGTTCATCAGTTCGC

CATTGCGCCTGCAAGCCGTGAAATTTTGCATCAGCGCATTGCAGCCCGATTTGAAC

AGATGATCAAATCAGGGTTTGAAGATGAAGTTAAAGCGCTTTATGCTCGTAGCGAT

TTGCATACGGATTTACCCTCCATTCGTTGTGTTGGTTATCGTCAAATGTGGTCTTAC

CTCGCAGGCGAGATTTCTCATGATGAGATGGTTTATCGTGGTATCTGCGCAACTCG

CCAGCTGGCGAAGCGTCAGATAACCTGGCTCAGGGGGTGGGACGATGTGGCCTGG

TTGGACAGCGACCAGCCTGAGCAGGCCCTGAAAACAGTCATGCAGGTTATTGGTAC

ATAAATTCGTTGATTGTGTACAATTATCAGTACAAAGCGTCATTTTTGAGTAGTTAC

TTTTTCGAACCAACGGGTTCTTAGTTAAAAACAACAAAATAAGGAAAATATAGAAT

GGCTAAGGGGCAATCTTTGCAAGATCCATTCCTGAACGCATTACGTCGTGAAAGGG

Primer P2 Reward

TCCCGGTTTCTATTTATTTAGTCAACGGCATCAAATTGCAGGGTCAGATTGAGTCTT

TTGACCAGTTTGTCATTTTGCTGAAAAACACGGTTAGCCAGATGGTTTATAAACAC

GCCATCTCTACTGTTGTGCCTTCCCGTCCGGTATCTCACCACGGTAGCAATGCTAAT

Primer P3 Forward

ATGGCATCCAGCGTGGGAAATTATCAGGCTGGTAACAGTCCGGCAGCACAACAGG

AAAATGATATCGCTGAATAAATCAGTGATAATGCCTGACATAAATAAAAACATAG

GTAGGGAGACTTTACCTATGTTTTTCCTATGGAATTTTATACCCAATGGATTTCGAG

TTGCATCTCGGTAGCTTGAAAGACGAAGGGGATACTCAGCCTGAGGGTTGCACCAT

TGTTTGATCGTTACGAAGGCGGAGAACTAGCTGTTCTGGTGCATGTTTTTTTCTCAC

AGGAAAAAGACACGGAAAATCTCAGTGAATTTGAATCATTGGTGACTTCCGCAGG

TGTTTCTCCTGTGCAGATTGTGACAGGAAGCCGTAAGGCTCCGCATCCGAAATATT

TTGTCGGGGAAGGCAAGGCAGAAGAAATTGCTGAAGCAGTCAAAAACAGTGGTGC

AGATGTGGTGCTGTTTGATCACGCACTTTCTCCTGCTCAGGAACGTAATCTGGAAC

GCTTGTGCCAATGTCGTGTTGTTGATCGTACTGGTGTAATACTGGATATTTTTGCCC

AGCGGGCGAGAACTCATGAAGGTAAGTTGCAGGTAGAACTTGCACAGTTACGCCA

TTTATCTACTCGCTTAGTCCGAGGCTGGACCCATCTTGAACGCCAGAAAGGCGGAA

TTGGTTTACGTGGCCCCGGTGAAACCCAGCTGGAATCAGATCGCCGTATGTTGCGC

GATAAAATTAAACAGATTCTGGGGCGTCTTGGTAAAGTAGAAAGACAGCGTGAAC

AGGGGCGTCAGGCGCGCAACAAAGCAGATATTCCCACCGTTTCTCTTGTTGGTTAC

ACCAATGCCGGAAAATCAAGTTTATTCAATAGAATAACCTCGGCTGAGGTATATGC

Primer P4 Reward with overhang of plasmid pEB17 (in red alphabets)

TGCTGATCAGCTTTTTGCTACTCTCGACCCGACATTGCGTCGGATCGCTGTAAATGA

TGTCGGCCCGGTTGTTCTGGCTGACACCGTTGGTTTCATTCGTCACGTGACGAATGA

AACCAACGGTGTCTTACCCCATGATTTGGTGGCAGCGTTTAAGGCCACTTTGCAGG

Primer P6 Reward

AAACAAGGCAGGCAAGGTTATTGCTTCATGTTGTTGATGCGGCTGATAACCGGCTG

GATGAGAACATTCTTGCAGTGGACAGTGTTCTGGAAG

APPENDIX D GENE DELETION

A. **B.**

C.

Figure 22 Hfq Deletion. (A) *Xenorhabdus Stockiae* RT25.5 WT *(B) Xenorhabdus stockiae* RT25.5_Δ*hfq*; light-colored colonies were selected for PCR verification. (C) Colony PCR verification of selected colonies.

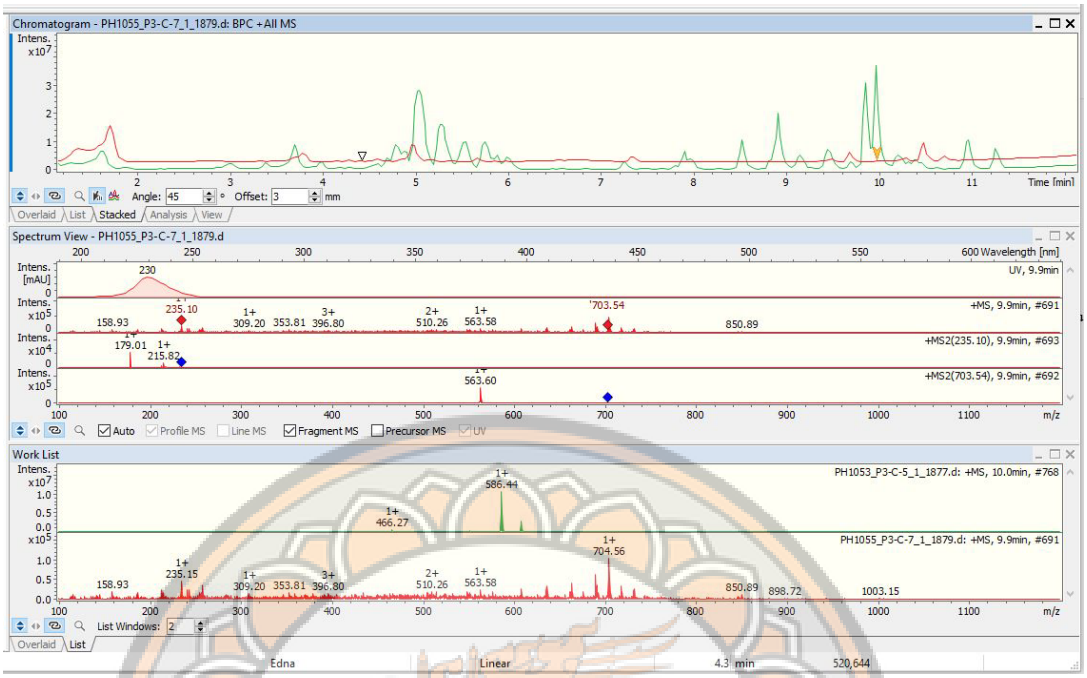

Figure 23 The base peak chromatograms (BPCs) of cell-free supernatants extracted with methanol from *Xenorhabdus stockiae* RT25.5 wild type (WT) and the *X. stockiae* RT25.5_Δ*hfq* mutant reveal differences in metabolite profiles, providing insights into the effects of the Δ*hfq* mutation on secondary metabolite production

Green Line: Represents the BPC of the methanol-extracted supernatant from the WT strain (*X. stockiae* RT25.5). This chromatogram displays peaks corresponding to various natural products (NPs) synthesized by the WT strain, reflecting the normal biosynthetic activity of its biosynthetic gene clusters (BGCs).

Red Line: Represents the BPC of the methanol-extracted supernatant from the Δ*hfq* mutant. The significant reduction or absence of peaks in this chromatogram suggests that the mutation in the *hfq* gene disrupts the expression or activation of many BGCs, resulting in reduced production of almost NPs

Figure 24 The results of antibacterial activity testing using crude compounds from bacteria.